DESIGN AND IMPLEMENTATION OF L AND X-BAND FILTERS FOR THE NEXTRAD FRONT END

A thesis submitted to the Department of Electrical Engineering,
UNIVERSITY OF CAPE TOWN, in fulfilment of the requirements for the degree of

Master of Science

at the

University of Cape Town

by

Dominique Gouveia

Supervised by :
ASSOCIATE PROFESSOR RIANA GESCHKE

June 19, 2017

Declaration

I know the meaning of plagiarism and declare that all the work in this dissertation, save for that which is properly acknowledged and referenced, is my own. It is being submitted for the degree of **Master of Science** in Electrical Engineering at the University of Cape Town. This work has not been submitted before for any other degree or examination in any other university.

Signature of Author: Signed by candidate Signature Removed

University of Cape Town

Cape Town
June 19, 2017

ABSTRACT

Microwave filters are required at the RF front end of a research radar called NeXtRAD to suppress out of band transmitted and received signals. NeXtRAD is a multistatic[1] pulse-Doppler radar[2] system, developed at the University of Cape Town (UCT) in collaboration with the University College London (UCL). It has been designed to operate in two frequency bands, designated as L and X-bands. NeXtRAD will be used as a research tool, for the purposes of measuring sea targets and detecting sea clutter. The measured data will be stored in a database, and it will be made freely available to the public for research purposes.

A coaxial comb-line filter was designed, manufactured and measured at L-band. The narrow band measurement results showed that the filter was centred at 1300 MHz, with an equal ripple bandwidth of 210 MHz. The filter has a spurious-free window of 2050 MHz at -60 dB, with the first spurious approximately at 2.86 times the operating frequency. The return loss of the filter was 19.52 dB, and the insertion loss at mid-band was 0.14 dB. The measured filter agreed extremely well with the L-band specifications.

The X-band iris coupled filter was also designed, manufactured and measured. The narrow band measurement results showed that the filter was centred at 8.5 GHz, with an equal ripple bandwidth of 121 MHz. The spurious-free window of the measured filter at -60 dB was 6.571 GHz, with the first spurious at 1.82 times the operating frequency. The insertion loss of the filter was measured to be 2 dB at mid-band and the return loss of the filter was measured to be 18.58 dB at mid-band. The filters are currently being used at the RF front end of the NeXtRAD system.

[1] A radar system having two or more transmitting or receiving antennas with all antennas separated by large distances when compared to the antenna sizes [1].

[2] A Doppler radar that uses pulsed transmissions [1]

ACKNOWLEDGEMENTS

I would like to express my gratitude to the following people, who assisted towards successful completion of this research project:

- **Associate Professor Riana Geschke**, my UCT supervisor, for your guidance during the entire research project. Thank you for taking me as one of your students for the past three years. Your enthusiasm in this field motivates me. I am grateful to you for putting time aside for us to go and visit manufacturing companies. I learned a great deal on how to plan builds of filters and interact with manufacturers, just by watching you in action.

- **National Research Foundation (NRF)-South Africa**, for the financial assistance throughout this research project.

- **Associate Professor Daniel O'Hagan**, for always being actively involved and interacting with students both, academically and personally. Thank you for running around with me in 2015, in an attempt to sort out my study visa. Also, I am grateful to you for keeping me posted on matters regarding application for permanent residence.

- **Mr. Ashiv Dhondea**, for always helping me out with Matlab and Latex. You have been a great source of help since my undergraduate thesis. I am grateful to you for your willingness to help me at all times. Also, thank you for proofreading my dissertation.

- **Mr. Adrian Steven**, for your guidance throughout the project and for always being ready to answer any question I have regarding the filters for NeXtRAD.

- **Mr. Philip Titus**, for allowing me to use the tools in the power lab. Thank you for always being willing to help me with the mechanical aspects of my filter, such as precisely cutting the feeding probes for my filters, ordering the tuning screws, etc.

- **Mr. Chris Wozniak**, for allowing me to use the measuring instruments in the machines lab.
- **Mr. Pierre Smith**, for lending me the hacksaw from the mechanical workshop to cut my probes.
- **Mr. John-Philip Taylor**, for proofreading the first two chapters of my dissertation.
- **NeXtRAD Team**, for allowing me to take part in this project.

CONTENTS

LIST OF FIGURES

List of Tables

LIST OF ABBREVIATIONS

- **CAD** – Computer-Aided Design
- **CST** – Computer Simulation Technology
- **EM** – Electromagnetic
- **HFSS** – High Frequency System Simulator
- **HPA** – High Power Amplifier
- **ICASA** – Independent Communications Authority of South Africa
- **IEEE** – Institute of Electrical and Electronic Engineers
- **L-Band** – Frequency Band Spanning 1 GHz to 2 GHz
- **LNA** – Low Noise Amplifier
- **RL** – Return Loss
- **S-Band** – Frequency Band Spanning 2 GHz to 4 GHz
- **SIW** – Substrate Integrated Waveguide
- **TEM** – Transverse Electromagnetic
- **TE**$_{n,m}$ – Transverse Electric
- **TM**$_{n,m}$ – Transverse Magnetic
- **UCL** – University College London
- **UCT** – University of Cape Town
- **X-Band** – Frequency band Spanning 8 GHz to 12 GHz

LIST OF SYMBOLS

f_m — Even mode frequency (Hz)

f_e — Odd mode frequency (Hz)

f_0 — Centre frequency (Hz)

f_c — Cutoff frequency of waveguide (Hz)

T_x — Transmitter

R_x — Receiver

P_{LR} — Power loss ratio of a filter response

ω — Angular frequency (rad/sec)

ω_c — Cutoff angular frequency (rad/sec)

$\Gamma(\omega)$ — Reflection coefficient

H_{IL} — Insertion loss (dB)

P and Q — Polynomials in ω^2

N — Filter order

τ — Chebyshev ripple factor

T_{N} — Chebyshev polynomials

L_{Ar} — Chebyshev pass band ripple (dB)

L_{As} — Minimum stop band attenuation (dB)

L_R — Minimum pass band return loss (dB)

Δ — Fractional bandwidth of the pass band

ω_0 — Angular centre frequency (rad/sec)

ω_1 — Lower angular cutoff frequency (rad/sec)

ω_2 — Upper angular cutoff frequency (rad/sec)

ω_s — Minimum stop band attenuation angular frequency (rad/sec)

K — Characteristic impedance of inverter (Ω)

J — Characteristic admittance of inverter (siemens)

Z_{in} — Input impedance of two port network (Ω)

Y_{in} — Input admittance of two port network (siemens)

Z_L — Load impedance of two port network (Ω)

Y_L — Load admittance of two port network (siemens)

Z_0 — Characteristic impedance of two port network (Ω)

$X(\omega)$ — Reactance of the distributed resonator (Ω)

$B(\omega)$ — Susceptance of the distributed resonator (siemens)

$x(\omega)$ — Reactance slope parameter

$b(\omega)$ — Susceptance slope parameter

λ_{g_0} — Guide wavelength (m)

λ_0 — Free space wavelength (m)

λ_{g_1} — Guide wavelength at lower band edge (m)

λ_{g_2} — Guide wavelength at upper band edge (m)

Q_e — External quality factor

κ — Physical coupling coefficient

κ_M — Inductive coupling coefficient

κ_E — Capacitive coupling coefficient

c_0 — Speed of light in free space (m/s)

CHAPTER 1

INTRODUCTION

The coaxial and the waveguide band pass filters are commonly used at the RF front end of radar systems, due to their power handling capability, relatively low loss and stop band performance [3], [4] , [5], and [6]. A coaxial comb-line and a waveguide inductive iris band pass filters were designed and implemented in this thesis. These filters are used at the RF front end of a dual band (L and X-band)[1] high power[2] networked radar system, known as NeXtRAD.

This chapter provides a brief overview of the NeXtRAD system in Section 1.1. Thereafter, Section 1.2 discusses the requirement of the filters at the RF front end of the NeXtRAD system. Following that, the electrical specifications for the filters are presented in Section 1.3. The chapter concludes with a layout of the thesis in Section 1.4.

1.1 NEXTRAD SYSTEM[2]

The University of Cape Town (UCT) and University College London (UCL) have collaborated in the development of a multistatic pulse-Doppler radar system, known as NetRAD, from 2009 to 2011. NetRAD operates in the frequency range spanning 2 GHz to 4 GHz (S-band) and is centred at f_0 = 2.45 GHz. S-band was strategically selected for two reasons: firstly, to take advantage of the fact that it is an unlicensed band. The other is because there were many readily available commercial off-the-shelf components at this band. The NetRAD system contains a single transceiver (active node) and single receiver (passive node), arranged in a bistatic-radar[3] configuration as illustrated in Figure 1.1 , with one passive node removed. NetRAD was used as a research tool, for the purpose of measuring sea targets and detecting sea clutter. The measured

[1] In the L-band, the radar is intended to operate from 1.2 GHz to 1.4 GHz. In the X-band, the radar is intended to operate from 8.5 GHz to 10.5 GHz. The X-band frequency range is limited by the current high power amplifier.

[2] The L-band peak power is 1.4 kW, with 20 % duty cycle. The X-band peak power is 400 W, with 20 % duty cycle.

[3] A radar using antennas for transmission and reception at sufficiently different locations that the angles or ranges to the target are significantly different [1].

data was stored in a database and is freely available to the public for research purposes.

To further enhance the discrimination between targets at sea and sea clutter, NetRAD is currently being upgraded as follows: Firstly, two different frequency bands, L and X-band replaced the single S-band. From an electrical point of view, objects look different at L and X-band. This allows the radar to electrically see the target from multiple perspectives, which could potentially enhance the detection of a target at sea. Like the S-band, the L and X-band were selected because they are traditional radar bands, making licensing easier, and due to the fact that there are commercially available components at these frequencies as well. Secondly, dual polarized antennas are used to improve the characterisation and to estimate the salient features of targets at sea. Lastly, an additional receiver is added to NetRAD to form the multistatic configuration illustrated in Figure 1.1. Such a configuration allows the radar to physically look at the target from multiple points of views, and could potentially enhance the detection of the target at sea. The new radar system is called NeXtRAD, the upgrade of NetRAD.

1.2 FILTERS REQUIRED AT THE RF FRONT END OF NEXTRAD

Figure 1.2 illustrates the setup of the NeXtRAD system during a measurement trial in Simons Town (RSA) in December 2016. The red arrow in Figure 1.2 points to the L and X-band filters inside the RF front end of NeXtRAD. The location of the filters in the RF front end can be seen in a block diagram of the RF front end shown in Figure 1.3. The location of the filters in Figure 1.3 is indicated by means of red rectangles.

In the L and X-band transmitter chains, the filters come after the high power amplifier (HPA) and are positioned between a high power directional coupler and a high power switch. In the L and X-band receiver chains, the filters come before the low noise amplifier (LNA). However, in the X-band receiver chain, the filters are positioned between the receiver antennas and low power limiter, and in the L-band receiver chain, the filters are positioned between a low power switch and low power limiter. NeXtRAD is specified to transmit a peak power of 1.4 kW and 400 W with a 20 % duty cycle in the L and X-band respectively. Microwave filters are required in the transmit chains of the RF front end of NeXtRAD to suppress out-of-band signals from the high power amplifier, so as to ensure that NeXtRAD complies with the Independent Communication Authority of South Africa (ICASA) out-of-band emission regulations. Additionally, filters are required at the receive chains to prevent the low noise amplifier (LNA) from saturating due to the out-of-band received signals.

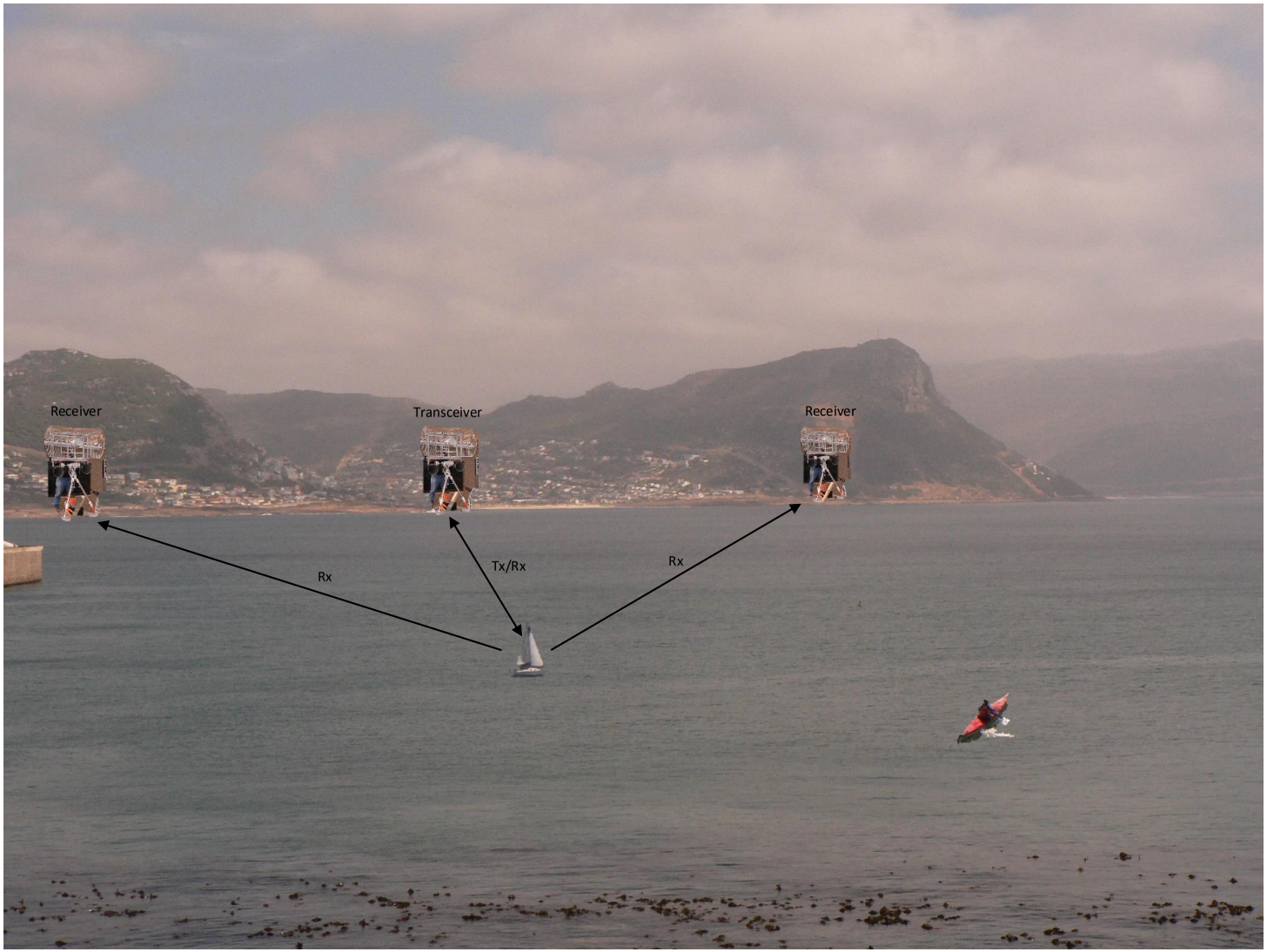

Figure 1.1: A basic illustration of the NeXtRAD system in a multistatic arrangement containing a transceiver and two receivers, for detecting a target at sea. In the case of NetRAD, only a single receiver was considered.

Figure 1.2: L and X-band filters being used at the RF front end of NeXtRAD at the test site: Simon's Town (RSA)

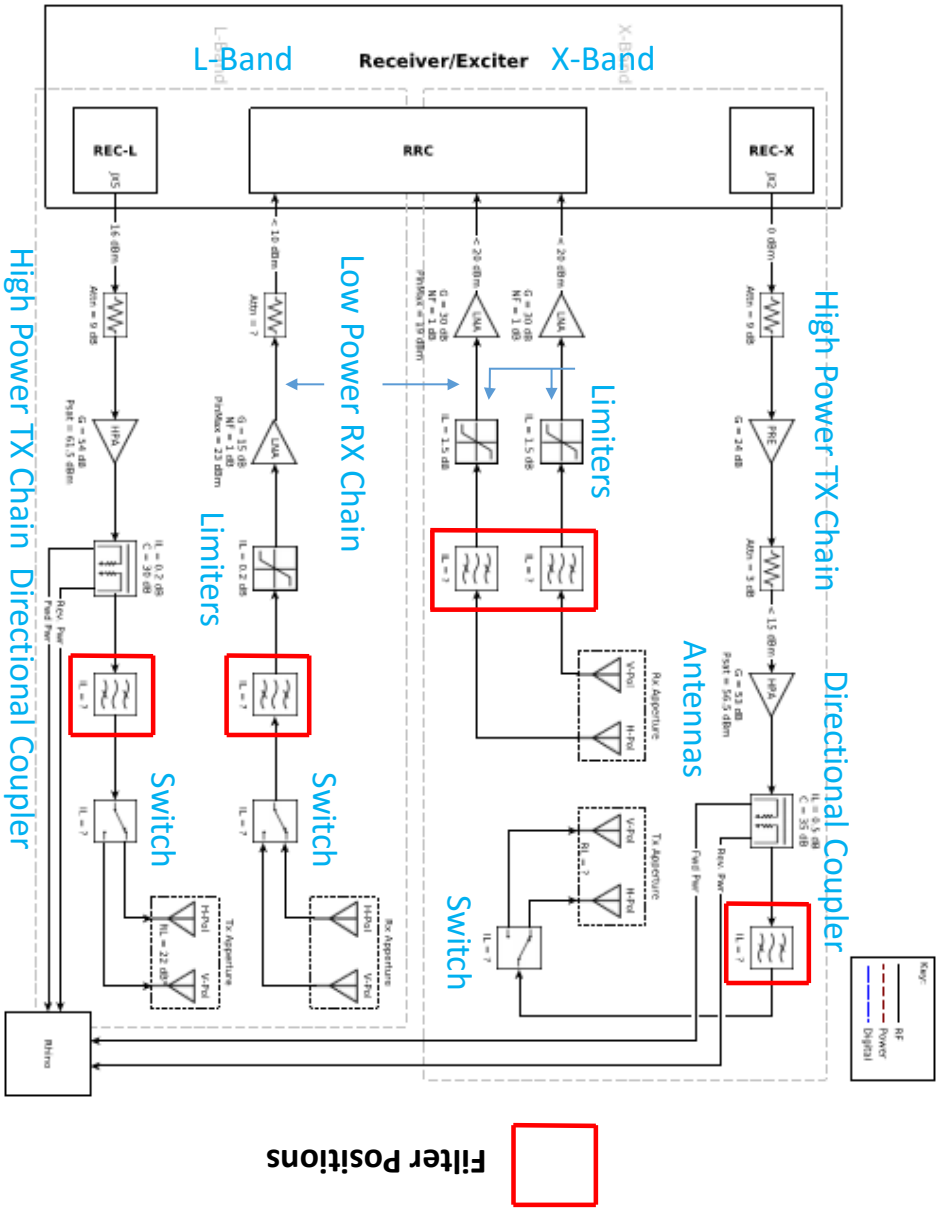

Figure 1.3: Block diagram of the RF front end of NeXtRAD

1.3 FILTER SPECIFICATIONS

NeXtRAD is currently at its early stage of development and is operating on a limited budget. For these reasons, there are no exact specifications for the filters at the moment. As NeXtRAD grows through various stages of development, so will the specifications of the filters be updated. To save on cost, the author was given the task to design temporary filters which could be used at the RF front end of NeXtRAD, to perform preliminary trial measurements. At the time of writing this document, NeXtRAD specified the L-band filter to be centred at 1300 MHz, with a bandwidth of 200 MHz and 1.4 kW peak power at 20% duty cycle. The X-band filter was specified to be centred at 8.5 GHz, with a bandwidth of 50 MHz and 400 W peak power at 20% duty cycle.

The filter specifications provided by NeXtRAD were not adequate to practically characterize the filters. An investigation was done to study the characteristics of practical filters from various manufacturers. The aim was to find filters with characteristics suitable for NeXtRAD. Once these filters were found, the filters were used as reference filters to specify the NeXtRAD L and X-band filters.

Reutech Radar donated an interdigital band pass filter to NeXtRAD, this filter is currently being used at the L-band in the NeXtRAD system. The filter was measured in order to study its electrical characteristics, which is presented in Appendix A, Table A.1. The response of the filter is given in Appendix A, Figures A.4 to A.6. Practical specifications for the L-band filter for NeXtRAD was then estimated from Appendix A, Table A.1, and is presented in Table 1.1.

The specifications of the X-band filter were determined by communicating with the system engineer, Adrian Steven. The specifications for the X-band filter were estimated as provided in Table 1.2.

1.4 REPORT LAYOUT

The material in this report is organised in three chapters as follows:

- **Chapter 2** presents a very basic theory of the insertion loss method, with the focus on combining circuit models and computer-added design (CAD) software to design coupled resonator filters.

  Section 2.1 introduces the Chebyshev filter function. This is a commonly used filter function and is derived from the approximation problem [5]. In Section 2.2, the low pass prototype circuit for the Chebyshev filter function is presented. The section does not

Table 1.1: Specifications for L-band filter

Pass band	1200 MHz to 1400 MHz
Centre Frequency	1300 MHz
Insertion Loss	0.5 dB (max)
Return Loss	20 dB (min)
Equal Ripple Bandwidth	200 MHz
Fractional Bandwidth	15.38 %
Stop band	
Frequency/MHz	Attenuation/dB (min)
880 to 890	60
925 to 935	55
1710 to 1785	70
1805 to 1880	80
Input/output Impedance	50 Ω

focus on the actual synthesis procedure but rather presents formulas and tables which can be used to determine the element values and the order of the low pass prototype circuit for the Chebyshev filter function.

The low pass prototype circuit discussed in Section 2.2 are normalized in frequency and impedance. In order to implement practical filter responses, such as a band pass response using this prototype, the low pass prototype circuit in Section 2.2 must be denormalized in frequency and impedance. Section 2.3[4] gives the necessary equation to denormalise the low pass prototype circuit of Section 2.2.

The denormalised prototypes of Section 2.3 have both series and shunt elements. It is often desirable when implementing microwave filters to have a prototype with only series or shunt elements. For this, impedance and admittance inverters are required, which is the subject of Section 2.4. Section 2.4 also presents the concepts of the coupling coefficients and external quality factor. These two concepts are central to coupled resonator filter design. It relates the electrical elements of the band pass filter prototypes presented in Section 2.4 to the elements of the physical filter. Section 2.5 illustrate these relationships, and will show how the external quality factor and coupling coefficients along with the resonant frequencies of the resonators can be combined with an electromagnetic (EM) simulators to determine the physical dimensions of coupled resonator filters, and hence concluding the chapter.

[4] Note: the frequency transformation in this report is limited to the low pass to band pass transformation.

Table 1.2: Specifications for X-band filter

Pass band	8.475 GHz to 8.525 GHz
Centre Frequency	8.5 GHz
Return Loss	20 dB (min)
Equal Ripple Bandwidth	50 MHz
Fractional Bandwidth	0.588 %
Stop band	
Frequency/GHz	Attenuation/dB (min)
8.2	45
8.8	45
Input/output Impedance	50 Ω

- **Chapter 3** deals with the design of the coaxial comb-line filter. The comb-line filter order and stop band rejection that will meet the NeXtRAD specifications is estimated in Section 3.2. Section 3.3 provides a brief literature review on the special properties of the coaxial transmission line and the comb-line filter. Once the filter order is known and the properties of the comb-line filter understood, the design and analysis of the comb-line filter begin in Section 3.4. First, the physical dimensions of the resonators were determined using the eigenmode analysis. Thereafter, two resonators with previously determined physical dimensions were coupled together in order to determine the physical dimensions, which realizes the desired interresoantor coupling coefficient. Finally, the resonators were used to determine the physical dimensions to realize the required input/output external quality factors.

  Thereafter, a complete filter was modeled and simulated in CST [7], with the obtained physical dimensions. This filter was tuned and compared to the ideal filter response. Section 3.5 discusses the fabrication of the comb-line filter. Section 3.6 provides the measured results of the comb-line filter. These measured results are compared to the simulated results in this section, and the discussions of these results follow in Section 3.7 to conclude the chapter.

- **Chapter 4** addresses the design of an inductive iris coupled waveguide filter. It follows the same procedure as Chapter 3 to design the waveguide filter. The only exception is the literature review on the special properties of the rectangular waveguide and the inductive iris coupled filter, presented in Section 4.3.

- **Chapter 5** concludes this thesis. This chapter gives the main conclusions about the characteristics of the filters, and its use at the RF front end of the NeXtRAD system. It also

provides recommendations on how to build better filters for the NeXtRAD system when the system is more developed.

CHAPTER 2

MICROWAVE FILTER DESIGN WITH THE INSERTION LOSS METHOD

This chapter presents a concise theory on microwave filter design with the insertion loss method. This well-known insertion loss method is a commonly used network synthesis technique, which is used to design microwave filters with a completely specified frequency response around the desired pass band [8]. The insertion loss method may be divided into two parts, namely the approximation and synthesis problems. The approximation is the process of finding a filter function that mathematically describes the desired frequency response of the filter. The synthesis, on the other hand, is the process of obtaining a filter circuit from the approximated filter function [9] and [10].

Section 2.1 introduces the commonly used all pole Chebyshev filter function[1]. In Section 2.2, the normalized low pass prototype circuit for the Chebyshev filter function along with the tables and equations necessary to calculate the elements of this circuit and the filter order are presented. The low pass to band pass transformation equations used to implement practical filter responses using the low pass prototype are given in Section 2.3. The impedance and admittance inverters are required to implement microwave filters with either series or parallel elements, these inverters are discussed in Section 2.4. The concepts of the coupling coefficients and external quality factor are central to the design of coupled resonator filter and are also discussed in Section 2.4. The coupling coefficients and external quality factor concepts along with the resonant frequencies of the resonators are used to determine the physical dimensions of the coupled resonator filter.

[1] There are other types of Chebyshev filter functions, as well as many other types of filter function prototype that can be used. The choice of the filter function depends on the filter specifications

2.1 CHEBYSHEV FILTER FUNCTION

The insertion loss, or power loss ratio, of a filter, may be used to define the response of the filter [8]. The power loss ratio P_{LR} is given in [8] as

$$P_{LR} = \frac{1}{1 - |\Gamma(\omega)|^2}, \tag{2.1}$$

where ω is the angular frequency in (rad/sec), and $|\Gamma(\omega)|$ is the reflection coefficient. The insertion loss (H_{IL}) in dB is [8]

$$H_{IL} = 10 \log P_{LR}. \tag{2.2}$$

Equation (2.1) can be expressed as a polynomial in ω^2, because $|\Gamma(\omega)|^2$ is an even function of ω [8]. This means that $|\Gamma(\omega)|^2$ can be written as [8]

$$|\Gamma(\omega)|^2 = \frac{P(\omega^2)}{P(\omega^2) + Q(\omega^2)}, \tag{2.3}$$

where P and Q are real polynomials in ω^2. Thus by substituting (2.3) in (2.1), the new expression for the power loss ratio is

$$P_{LR} = 1 + \frac{P(\omega^2)}{Q(\omega^2)}. \tag{2.4}$$

Therefore, physically realizable filters must have their power loss ratio of the form in (2.4) [8]. Practical filter functions or responses, such as a Chebyshev response may then be derived from (2.4).

2.1.1 Classical Band-forms of Filters

An electronic filter can be described by its frequency response [5]. The frequency response of a filter can be represented by a transfer function, such as the transmission coefficient, which can be of various forms and characteristics.

The low pass, high pass, band pass and band reject are the four basic prototype band-forms a filter may have. By carefully selecting the correct type of band-form for a given application, it is possible to accept the desired signals and reject the undesired signals. These four band-forms

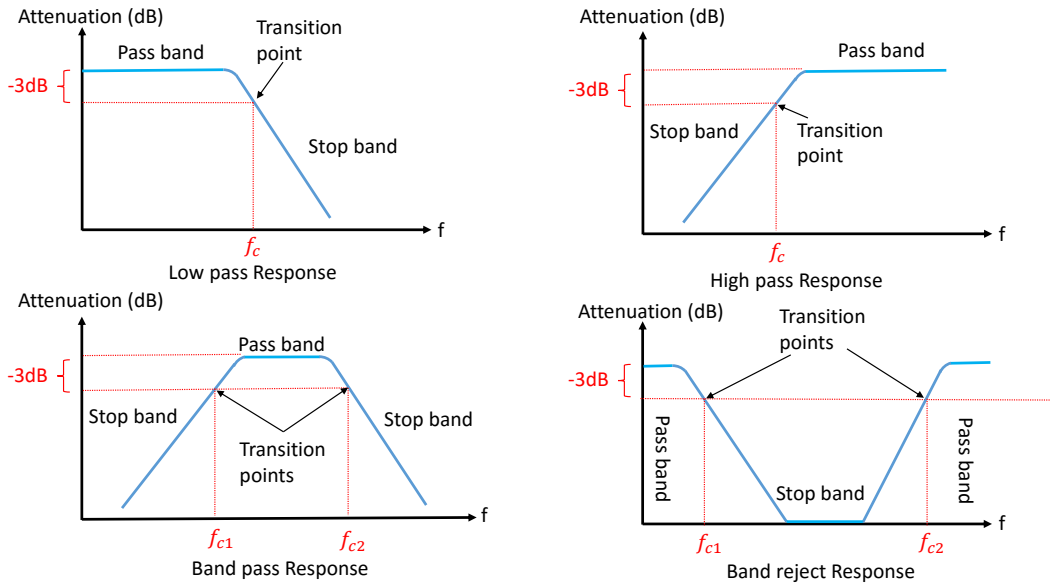

Figure 2.1: Low pass, high pass, band pass and band reject band-forms

are illustrated in Figure 2.1.

The frequency response of a filter has several regions. These regions define the band-forms type. It is important to have a description of these regions in mind. These regions are called: the pass band, transition point, and the stop band. The transition point between the pass band and the stop band is termed the cutoff frequency. The pass band of the filter is the range of frequencies within which the attenuation of a filter is lower than at frequencies outside this band. The stop band is the range of frequencies within which the attenuation of a filter is higher than at frequencies outside this band [11]. The transition point is between the pass band and the stop band. This point is marked by the cutoff frequency of the filter, which is usually defined at the 3 dB point, depending on the filter function used.

2.1.2 **Chebyshev Characteristic Polynomial**

Ideally, when designing a filter, one would like to have zero insertion loss in the pass band, infinite attenuation in the stop band and a linear phase response in the pass band [8]. Such filters are not practical. There is always a trade-off between these three desired filter characteristics [8]. For this reason, typical standard filter functions, such as the Chebyshev and the Butterworth functions, are used to make the design procedure easier. These functions ensure that the necessary trade-offs can be made. For example, if a flat pass band response is needed, then the Butterworth function is preferred, for an excellent selectivity, the Chebyshev function is chosen as shown in Figure 2.2.

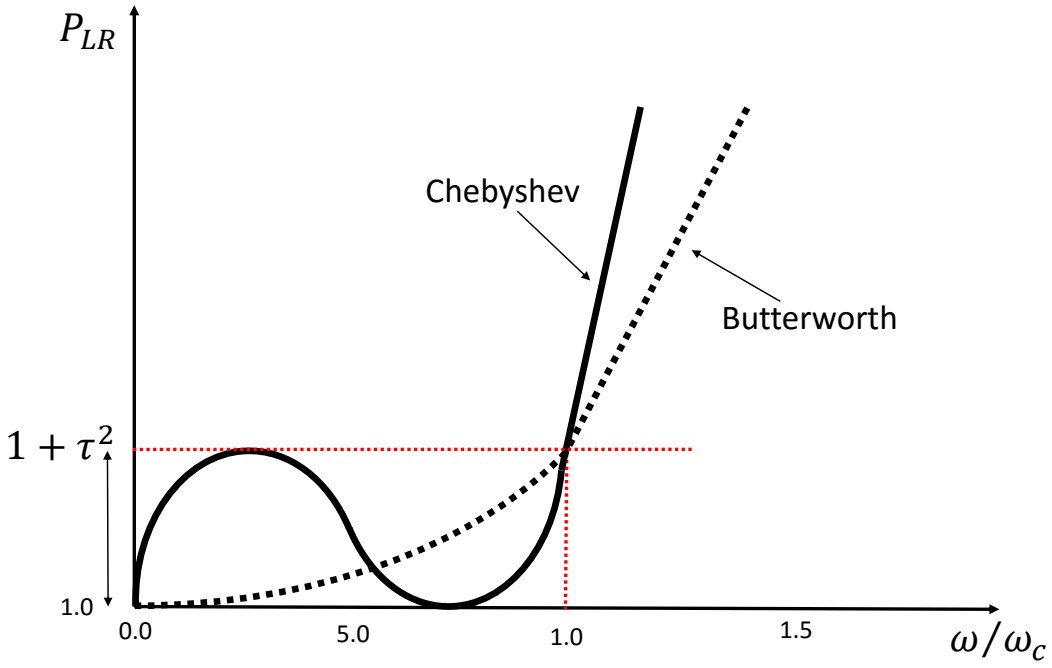

Figure 2.2: Chebyshev and Butterworth low pass filter response

The Chebyshev characteristic polynomial has an equal-ripple attenuation variation in its pass band, with consistently increasing attenuation as the frequency moves away from the pass band [11]. The polynomial used to specify the insertion loss of an N-order Chebyshev low pass filter is given by [8] as

$$P_{LR} = 1 + \tau^2 T_{\mathrm{N}}^2\left(\frac{\omega}{\omega_c}\right), \tag{2.5}$$

where τ is the ripple factor and $T_{\mathrm{N}}\left(\frac{\omega}{\omega_c}\right)$ are Chebyshev polynomials.

The low pass filter will have a sharp cutoff response, at the expense of pass band ripple. This is due to the fact that $T_{\mathrm{N}}(y)$ oscillates between ± 1 for $|y| \leq 1$. The amplitude of the pass band ripple is given by $1 + \tau^2$ [8]. This behavior can be seen in Figure 2.2.

2.2 Low Pass Prototype Filter Circuits and Elements

An electrical circuit can be synthesized from the characteristic polynomials of the Chebyshev filter function. The resulting electric circuit is the so-called low pass prototype circuit [10].

A low pass prototype filter circuit is generally defined as a filter whose element values are normalized to make the source resistance/conductance equal to one, and the cutoff angular frequency to be unity. The source resistance/conductance and the cutoff angular frequency are denoted by $g_0 = 1$ and $\omega_c = 1$ rad/sec [12]. Figures 2.3 and 2.4 demonstrate example of two possible forms of an N-order low pass prototype filter circuit used to realise an all-pole filter response, such as the Chebyshev responses.

In Figure 2.3, the low pass prototype begins with a series element, while in Figure 2.4 it begins with a shunt element. Either form of these prototype circuits may be used, because both circuits are equivalent [12].

The element values of the prototypes are numbered from g_0 starting at the generator impedance to g_{N+1} ending at the load impedance, for a filter having N reactive elements [8]. These elements alternate between series and shunt connections, as seen in Figures 2.3 and 2.4. The element values of the demonstrated low pass filter prototypes are interpreted in [13] as follows:

- g_1 to g_N are the inductance of a coil connected in series or the capacitance of a shunt capacitor.
- g_0 the source resistance if g_1 is a capacitor or the source conductance if g_1 is inductor.
- g_{N+1} is the load resistance if g_N is a capacitor, but is defined as the load conductance if g_N is an inductor.

Unless otherwise specified, the g values are supposed to be the inductance in henries, the capacitance in farads, the resistance in ohms, and the conductance in Siemens [12]. The normalized element values of the low pass filter prototypes for the Chebyshev response as well as the degree of the prototype filter can be determined from equations and tables [5] and [12].

2.2.1 Equations and Tables for the Chebyshev Filter

For the Chebyshev low pass prototype filter with pass band ripple L_{Ar} dB and at $\omega_c = 1$ the element values can be computed from (2.6) [5]:

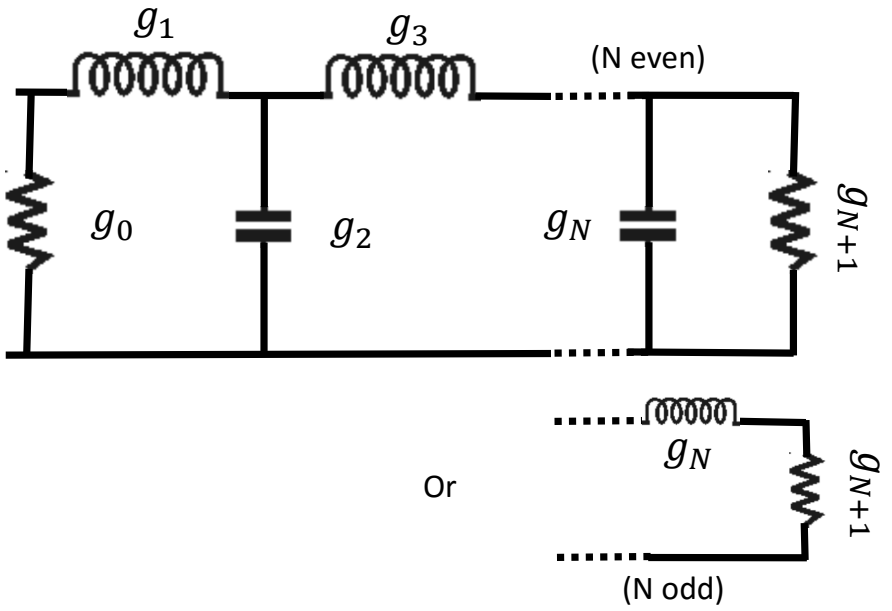

Figure 2.3: Low pass prototype beginning with a series element

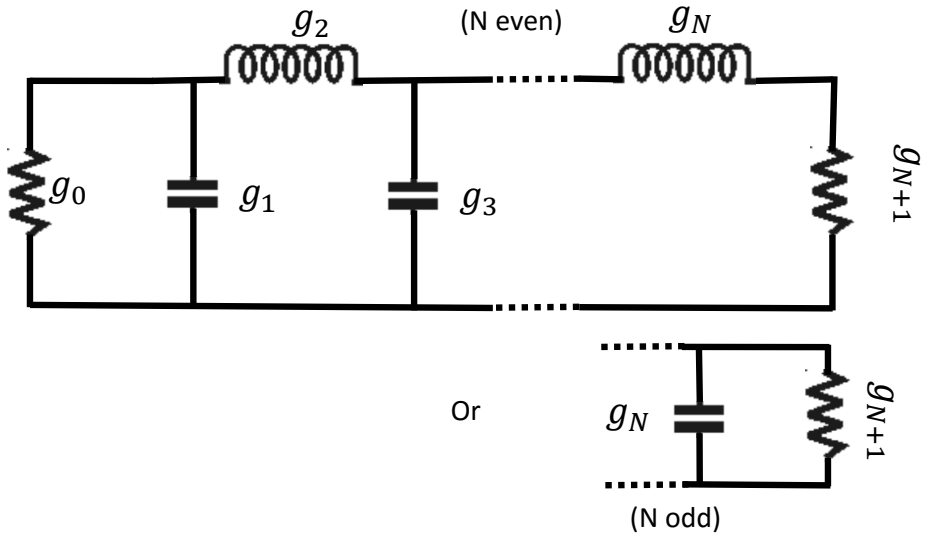

Figure 2.4: Low pass prototype beginning with a shunt element

$$
\begin{aligned}
g_0 &= 1 \\
\beta &= \ln\left(\coth\left(\frac{L_{AR}}{17.37}\right)\right) \\
\gamma &= \sinh\left(\frac{\beta}{2N}\right) \\
a_j &= \sin\left[\frac{(2j-1)\pi}{2N}\right], \qquad j = 1, 2, ..., N \\
b_j &= \gamma + \sin^2\left(\frac{j\pi}{N}\right), \qquad j = 1, 2, ..., N \\
g_1 &= \frac{2a_1}{\gamma} \\
g_j &= \frac{4a_{j-1}a_j}{b_{j-1}g_{j-1}}, \qquad j = 2, 3, ..., N \\
g_{N+1} &= \begin{cases} 1 & \text{N odd} \\ \coth^2\left(\frac{\beta}{4}\right) & \text{N even} \end{cases}
\end{aligned}
\tag{2.6}
$$

where N is the filter order and L_{Ar} is the pass band ripple level that can be calculated from the return loss. Figures 2.5 and 2.6 present tabulated results of some typical element values for the Chebyshev filter having various pass band ripples L_{Ar}, and for filters of order N = 1 to N = 10.

For a specified pass band ripple L_{Ar} dB and a minimum stop band attenuation L_{As} dB at $\omega_s = 1$ the order of the the Chebyshev low pass prototype that meets this requirement, can be found from (2.7) [12].

$$
N \geq \frac{\cosh^{-1}\sqrt{\frac{10^{0.1L_{As}}-1}{10^{0.1L_{Ar}}-1}}}{\cosh^{-1}\omega_s} \tag{2.7}
$$

Where L_{As} is the minimum stop band attenuation at $\omega = \omega_s$, and $\omega_s > 1$. The relationship

For passband ripple $L_{Ar} = 0.04321$ dB

n	g_1	g_2	g_3	g_4	g_5	g_6	g_7	g_8	g_9	g_{10}
1	0.2000	1.0								
2	0.6648	0.5445	1.2210							
3	0.8516	1.1032	0.8516	1.0						
4	0.9314	1.2920	1.5775	0.7628	1.2210					
5	0.9714	1.3721	1.8014	1.3721	0.9714	1.0				
6	0.9940	1.4131	1.8933	1.5506	1.7253	0.8141	1.2210			
7	1.0080	1.4368	1.9398	1.6220	1.9398	1.4368	1.0080	1.0		
8	1.0171	1.4518	1.9667	1.6574	2.0237	1.6107	1.7726	0.8330	1.2210	
9	1.0235	1.4619	1.9837	1.6778	2.0649	1.6778	1.9837	1.4619	1.0235	1.0

Figure 2.5: Table of element values for the Chebyshev low pass prototype filters ($g_0 = 1.0$, $\omega_c = 1$, $L_{Ar} = 0.04321$ dB at ω_c) from [12]

	0.5 dB Ripple										
N	g_1	g_2	g_3	g_4	g_5	g_6	g_7	g_8	g_9	g_{10}	g_{11}
1	0.6986	1.0000									
2	1.4029	0.7071	1.9841								
3	1.5963	1.0967	1.5963	1.0000							
4	1.6703	1.1926	2.3661	0.8419	1.9841						
5	1.7058	1.2296	2.5408	1.2296	1.7058	1.0000					
6	1.7254	1.2479	2.6064	1.3137	2.4758	0.8696	1.9841				
7	1.7372	1.2583	2.6381	1.3444	2.6381	1.2583	1.7372	1.0000			
8	1.7451	1.2647	2.6564	1.3590	2.6964	1.3389	2.5093	0.8796	1.9841		
9	1.7504	1.2690	2.6678	1.3673	2.7239	1.3673	2.6678	1.2690	1.7504	1.0000	
10	1.7543	1.2721	2.6754	1.3725	2.7392	1.3806	2.7231	1.3485	2.5239	0.8842	1.9841

Figure 2.6: Table of element values for the Chebyshev low pass prototype filters ($g_0 = 1.0$, $\omega_c = 1$, $L_{Ar} = 0.5$ dB at ω_c) from [8]

between the pass band ripple and the minimum pass band return loss is given by [12] as

$$L_{Ar} = -10\log(1 - 10^{0.1L_R}) \quad \text{dB}. \tag{2.8}$$

(2.8) is useful when the minimum return loss L_R in the pass band is specified instead of the pass band ripple L_{Ar}. For example, if a return loss of $L_R = 20$ dB is given, then $L_{Ar} = 0.04364$ dB.

2.3 Frequency and Impedance Scaling

The low pass prototype filters considered in Section 2.2, have normalised source and load resistance/conductance $g_0 = 1$[2] and a cutoff angular frequency $\omega_c = 1$. In order to obtain a filter with practical frequency characteristics and element values, based on the low pass prototype filters, one may apply frequency and impedance scaling to the normalized low pass prototype circuits [12] and [8].

The frequency transformation will only have an effect on the reactive elements of the low pass prototype. It will have no effect on the resistive elements [12]. This assumes that the resistance of the low pass prototype does not vary with frequency. The impedance scaling, which is required to shift the impedance level of the filter, will have an effect on both the reactive and resistive elements of the low pass prototype filters.

2.3.1 Impedance Scaling

A low pass prototype with a source resistance of R_0 can be obtained by simply multiplying the lumped element values of the prototype circuit by the quantity R_0. Therefore, if the impedance-scaled lumped element values are denoted by primes, the new lumped element values of the filter is given by (2.9) [8]

$$\begin{aligned} L^{'} &= R_0 L \\ C^{'} &= C/R_0 \\ R_s^{'} &= R_0 R_s \\ R_L^{'} &= R_0 R_L \end{aligned} \tag{2.9}$$

where L, C, R_s and R_L are the original component values of the low pass prototype filters.

[2] Except for Chebyshev filters with even N, which have non-unity load resistance/conductance

2.3.2 Frequency Scaling

Here the frequency transformation from the low pass prototype to the band pass prototype filter is considered. If ω_1 and ω_2 denote the lower and upper pass band edges frequencies respectively, the band pass response can then be obtained from the low pass filter by using the following frequency substitution [8]:

$$\omega = \frac{1}{\Delta}\left(\frac{\omega}{\omega_0} - \frac{\omega_0}{\omega}\right) \tag{2.10}$$

$$\Delta = \frac{\omega_2 - \omega_1}{\omega_0} \tag{2.11}$$

$$\omega_0 = \sqrt{\omega_1 \omega_2} \tag{2.12}$$

where Δ is the fractional bandwidth of the pass band. ω_0 is the centre frequency of the pass band and is calculated as the geometric mean of the band cutoff frequencies ω_1 and ω_2.

Figure 2.7 shows the transformation of the low pass prototype elements to the band pass prototype elements. Figure 2.8 shows the resulting band pass filter, after performing the low pass to band pass transformation.

2.3.3 Chebyshev Band Pass Filter

Suppose one would like to design a band pass filter with the specifications given in [8]. The band pass filter must have a 0.5 dB equal-ripple response, with N = 3. The centre frequency of the filter must be 1000 MHz, with a 10 % fractional bandwidth. Finally, the filter must have an input impedance of 50 Ω.

By inspecting these specifications, it is clear that the Chebyshev response is required, this is due to the equal-ripple requirement. Moreover, the centre frequency of the filter is at 1000 MHz, therefore, a filter transformation from the low pass to the band pass prototype is needed. Finally, the filter will have to be matched to 50 Ω at the input, implying impedance scaling. It can also be seen that since N is odd, the load impedance for the filter will also be 50 Ω. The results of the low pass element to band pass element transformation are presented in Table 2.1. The element values of the low pass prototype were obtained from Figure 2.6.

Figure 2.9 shows a 3$^{\text{rd}}$ order Chebyshev band pass prototype filter implemented in CST [7]. The

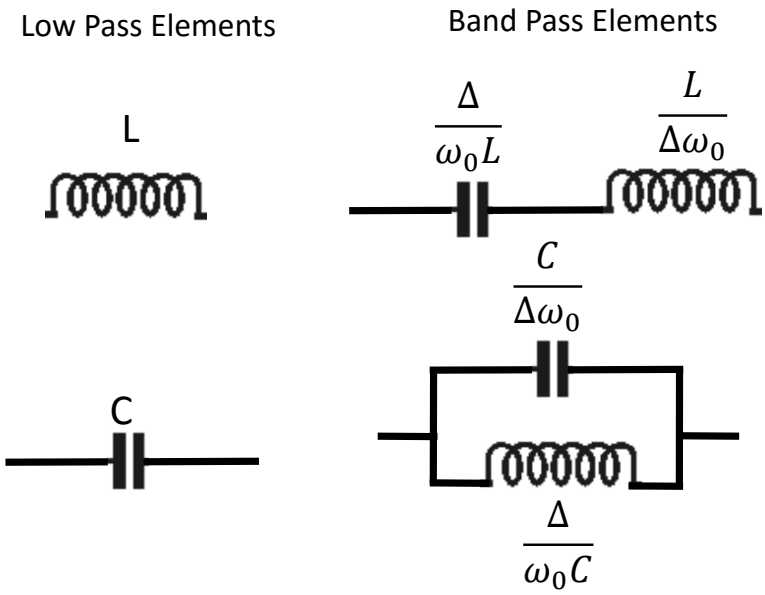

Figure 2.7: Low pass to band pass transformation circuits and equations

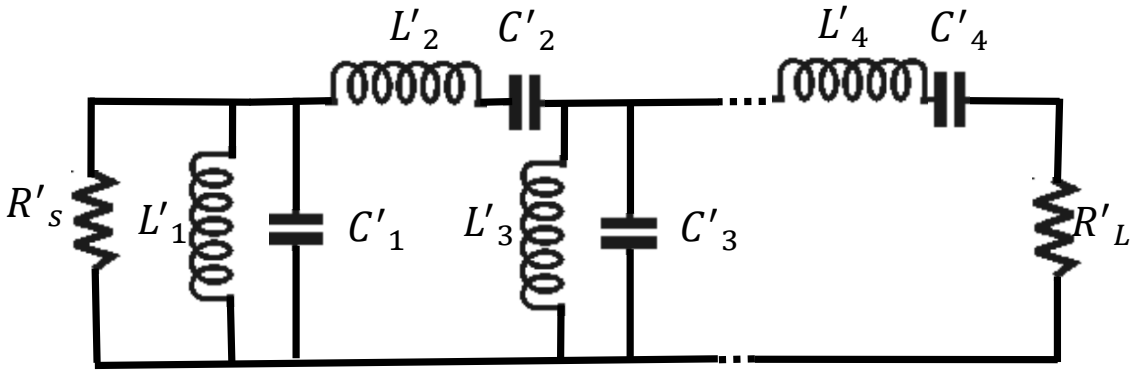

Figure 2.8: Band pass filter obtained after transforming low pass prototype

Table 2.1: Low pass element values and their band pass transformed equivalent values

Low pass element values	Band pass element values
$g_0 = 1.00 = R_s$	$R_s' = R_0 R_s = 50\ \Omega$
$g_1 = 1.5963 = L_1$	$L_1' = \frac{L_1 R_0}{\omega_0 \Delta} = 127$ nH $C_1' = \frac{\Delta}{\omega_0 L_1 R_0} = 0.199$ pH
$g_2 = 1.0967 = C_2$	$L_2' = \frac{\Delta R_0}{\omega_0 C_2} = 0.726$ nH $C_2' = \frac{C_2}{\omega_0 \Delta R_0} = 34.91$ pH
$g_3 = 1.5963 = L_3$	$L_3' = \frac{L_3 R_0}{\omega_0 \Delta} = 127$ nH $C_3' = \frac{\Delta}{\omega_0 L_3 R_0} = 0.199$ pH
$g_4 = 1.00 = R_L$	$R_L' = R_0 R_L = 50\ \Omega$

circuit has 2 series resonators and one shunt resonator and is fed with 50 Ω ports. The response of this circuit is shown in Figure 2.10. Figure 2.10 shows that, indeed, the low pass prototype has been transformed to the desired band pass filter.

2.4 Impedance and Admittance Inverters

The band pass filter in Figure 2.8 has both shunt and series elements. In practice, it is often desirable to use either a series or shunt elements to implement filters with a particular transmission line. The conversion of the band pass prototype filter in Figure 2.8 to use either series or shunt elements can be done with idealised impedance or admittance inverters, as shown in Figures 2.11 and 2.12, respectively [12], [8] and [13].

An ideal impedance inverter operates like a quarter wavelength transmission line of characteristic impedance $K_{k,k+1}$, at all frequencies. For this reason, if the output port in Figure 2.11 is terminated in an impedance Z_L, the impedance seen at the input port is given by (2.13) [13]

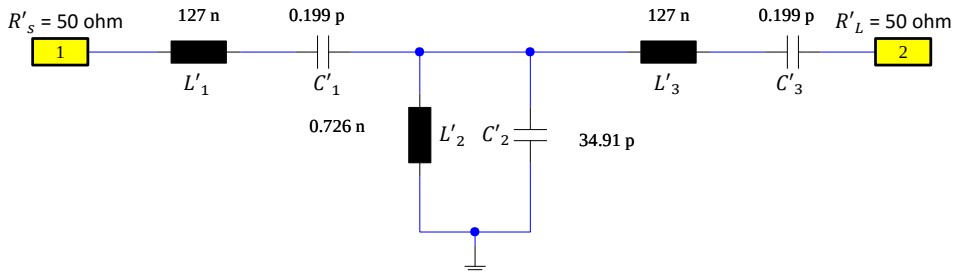

Figure 2.9: 3rd order all pole Chebyshev band pass prototype filter circuit CST [7]

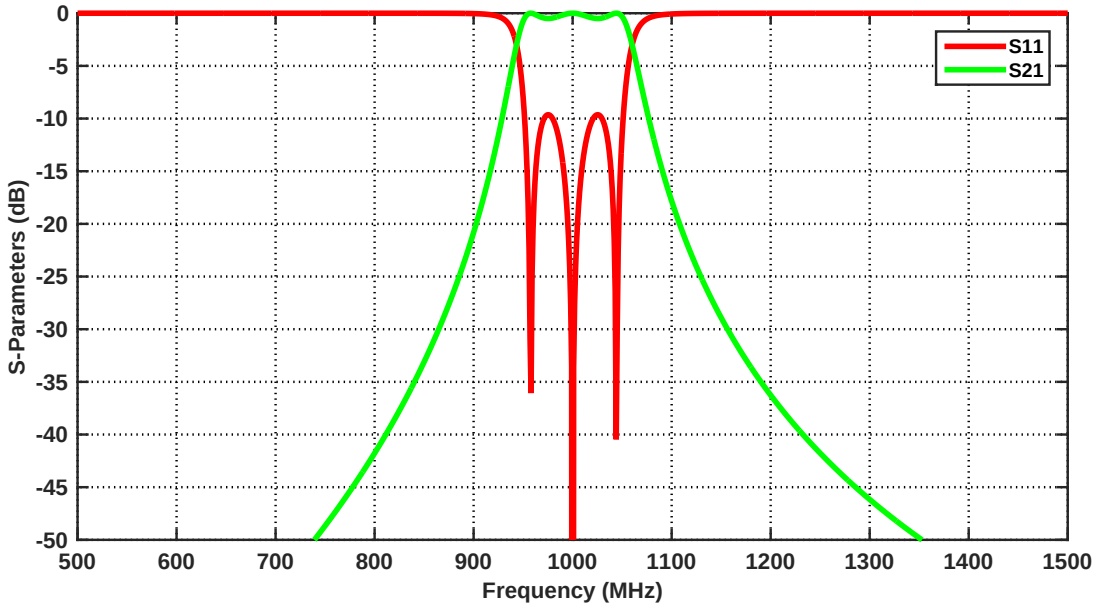

Figure 2.10: Response of the 3rd an all pole Chebyshev band pass filter (N= 3, f_0 = 1000 MHz, Δ = 10 %)

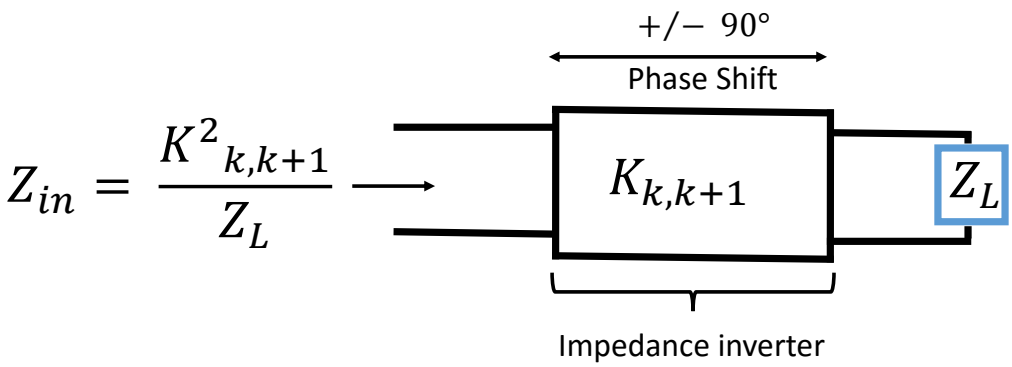

Figure 2.11: Definition of impedance inverter

$$Z_{in} = \left(\frac{1}{Z_L}\right) K^2_{k,k+1}. \tag{2.13}$$

Likewise, an ideal admittance inverter operates like a quarter wavelength transmission line, of characteristic admittance $J_{k,k+1}$, at all frequencies. For this reason, if the output port in Figure 2.11 is terminated in an admittance Y_L, the admittance seen at the input port is given by (2.14) [13]

$$Y_{in} = \left(\frac{1}{Y_L}\right) J^2_{k,k+1}. \tag{2.14}$$

Equations (2.13) and (2.14) demonstrates the two actions performed by the impedance and admittance inverters. The first term of both equations indicates the inverting action that the transmission line performs, through a phase shift of $\pm 90°$ or an odd multiple thereof. The second term indicates that the inverters have the ability to shift impedance or admittance levels, depending on the characteristic impedance or admittance of the inverters [8], [12] and [13].

2.4.1 Filters with Impedance and Admittance Inverters

Due to the inverting action of the inverters, as indicated by Equations (2.13) and (2.14) it can be shown, by means of simple matrix multiplication, that a series inductance with an inverter on each side looks like a shunt capacitance from its exterior terminals, as indicated in Figure 2.13 (a) [12]. Likewise, a shunt capacitance with an inverter on each side looks like a series inductance from its external terminals, as in Figure 2.13 (b) [12]. These properties of the inverters enable one to convert the low pass prototype circuits and hence, band pass prototype circuits, into an equivalent form that will be more convenient for implementation with microwave struc-

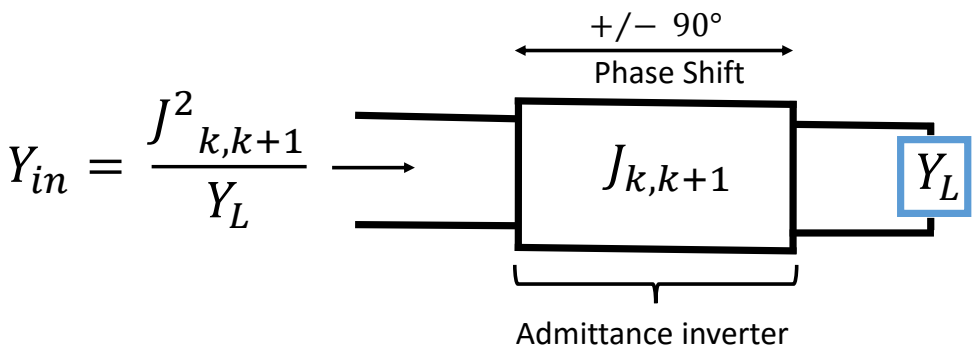

Figure 2.12: Definition of admittance inverter

tures.

Figure 2.14 illustrates two band pass filters using impedance and admittance inverters. For the case of impedance inverters, only series resonators are used, whereas in the case of admittance inverters only shunt parallel resonators are used. However, the models are equivalent.

Figure 2.14 can be made more general by replacing the lumped LC resonators by distributed circuits [12], which can be microstrip resonators, microwave cavities, or any other suitable resonator structure. For this to be done, two important parameters, namely the reactance and susceptance slope parameters, are introduced. So as to equate the reactance/ susceptance and reactance/ susceptance slopes of the distributed elements and the lumped elements near resonance. The reactance slope parameter for resonators having zero reactance at the centre frequency ω_0 is defined by (2.15) [12]

$$x = \frac{\omega_0}{2}\frac{\mathrm{d}X(\omega)}{\mathrm{d}\omega}\bigg|_{\omega=\omega_0}. \tag{2.15}$$

where $X(\omega)$ is the reactance of the distributed resonator. The susceptance slope parameter for resonators having zero susceptance at centre frequency ω_0 is defined by (2.16) [12]

$$b = \frac{\omega_0}{2}\frac{dB(\omega)}{d\omega}\bigg|_{\omega=\omega_0}. \tag{2.16}$$

where $B(\omega)$ is the susceptance of the distributed resonator. Figure 2.14 becomes more general as presented in Figure 2.15. The equations corresponding to the general model given by [12] are as follow:

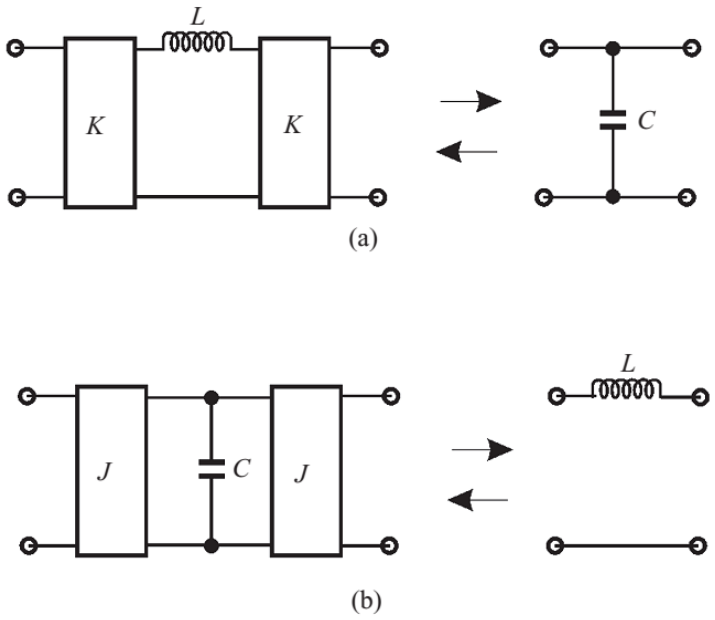

Figure 2.13: (a) K-inverter used to convert shunt capacitance into an equivalent circuit with series inductance. (b) J-inverter used to convert series inductance into an equivalent circuit with shunt capacitance from [12].

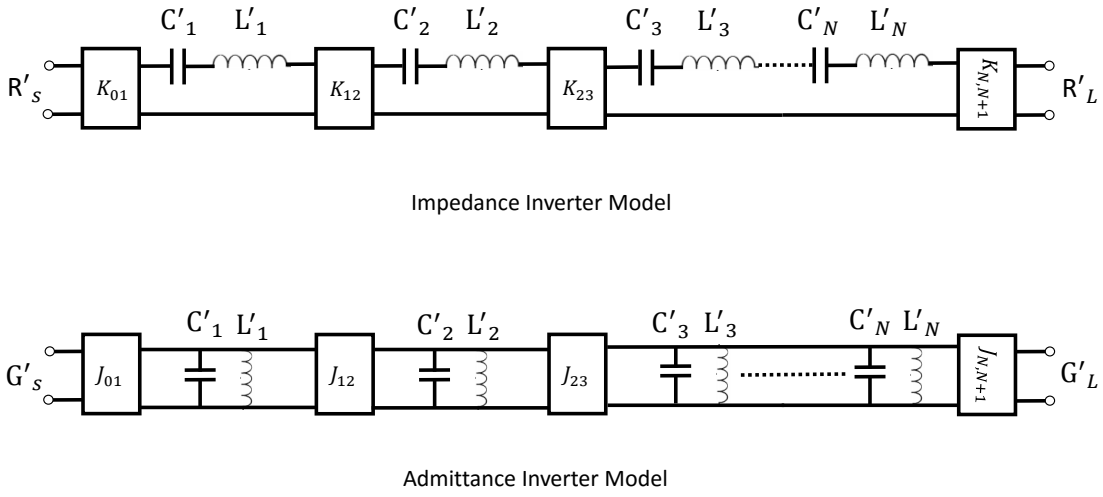

Figure 2.14: Band pass filters using impedance and admittance inverters

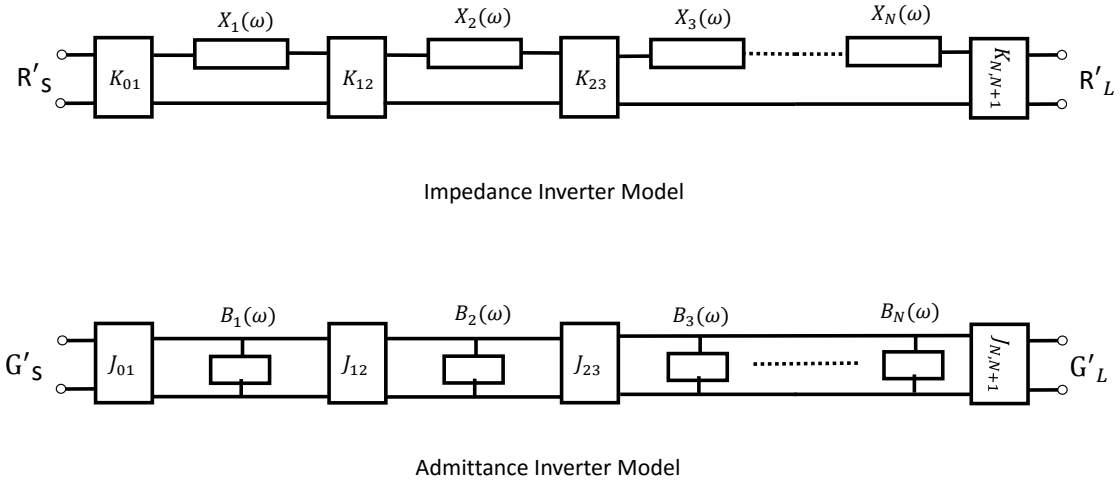

Figure 2.15: General band pass filters (including distributed elements) using impedance and admittance inverters

K-impedance inverter model equations:

$$K_{j,j+1} = \frac{\Delta}{\omega_c}\sqrt{\frac{x_j x_{j+1}}{g_j g_{j+1}}}, \qquad j = 1, 2, ..., \mathrm{N}-1$$
$$K_{0,1} = \sqrt{\frac{R'_s x_1 \Delta}{\omega_c g_0 g_1}}, \qquad K_{\mathrm{N,N+1}} = \sqrt{\frac{R'_L x_{\mathrm{N}} \Delta}{\omega_c g_{\mathrm{N}} g_{\mathrm{N+1}}}} \tag{2.17}$$

J-admittance inverter model equations:

$$J_{j,j+1} = \frac{\Delta}{\omega_c}\sqrt{\frac{b_j b_{j+1}}{g_j g_{j+1}}}, \qquad j = 1, 2, ..., \mathrm{N}-1$$
$$J_{0,1} = \sqrt{\frac{G'_s b_1 \Delta}{\omega_c g_0 g_1}}, \qquad J_{\mathrm{N,N+1}} = \sqrt{\frac{G'_L b_{\mathrm{N}} \Delta}{\omega_c g_{\mathrm{N}} g_{\mathrm{N+1}}}} \tag{2.18}$$

The parameters $g_0, g_1, g_2, ..., g_{N+1}$ in equations (2.17) and (2.18) are the elements of the low pass prototype. These values can be calculated from the equations and tables presented in

Section 2.2. Δ is the fractional bandwidth in (2.17) and (2.18).

For a dispersive medium, Δ is given by $\Delta = \frac{(\lambda_{g_1} - \lambda_{g_2})}{\lambda_{g_0}}$ [13], where λ_{g_0} is the guide wavelength at the centre frequency and λ_{g_1} and λ_{g_2} are the guide wavelengths at the band edge frequencies.

According to [13] the external quality factor Q_e and the physical coupling coefficient $\kappa_{j,j+1}$ are related to the impedance and admittance inverters and the reactance/susceptance parameters through the following equations:

Q_e and $\kappa_{j,j+1}$ using K-inverter model:

$$
\begin{aligned}
(Q_e)_s^{'} &= \frac{x_1}{K_{0,1}^2/R_s'} = \frac{\omega_c g_0 g_1}{\Delta}, \qquad (Q_e)_L^{'} = \frac{x_{\mathrm{N}}}{K_{\mathrm{N,N+1}}^2/R_L'} = \frac{\omega_c g_{\mathrm{N}} g_{\mathrm{N+1}}}{\Delta} \\
\kappa_{j,j+1} &= \frac{K_{j,j+1}}{\sqrt{x_j x_{j+1}}} = \frac{\Delta}{\omega_c \sqrt{g_j g_{j+1}}}, \qquad j = 1, 2, ..., \mathrm{N}-1
\end{aligned}
\tag{2.19}
$$

Q_e and $\kappa_{j,j+1}$ using J-inverter model:

$$
\begin{aligned}
(Q_e)_s^{'} &= \frac{b_1}{J_{0,1}^2/G_s'} = \frac{\omega_c g_0 g_1}{\Delta}, \qquad (Q_e)_L^{'} = \frac{b_{\mathrm{N}}}{J_{\mathrm{N,N+1}}^2/G_L'} = \frac{\omega_c g_{\mathrm{N}} g_{\mathrm{N+1}}}{\Delta} \\
\kappa_{j,j+1} &= \frac{J_{j,j+1}}{\sqrt{b_j b_{j+1}}} = \frac{\Delta}{\omega_c \sqrt{g_j g_{j+1}}}, \qquad j = 1, 2, ..., \mathrm{N}-1
\end{aligned}
\tag{2.20}
$$

2.4.2 Practical Realization of Impedance and Admittance Inverters

These inverters can be realized using any of the lumped element circuits. Such as those shown in Figure 2.16, which presents lumped element circuits and the relationship between the elements of the circuit and the impedance and admittance inverters.

These inverters are practically realized with irises, posts, stubs, and vias. Figure 2.17 shows different kinds of discontinuities used to realize the impedance/admittance inverters.

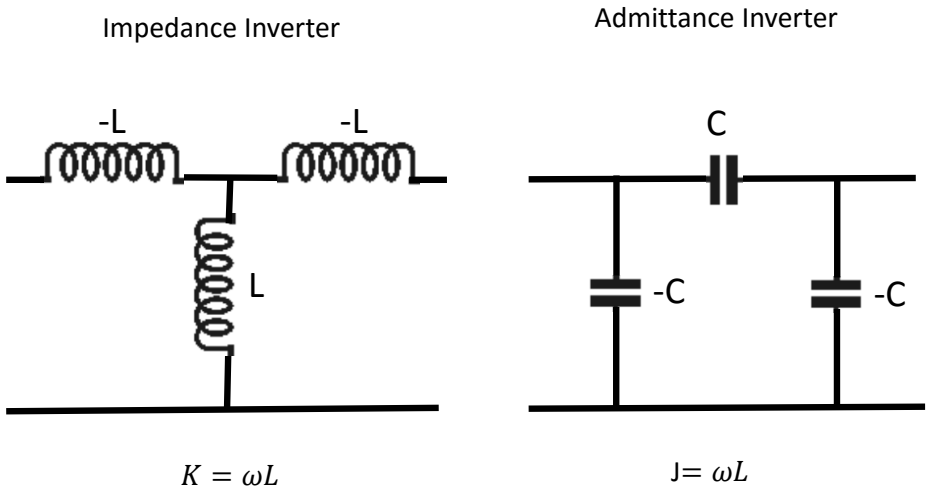

Figure 2.16: Lumped element circuit representation of impedance/admittance inverters

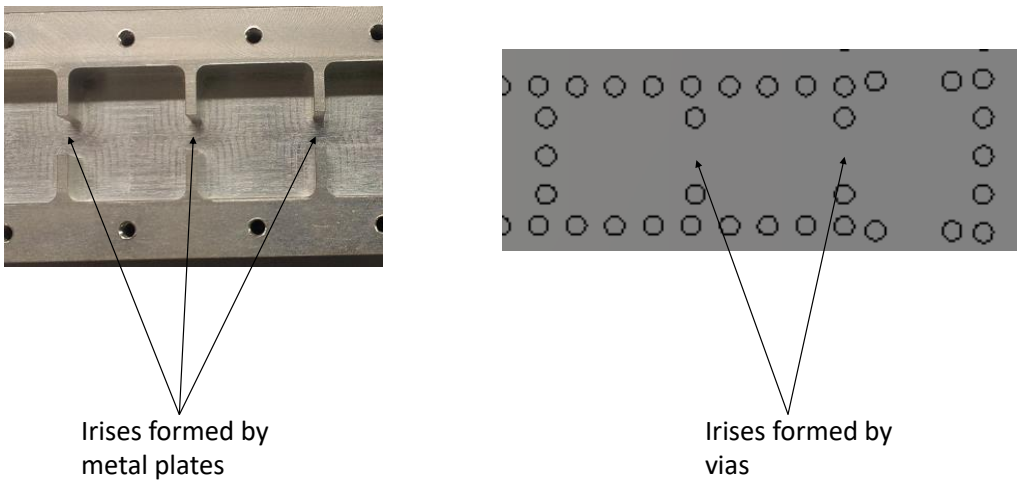

Figure 2.17: Metal plate irises and via irises used to realise practical impedance inverters

2.5 Design and Physical Realisation of Coupled-Resonator Filters

Coupled-resonator filters, in particular, narrow-band band pass filters, play a significant role in many RF/microwave applications [12]. Coupled-resonator filters are a class of filter, which contain a set of resonators inter-coupled by means of coupling structures. Iris, post and via structure are some examples of such coupling structures. Figure 2.18 to 2.20 shows some examples of coupled resonator filters.

Figure 2.18 shows a 1^{st} order multiband (3 bands) Substrate Integrated Waveguide (SIW) filter (designed by the author for another project). The coupling between the resonators is achieved through vias. The vias also couple the input/output resonators to the feed. An interdigital filter (designed by Reutech Radar Systems) is presented in Figure 2.19. For this filter, the interresonator coupling is achieved without any coupling structure in between the resonators. The magnitude of the coupling is controlled by the distance between the resonator rods inside the cavity. Figure 2.20 shows a waveguide filter, where the resonators are inter-coupled by irises or inductive windows. The irises are also used to couple the input/output resonators to the feed. Figure 2.21 shows the relationship between the components of the J-admittance circuit models and the components of a practical filter.

There exists a general technique for designing coupled-resonator filters, which can be applied to any type of resonator despite its physical structure [12]. This technique has been applied to the design of many filters, such as a waveguide, microstrip and dielectric resonator filters [5]. This design method is based on the coupling coefficients of inter-coupled resonators and the external quality factors of the input/output resonators [12].

2.5.1 Microwave Resonators

Resonators are the basic building blocks for any coupled-resonator filter. A resonator is capable of storing both frequency-dependent magnetic and electric energy. When the energy stored in the electric field equals the energy stored in the magnetic field, the resonator is said to resonate. The frequency at which this happens is termed the resonant frequency. Microwave resonators take on various shapes and forms, which affects the field distributions and hence the stored energy of the resonators. Therefore, the resonant frequency of a microwave resonator is determined by the structure's physical characteristics and dimensions [5].

Microwave resonators may be grouped into three categories: lumped element inductor and capacitor (LC) resonators, planar resonators, and three-dimensional (3D) cavity-type resonators[5]. These resonator types are shown in Figure 2.22.

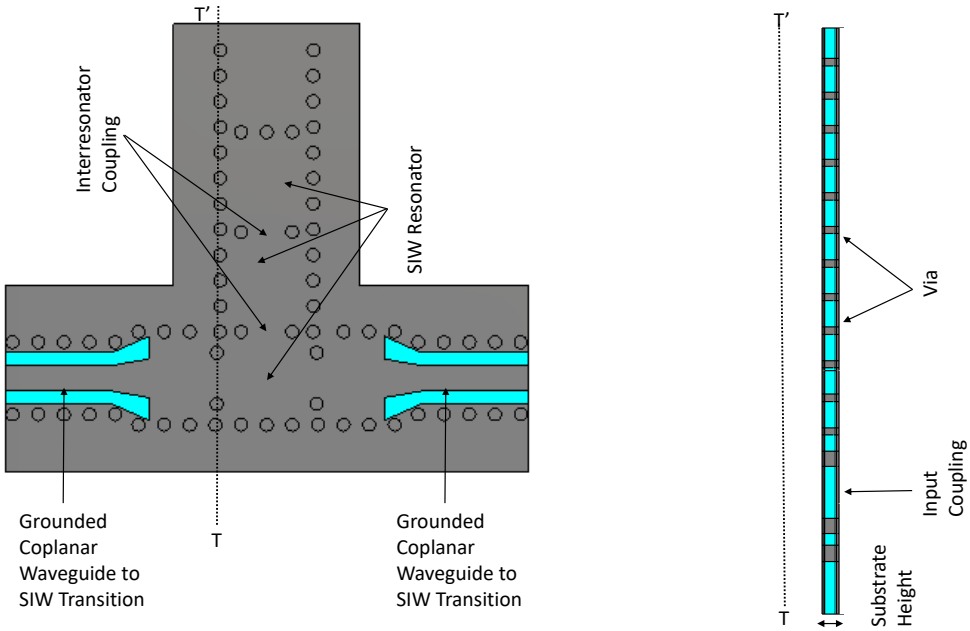

Figure 2.18: V-band (designed by the author) 1^{st} order 3 bands via coupled Chebyshev SIW filter CST [7]

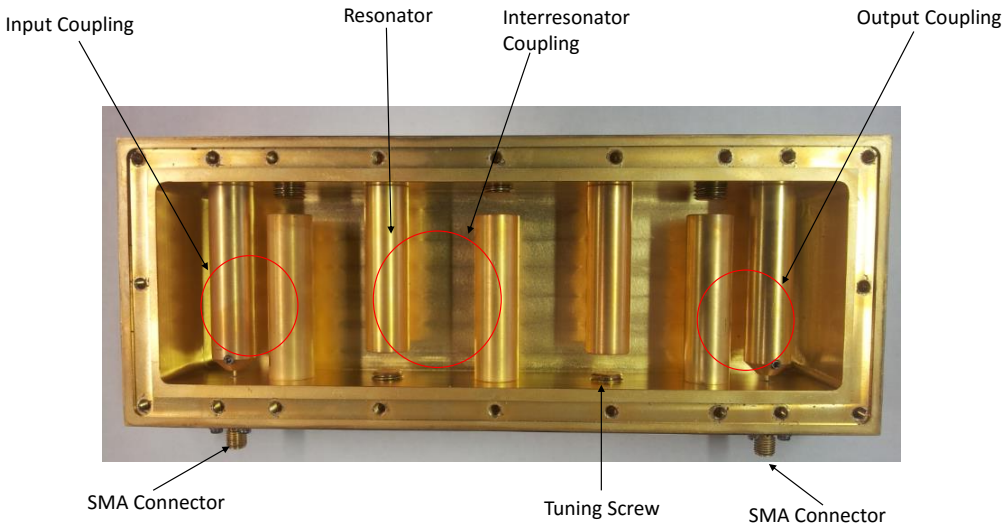

Figure 2.19: L-band interdigital filter from Reutech Radar Systems

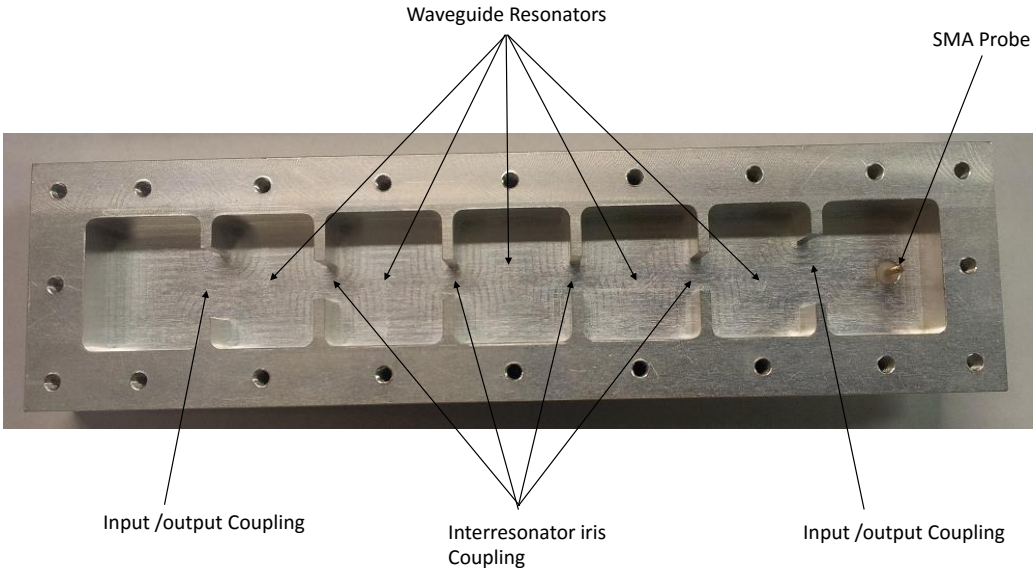

Figure 2.20: X-band inductive iris coupled waveguide filter

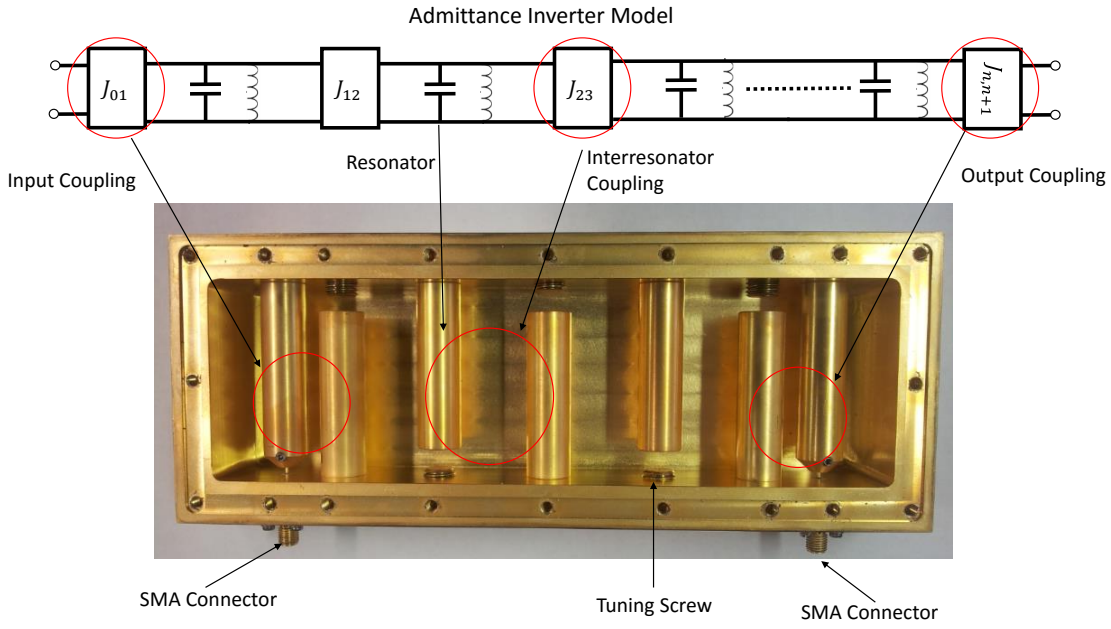

Figure 2.21: J-impedance circuit model related to a practical filter

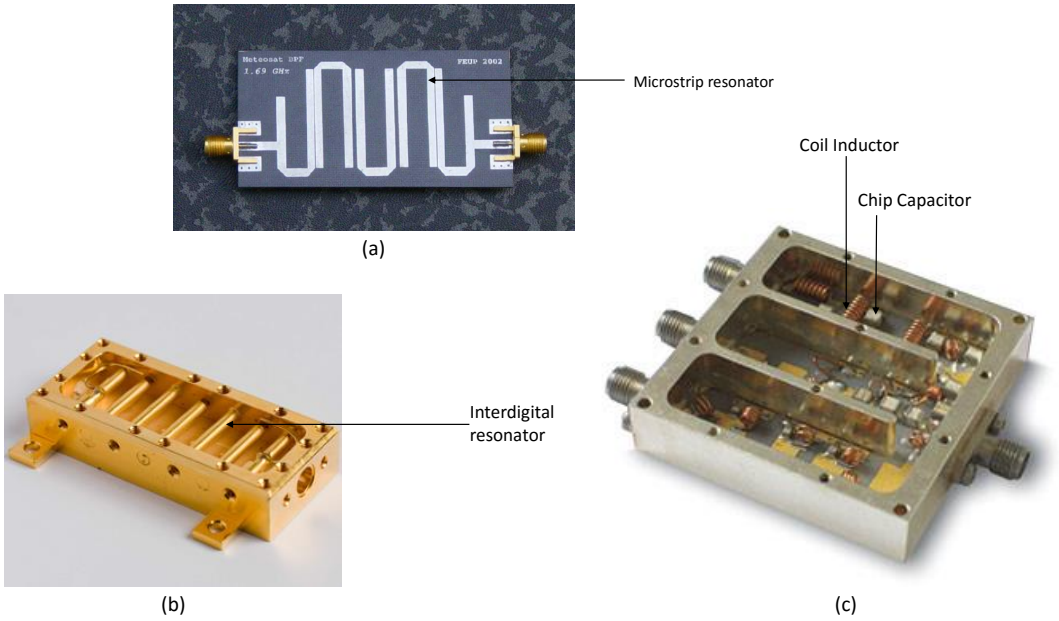

Figure 2.22: (a) Planar resonator from [14], (b) Cavity resonator from [15], (c) Lumped-element resonator from [16]

The main design considerations for microwave resonators are its size, unloaded quality factor (Q_u), spurious performance, and power handling capability [5]. Microwave resonators are scaled as a multiple or fraction of a wavelength. The resonant frequency of the resonator is determined by its size. The Q_u represents the losses in the resonators. The lower the Q_u value, the lossier the resonator is. Therefore, when low insertion loss and flat pass band are desired, resonators with high Q_u values must be used [5].

Unlike LC resonators, that theoretically have only a single resonant frequency, microwave resonators can support an infinite number of resonant modes (electromagnetic field configurations) [5]. This property of microwave resonators introduces the problem of spurious modes. The spurious performance of a resonator is evaluated based on how close the undesired modes are to the desired mode. The undesired modes act as spurious modes and hence interfere with the performance of the filter. Therefore, in order to improve the filter out of band rejection performance, one needs to have a reasonable separation or spurious-free window between the desired and undesired modes [5].

The resonant frequency of an arbitrarily shaped resonator can be determined by using an EM simulation tool. This is achieved by making use of an eigenmode or S-parameter analysis tools in an EM simulator. Both the fundamental and higher order resonant modes can be calculated by these techniques. Several EM packages such as CST and high frequency system simulator (HFSS) have eigenmode capabilities to analyze any microwave resonator and to provide

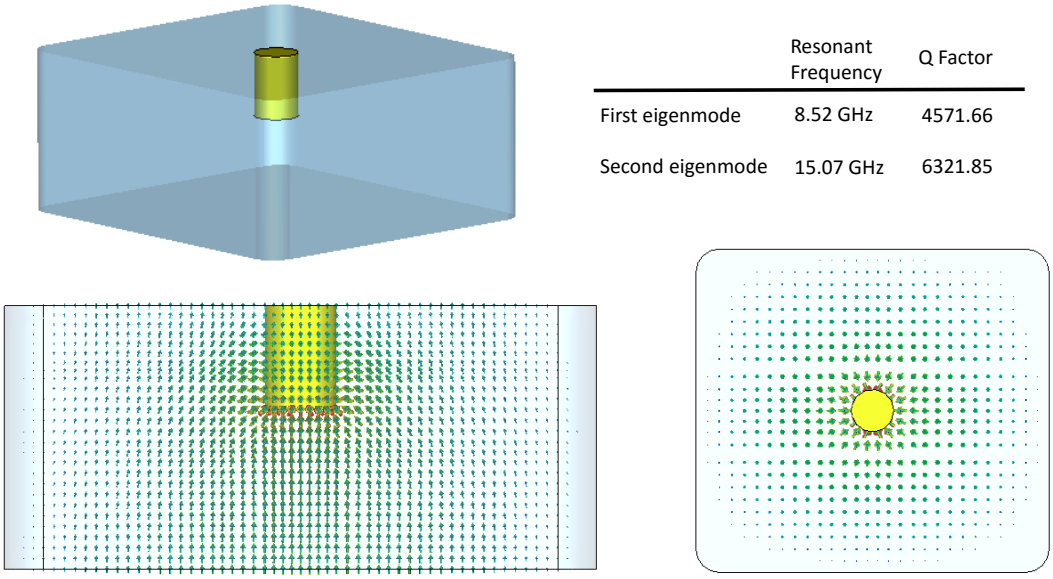

Figure 2.23: The field distribution of the first eigenmode solution for a X-band waveguide resonator CST [7]

information on its resonant frequency, unloaded Q_u factor and field distribution.

Figure 2.23 shows the eigenmode solution for a 27.57 mm long X-band waveguide resonator analyzed in CST [7]. In Figure 2.23 the first two resonant frequencies, the unloaded Q and the field distribution of the first $\mathrm{TE}_{1,0}$ mode are shown. The results show that the resonant frequency of the fundamental mode is 8.52 GHz, whereas that of the second mode is 15.07 GHz; thus, the resonator has a spurious-free window of 6.55 GHz.

An alternative to the eigenmode analysis is the S-Parameter analysis. This method is useful in the case where the available EM-software tool has no eigenmode analysis tool but has the capability to calculate the S-parameters. Figure 2.24 and 2.25 shows an example of a weakly coupled one port and two port S-parameter analysis for a 2.34 mm V-band SIW resonator, as calculated by CST [7]. The return loss of the single port analysis in Figure 2.24 shows that the resonator is lossy and it resonates at 54.22 GHz. While the transmission coefficient of the double port analysis in Figure 2.25 shows that the resonator resonates at 53.63 GHz.

2.5.2 **Interresonator Coupling**

It is well known that a single resonator is not sufficient to yield steep pass band skirts in coupled-resonator filters. This statement can be shown to be true, by using the example Chebyshev band pass filter circuit of Figure 2.9, with the response shown in Figure 2.10. Figure 2.9 was divided

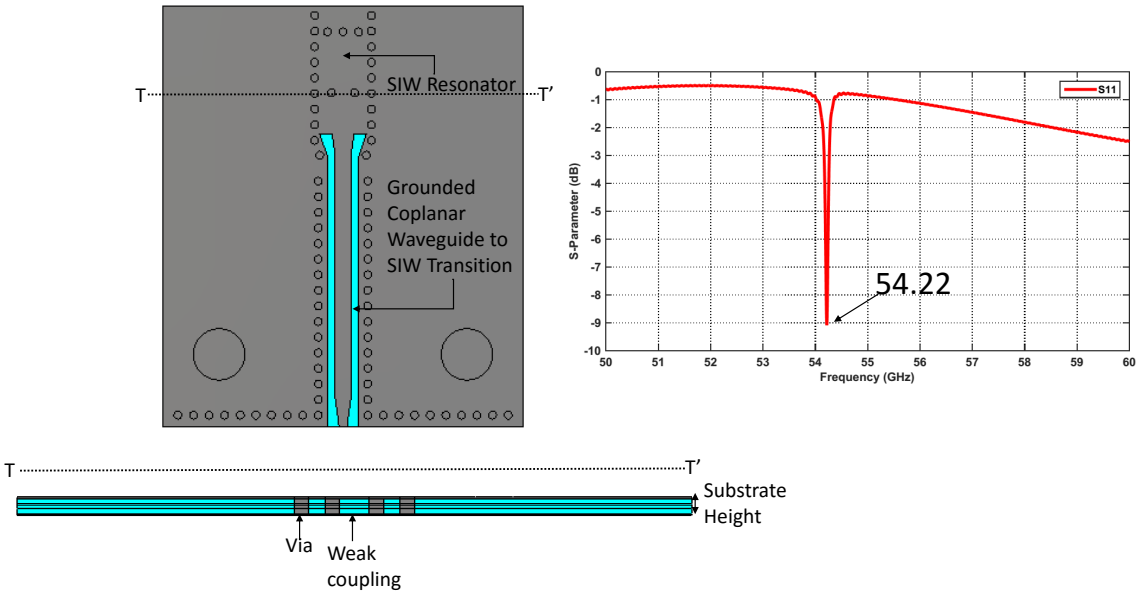

Figure 2.24: One port S-parameter analysis of the V-band SIW resonator (designed by the author) CST [7]

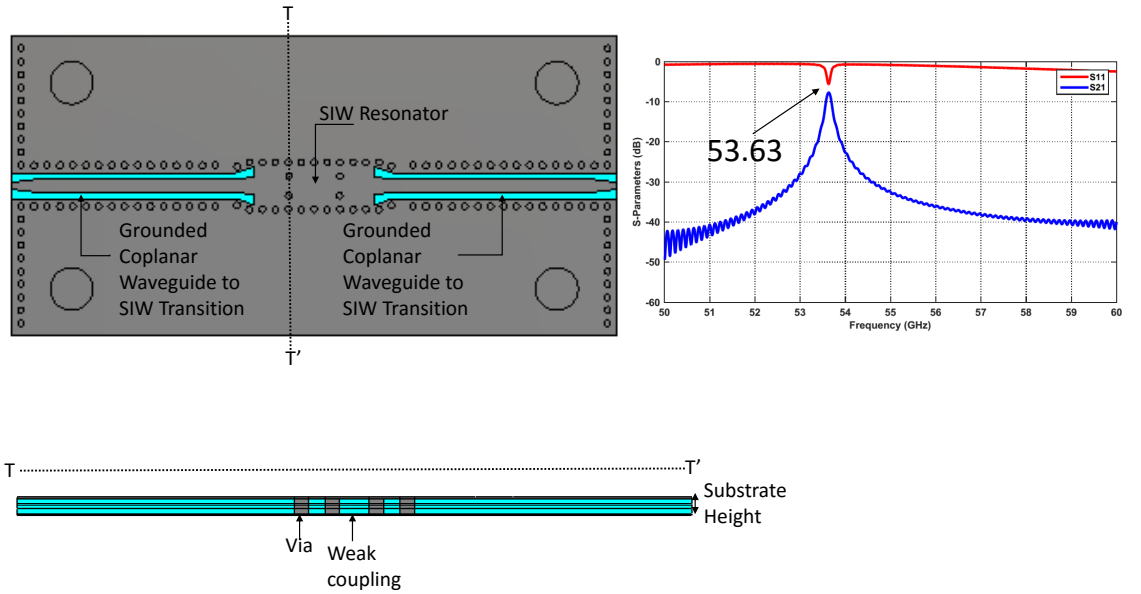

Figure 2.25: Two port S-parameter analysis of the V-band SIW resonator (designed by the author) CST [7]

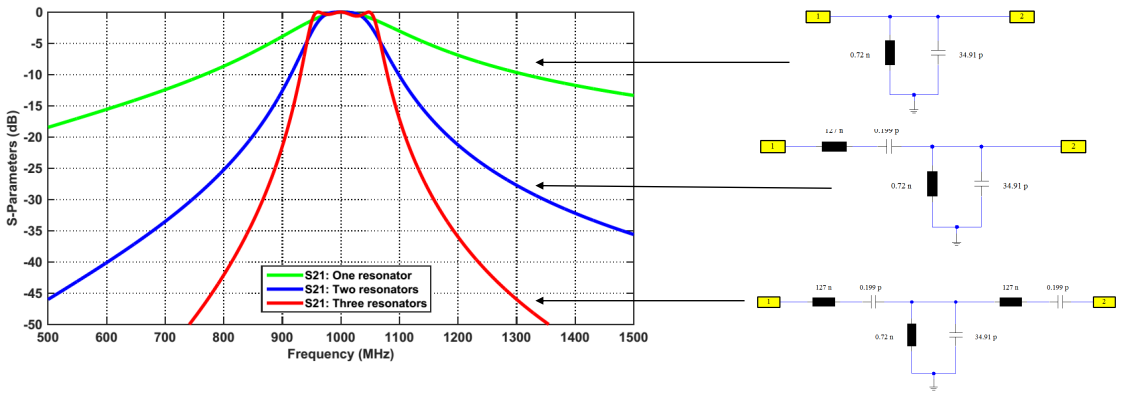

Figure 2.26: Pass band skirts for: Single, double and triple resonator configuration CST [7]

into three parts. The parts were made up of a single, double and triple resonators. Figure 2.26 shows the transmission response of each of the parts. It is clear from Figure 2.26 that the triple resonator configuration has the steepest skirts, followed by the double configuration, and lastly the single configuration. In situations where one would like to achieve more attenuation at certain frequencies outside the pass band, non-adjacent resonators must be coupled together.

In coupled-resonator filters, the most common forms of coupling are capacitive and inductive. This section will discuss the formulation of the coupling coefficient and methods to relate the coupling coefficient to the physical parameters of a practical filter through the eigenmode frequencies of the resonators. The discussion is limited to synchronously tuned coupled-resonators.

An equivalent circuit of two resonators separated by inductive coupling is shown in Figure 2.27. The coupling element is represented by a K-impedance inverter consisting of a shunt inductance L_m and two series inductances $-L_m$. The concept of symmetry is then used to divide the problem into single resonators terminated by magnetic and electric walls as indicated in Figure 2.27. From these circuits, the coupling coefficient can be computed by evaluating the resonant frequencies of the even (magnetic wall) and odd (electric wall) modes. By inspecting Figure 2.27 the resonant frequencies f_m (even mode) and f_e (odd mode) of the two circuits can be written as follows [5]:

$$f_m = \frac{1}{2\pi\sqrt{(L+L_m)C}} \tag{2.21}$$

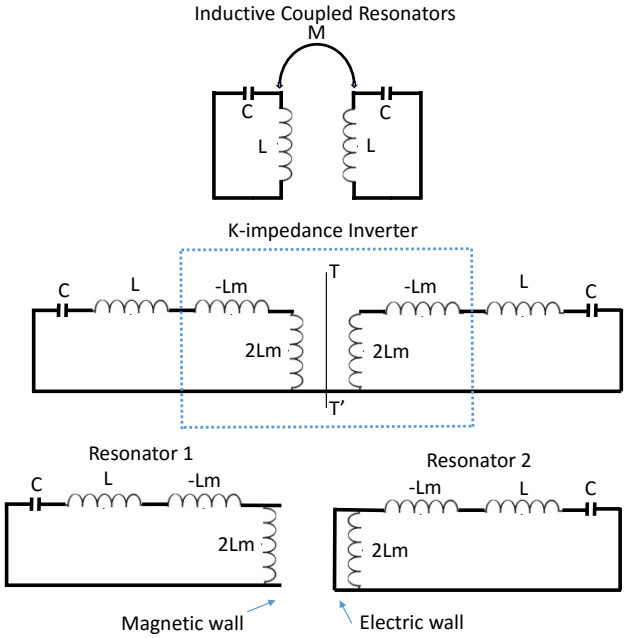

Figure 2.27: Impedance inverter equivalent circuit of two resonators separated by inductive coupling

$$f_e = \frac{1}{2\pi\sqrt{(L - L_m)C}}. \tag{2.22}$$

Solving equations (2.21) and (2.22) gives the inductive coupling coefficient κ_M between the two resonators as [5]:

$$\kappa_M = \frac{f_e^2 - f_m^2}{f_e^2 + f_m^2}. \tag{2.23}$$

A similar argument can be followed for a case where capacitive coupling is used instead of inductive coupling. The equivalent circuit is represented in Figure 2.28. Unlike the case for the inductive coupling, here the coupling is represented by a J-admittance inverter. After using symmetry to divide the circuit into two, the resonant frequencies f_m (even mode) and f_e (odd mode) of the two circuits in Figure 2.28 are given as follows [5]:

$$f_m = \frac{1}{2\pi\sqrt{(C - C_m)L}} \tag{2.24}$$

$$f_e = \frac{1}{2\pi\sqrt{(C + C_m)L}}. \tag{2.25}$$

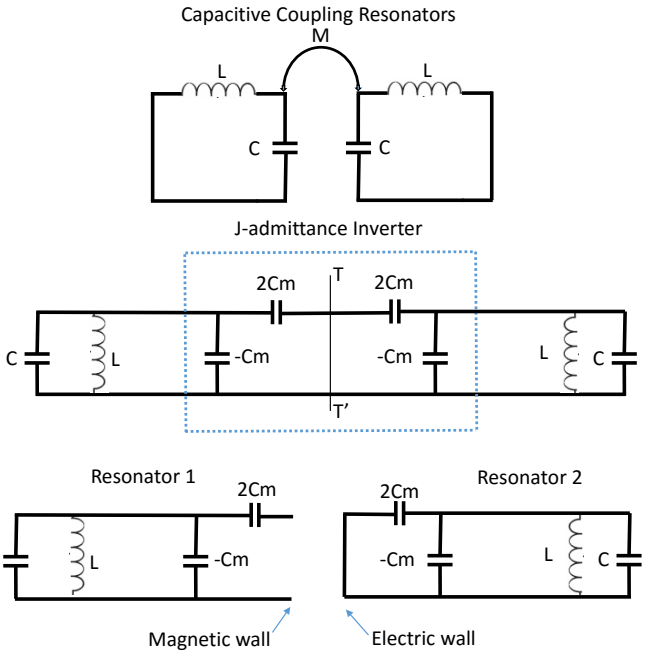

Figure 2.28: Impedance inverter equivalent circuit of two resonators separated by capacitive coupling

Solving equations (2.24) and (2.25) gives the capacitive coupling coefficient κ_E between the two resonators as [5]:

$$\kappa_E = \frac{f_m^2 - f_e^2}{f_m^2 + f_e^2}. \tag{2.26}$$

In general, for inductive coupling $f_e > f_m$, and for capacitive coupling $f_m > f_e$. These inequalities can be used to determine the nature of the coupling, but only the magnitude of the coupling is required to calculate the physical dimensions of the coupling devices [5]. By using an EM simulator such as CST [7] with eigenmode and S-parameter calculation capabilities, one can determine the odd and even mode frequencies f_e and f_m respectively. Figure 2.29 shows the magnetic and electric field intensity patterns of the even and odd mode frequencies for a pair of inductively coupled waveguide resonators.

The actual values of the even and odd mode frequencies f_m and f_e respectively was calculated using CST [7] eigenmode and S-parameter solvers. Figures 2.30 shows a table containing the even and odd mode frequencies as a function of the coupling aperture width for two inductively coupled X-band waveguide resonators obtained using the eigenmode solver in CST [7].

Another way to determine the values of the even and odd mode frequencies is to weakly couple a pair of resonators in a one or two port configuration and compute its return loss or transmis-

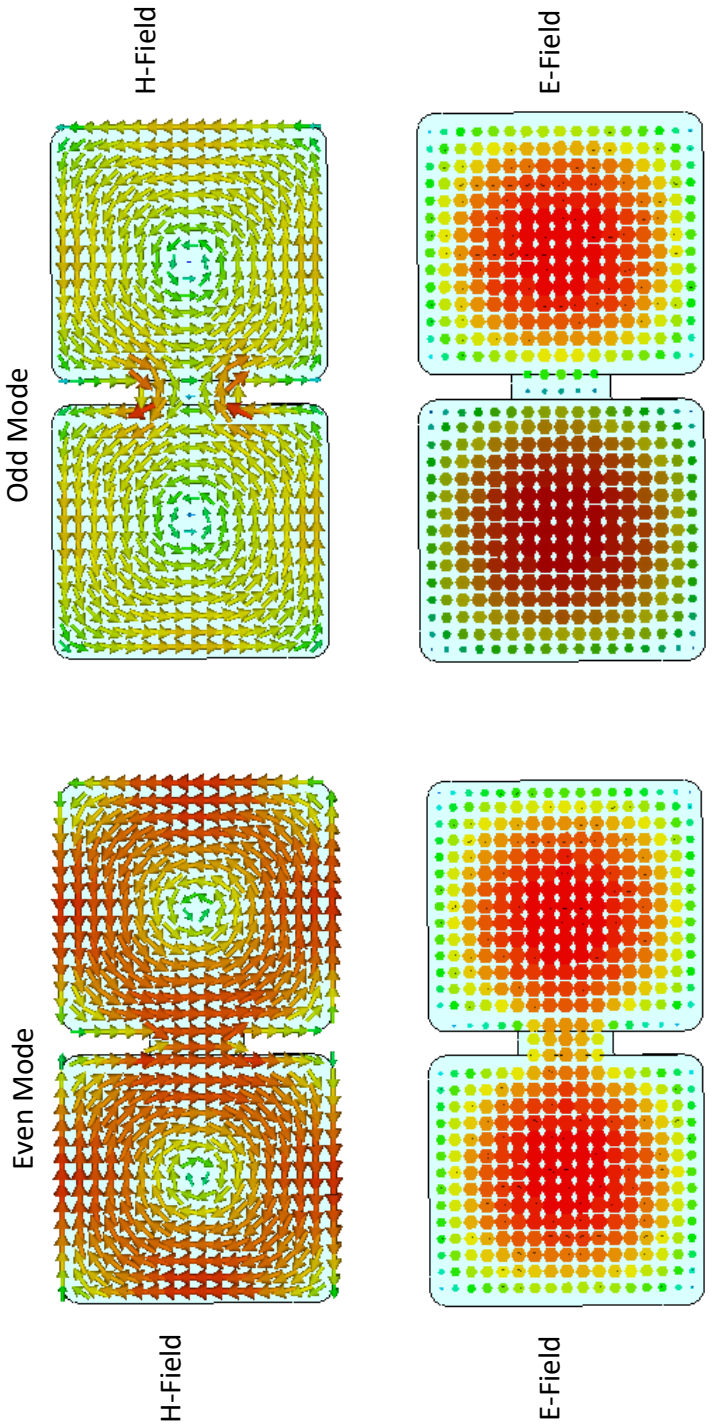

Figure 2.29: The magnetic and electric field intensity patterns of the even and odd modes frequencies for a pair of inductively coupled waveguide resonators

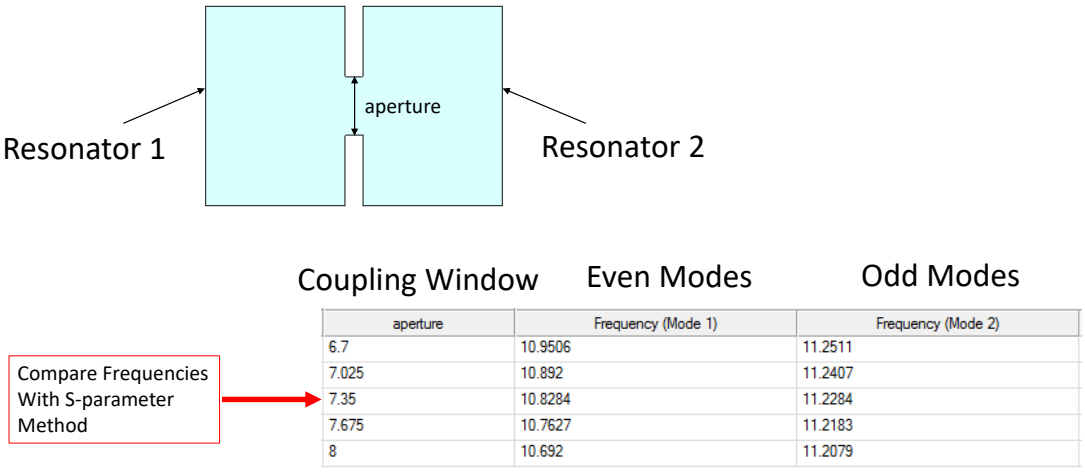

aperture	Frequency (Mode 1)	Frequency (Mode 2)
6.7	10.9506	11.2511
7.025	10.892	11.2407
7.35	10.8284	11.2284
7.675	10.7627	11.2183
8	10.692	11.2079

Figure 2.30: Even and odd mode frequencies of eigenmode analysis CST [7]

sion profile. Figure 2.31 shows the transmission coefficient of a pair of weakly fed, X-band waveguide resonators as a function of the aperture width. The peaks of the transmission coefficient profiles correspond to the even and odd mode frequencies, as clearly indicated in Figure 2.31.

The coupling coefficient κ was then extracted from these frequencies. Figure 2.32 shows the coupling coefficient obtained from the eigenmode and S-parameter method. The results show that the profiles of both methods are well matched, however, it also indicates that the profile of the S-parameter method is 2.8 % higher on average in comparison to the eigenmode method for this case. This error is not critical, as it might only affect the initial filter solution and hence, the optimization time depending on the model used to obtain the coupling coefficient. If the required coupling is known, the corresponding aperture width can be found in Figure 2.32.

2.5.3 Input/Output Coupling

Microwave filters are not used in isolation. The filter has to interface with other microwave components, so the input/output resonators of the filter must be fed somehow. Figure 2.33 shows a model for the first resonator when coupled to the input/output Norton equivalent feed source. L and C represent the inductance and capacitance of the resonator model. For narrow bandwidth, it can be shown that the reflection coefficient looking into the resonator at the reference plane T is given approximated as [5]

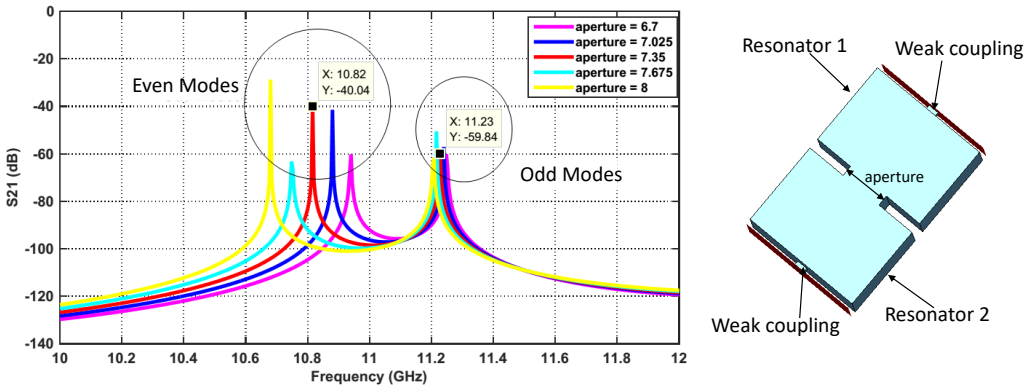

Figure 2.31: Even and odd mode frequencies of S-parameter analysis CST [7]

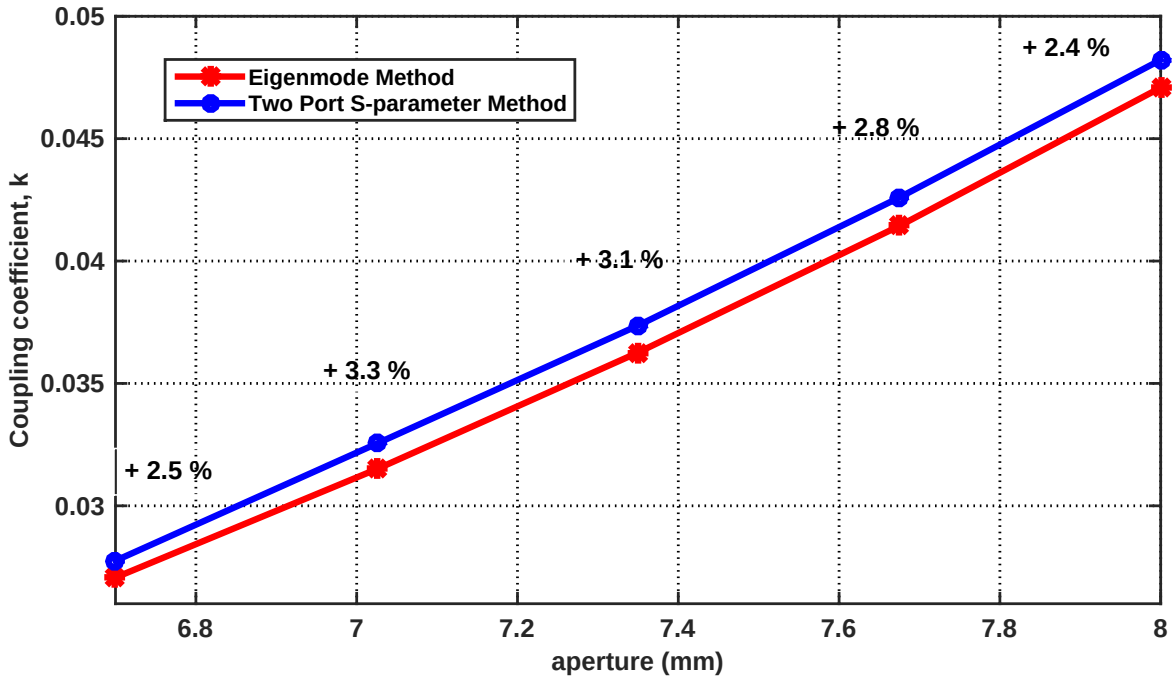

Figure 2.32: Comparison of coupling coefficient obtained from S-parameter and eigenmode analysis

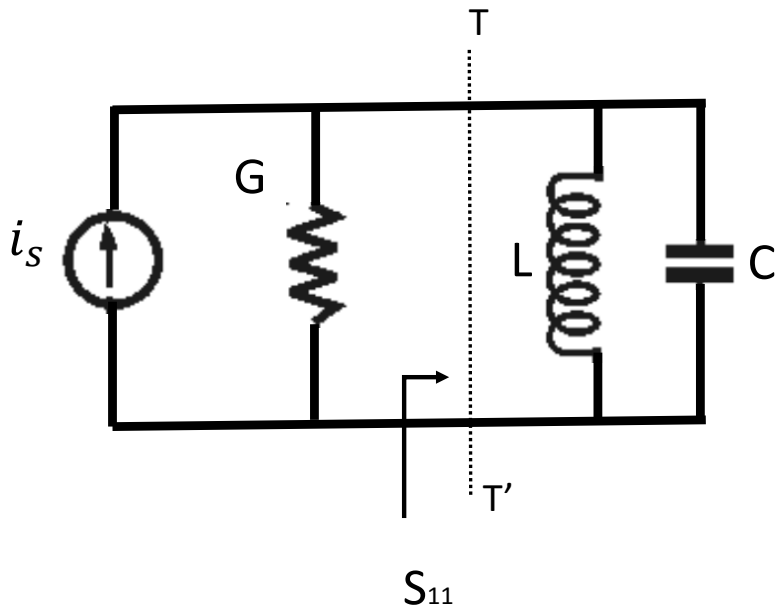

Figure 2.33: Equivalent circuit of the input/output coupling and the first resonator

$$S_{11} = \frac{1 - jQ_e\left(\frac{2\Delta\omega}{\omega_0}\right)}{1 + jQ_e\left(\frac{2\Delta\omega}{\omega_0}\right)}, \tag{2.27}$$

where Q_e is the external quality factor, ω_0 is the angular resonant frequency and $\Delta\omega$ is a small frequency shift near the resonant frequency.

The importance of (2.27) is that the external quality factor can be related to a practical filter through the phase of the reflection coefficient. This can be done either through the frequency domain method or the group delay method.

Using the frequency domain method, when the frequency offset from resonance is $\Delta\omega_{\mp} = \mp\omega_0/2Q_e$, the phase of S_{11} is $\pm 90°$. Thus it can be shown that the external quality factor is related to the $\pm 90°$ and expressed as [5]

$$Q_e = \frac{\omega_0}{\Delta\omega_{\pm 90}}. \tag{2.28}$$

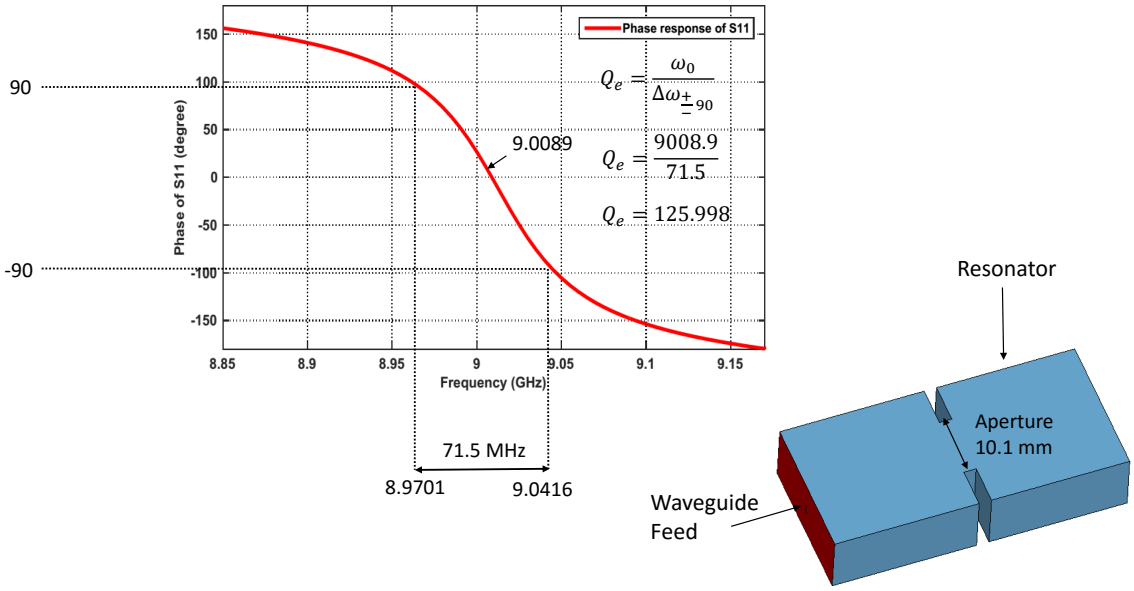

Figure 2.34: External quality factor obtained from the phase of the reflection coefficient

Using the group delay method the maximum group delay at resonance can be expressed as [5]

$$\tau_{(\omega_0)} = \frac{4Q_e}{\omega_0}. \tag{2.29}$$

From 2.29, the external quality factor can be expressed as [5]

$$Q_e = \frac{\tau_{(\omega_0)}\omega_0}{4}. \tag{2.30}$$

The Q_e was calculated using both the frequency domain and group delay methods as shown in Figure 2.34 and 2.35. Using CST [7], a model of a waveguide fed X-band waveguide resonator was built as seen on the bottom right of Figure 2.34 and 2.35. The aperture width between the feed and resonator waveguides is the physical parameter of interest, and this width can be swept to get a curve of the Q_e versus the aperture width. The aperture width of Figure 2.34 and 2.35 is kept constant at an arbitrary value of 10.1 mm for the sake of showing how to extract the Q_e from frequency domain and group delay methods. Figure 2.34 and 2.35 indicates that the Q_e of the frequency domain method is 1.56 % greater than that of the group delay method. Here again, this error may not be that significant, as it may only affect the initial solution and optimization time of the complete filter.

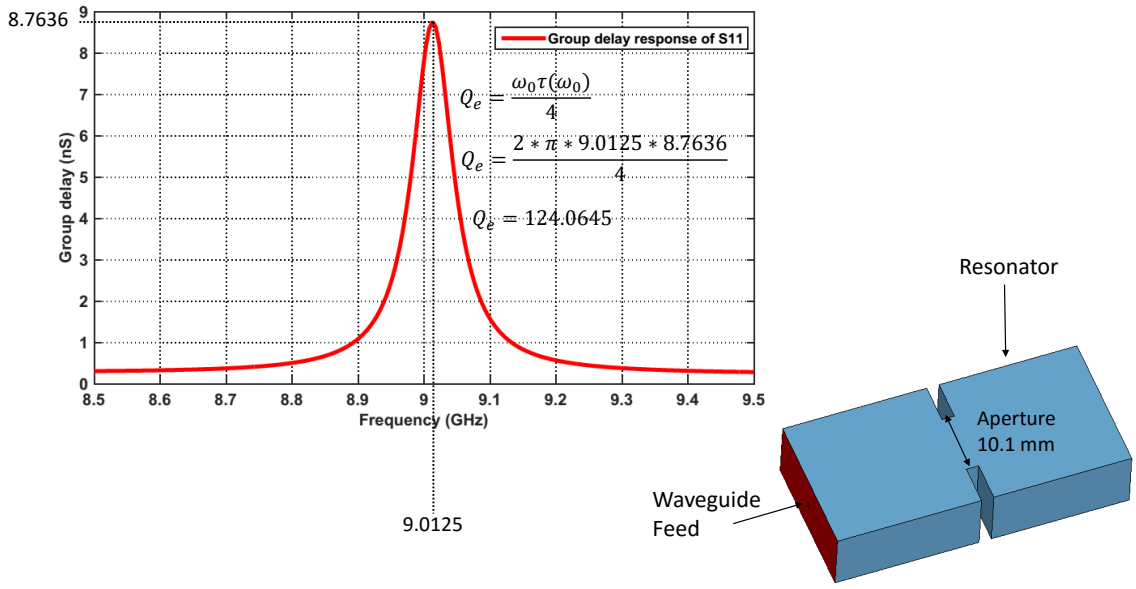

Figure 2.35: External quality factor obtained from the group delay of the reflection coefficient

2.6 CONCLUSION

The aim of this chapter was to present the impedance/admittance inverter models for the band pass filter and to demonstrate the concept of using these models and an EM simulator to synthesize the physical dimensions of a coupled-resonator filter. A general band pass filter models (including distributed elements) using impedance/admittance inverters was presented in Section 2.4. The element values of these models can be calculated by the equations presented in Section 2.2 and Section 2.4. The relationship between the impedance/admittance inverters and the coupling coefficient and external quality factors were also shown in Section 2.4. The chapter is concluded in Section 2.5, by showing how the external quality factor and the coupling coefficients can be used to synthesize the physical dimensions of a coupled resonator filter.

CHAPTER 3

L-BAND COAXIAL COMB-LINE FILTER DESIGN

3.1 INTRODUCTION

The comb-line band pass filter is widely used in many communication systems [17]. It can be designed to be compact, to have a relatively low loss, to have a good spurious performance and to have bandwidths up to 15 % or more of its centre frequency [17], [18], [4] and [19]. This chapter deals with the design, fabrication, and measurement of a coaxial comb-line band pass filter.

Section 3.2 discusses the estimation of the required order of the comb-line filter, which will satisfy the specifications of NeXtRAD. Thereafter, the special properties of the coaxial transmission line and the comb-line filter are briefly reviewed in Section 3.3. Following that, the design and analysis of the comb-line filter are presented in Section 3.4. Subsequently, the fabrication and the measurement results of the comb-line filter are discussed in Section 3.5 and Section 3.6 respectively. Finally, the chapter concludes with the interpretation of the measured results as discussed in Section 3.7.

3.2 ESTIMATION OF L-BAND FILTER ORDER AND STOP BAND REJECTION LEVEL

The specifications for the L-band filter, as given by NeXtRAD, are presented in Table 1.1. In this table, the equal ripple bandwidth of the L-band filter is 200 MHz; in order to compensate for any drift in the centre frequency of the filter due to temperature changes, an additional 10 MHz was added to the 200 MHz, to give a total equal ripple bandwidth of 210 MHz. The modified specifications are presented in Table 3.1, from which the required filter order and stop

band performance were estimated.

A Chebyshev response was selected because it offers a steeper stop band skirts, as oppose to a Butterworth response, for the same filter order. For an all pole Chebyshev response, the order of the filter can easily be estimated from Equation (2.7). This equation assumes that the filter is symmetrical. However, it is well-known that the insertion loss of a comb-line filter is asymmetrical, and it is practically much weaker on the low-frequency side of the pass band, especially for broad bandwidths [20]. When the fractional bandwidth is small, typically 1% to 2%, one can use the approximate Equation (2.7) to estimate the order of the filter. However, NeXtRAD requires a fractional bandwidth of 16.153 %. Such a moderate fractional bandwidth will result in an asymmetry or skewing of the comb-line filters insertion loss. Therefore, to get a better estimate of the stop band performance of the filter and the required filter order, the admittance circuit theory model, as shown in Figure 3.1 was used. This model served two purposes: first, to estimate the order of the comb-line filter and the stop band performance; second, to act as a reference filter for tuning the simulated 3D model and the fabricated filter.

The circuit model in Figure 3.1 consists of six synchronously tuned shunt lumped element resonators, which are coupled together by means of seven admittance inverters and are fed by a pair 50 Ω input/output ports. The response of this 6^{th} order prototype circuit, as well as those for the 5^{th} and the 4^{th} order prototype circuits are all plotted in Figure 3.2. From Figure 3.2, it can be deduced that the 4^{th} order prototype circuit will not be sufficient to estimate the required stop band response of the comb-line filter because the insertion loss of this prototype circuit is already in the forbidden regions above and below the pass band of the insertion loss. Unlike the 4^{th} order prototype circuit, the 5^{th} order prototype circuit seems like a reasonable choice, but there is no guarantee that the insertion loss response of this circuit at the lower frequency side of the insertion loss response will not enter the forbidden region when the filter is simulated in CST [7]. Furthermore, there is no guarantee that the insertion loss response at the high-frequency side of the pass band will get out of the undesired region.

Therefore, to overcome the uncertainty associated with selecting the 5^{th} order prototype circuit, the 6^{th} order prototype circuit was selected to estimate the comb-line filter stop band response. Two 6^{th} order prototype circuits were synthesized: the one uses resonators with inductors and capacitors (LC) as shown in Figure 3.1, and the other uses resonators with capacitors and transmission lines as shown in Appendix A, Figure A.1 to implement the prototype circuits. The responses of both prototype circuits are shown in Figure 3.2 and these responses agree reasonably well. The result of the ideal 6^{th} order filter in Figure 3.1 is compared to the NeXtRAD specifications presented in Table 3.1 and the results agree very well.

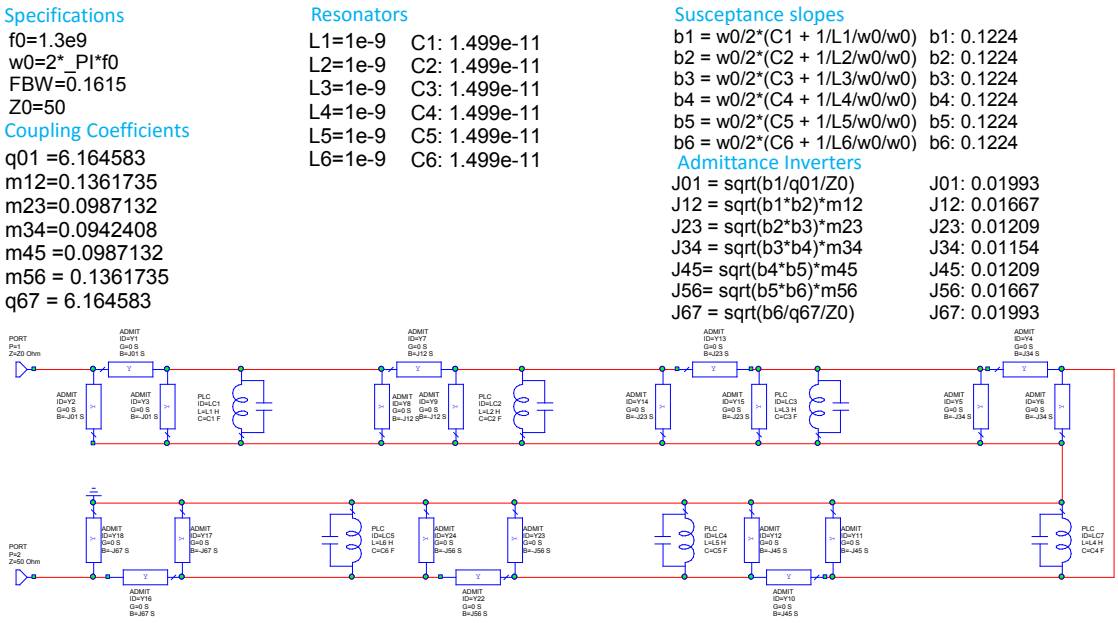

Figure 3.1: J-inverter prototype circuit model of a 6^{th} order Chebyshev band pass filter

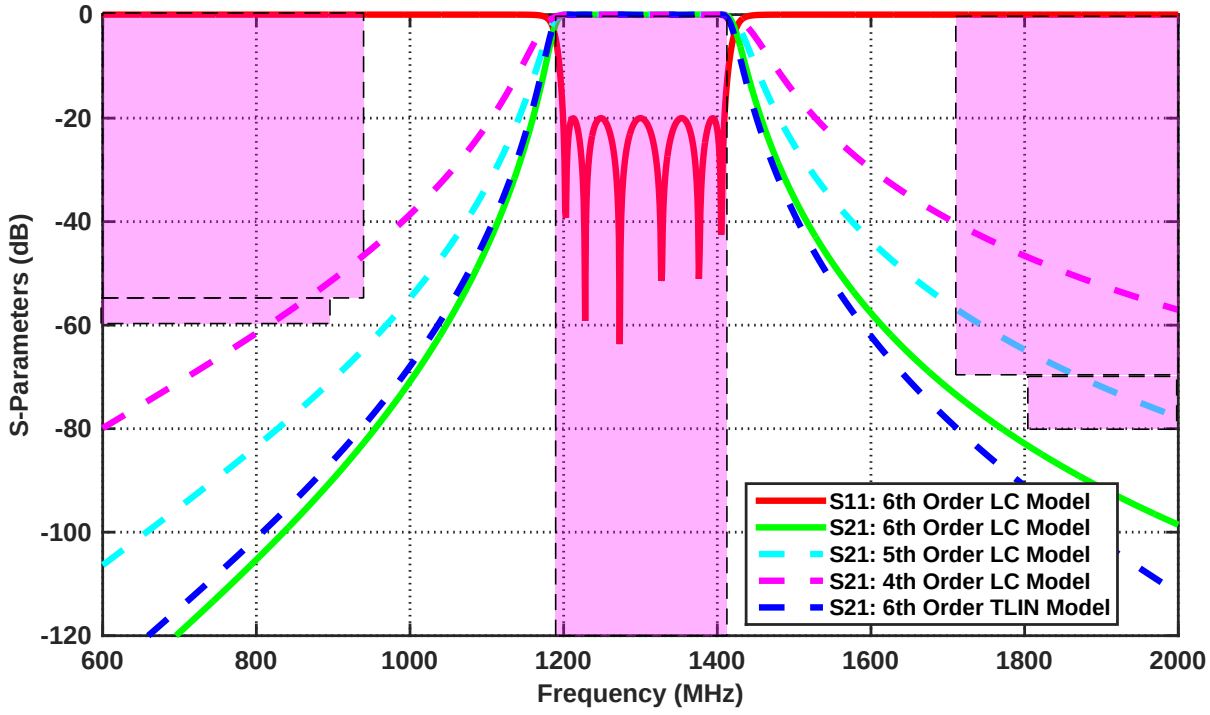

Figure 3.2: Circuit theory model responses for Chebyshev filters (N= 4, 5 and 6, RL = 20, $f_0 = 1300\,\text{MHz}$, $\Delta = 16.153\,\%$)

Table 3.1: NeXtRAD specifications versus ideal 6^{th} order circuit theory filter response

Parameters	Specifications	Ideal circuit model
Pass band	1195 MHz to 1405 MHz	1199 MHz to 1409 MHz
Centre Frequency	1300 MHz	1299.77 MHz
Insertion Loss	0.5 dB (max)	0.043 dB
Return Loss	20 dB (min)	20 dB
Equal Ripple Bandwidth	210 MHz	210 MHz
Fractional Bandwidth	16.153 %	16.156 %
Stop band		
Frequency/MHz	Attenuation/dB (min)	Attenuation/dB (min)
880 to 890	60	91.37
925 to 935	55	83.6
1710 to 1785	70	73.34
1805 to 1880	80	83.37
Input/output Impedance	50 Ω	50 Ω

3.3 REVIEW OF THE COAXIAL TRANSMISSION LINE AND THE COMB-LINE FILTER

The coaxial technology was selected at L-band because it is more compact than the waveguide technology at L-band. The coaxial technology also has lower loss compared to lumped element and microstrip technologies.

3.3.1 Properties of the Coaxial Transmission Line

Figure 3.3 describes a coaxial transmission line geometry, consisting of a centre conductor, enclosed within a dielectric material, which is in turn surrounded by a continuous outer conductor or shield, all sharing the same geometric centre. When a signal propagates along the transmission line, a transverse electromagnetic (TEM)[1] field is set up between the outer surface of the centre conductor and the inner surface of the shield, as clearly shown on the right hand side of Figure 3.3. The electric field lines are radial to the inner conductor, while the magnetic field lines circulate around the inner conductor.

The characteristic impedance for an infinitely long coaxial transmission line of the geometry in Figure 3.3 is given in [13] and [21] as

[1] Note: the TEM mode is the fundamental mode of a coaxial cable, however, higher order modes are also possible

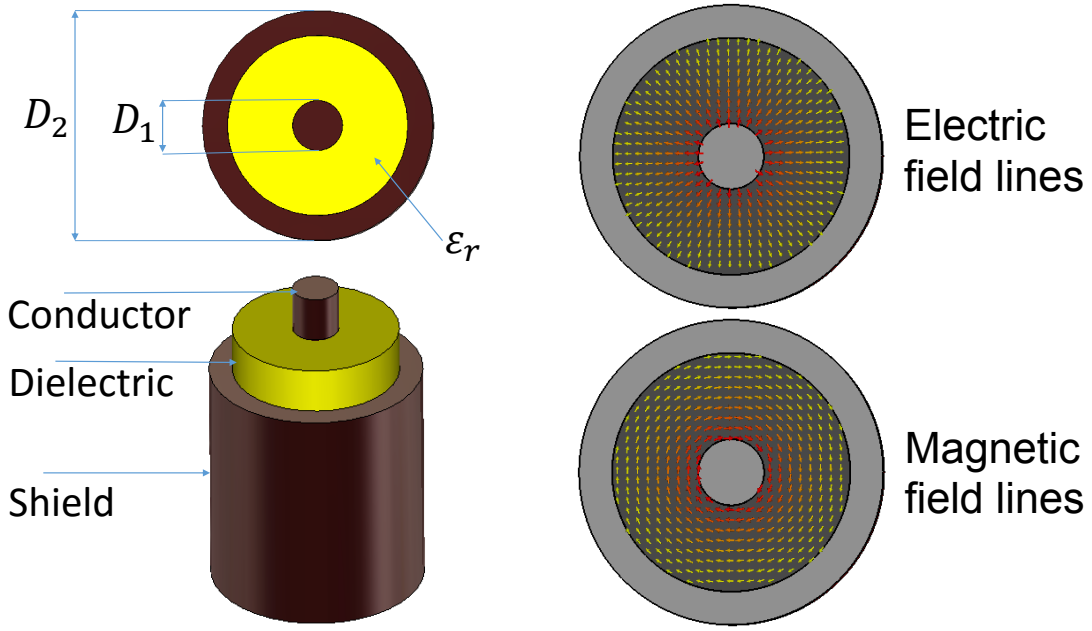

Figure 3.3: A basic coaxial transmission line geometry and the electromagnetic field patterns of the dominant TEM mode

$$Z_0 = \frac{\eta_0}{2\pi\sqrt{\epsilon_r}} \ln\left(\frac{D_2}{D_1}\right) \quad (\Omega). \tag{3.1}$$

Where $\eta_0 = 376.7\,\Omega$ is the impedance of free space, ϵ_r is the relative permittivity and D_2 and D_1 are the diameter of the outer and inner conductors respectively.

For a coaxial transmission line with inner and outer conductors having the same conductivity, the optimal ratio $\frac{D_2}{D_1}$ for minimum attenuation is 3.6, corresponding to $\sqrt{\epsilon_r} Z_0$ = 77 ohms [13] and [21]. Also, it is often desirable to have a coaxial transmission line with a square outer conductor as opposed to a circular outer conductor. The square outer conductor makes for easier fabrication than the round outer conductor. Therefore, Equation (3.1) is modified as follow to account for the square outer conductor, as given by [21]

$$Z_0 = \frac{\eta_0}{2\pi\sqrt{\epsilon_r}} \ln\left(\frac{1.0787 D_2}{D_1}\right) \quad (\Omega). \tag{3.2}$$

When the coaxial cable in Figure 3.3 is used as a resonator, its guide wavelength λ_g is given by Equation (3.3) [5]

$$\lambda_g = \frac{c_0}{f\sqrt{\epsilon_r}}, \qquad f_{0q} = q\frac{c_0}{2l\sqrt{\epsilon_r}}, \qquad q = 1, 2, 3, \ldots . \tag{3.3}$$

Where $c_0 = 2.998 \times 10^8$ m/s is the speed of light in free space, q is an integer number, l is the length of the resonator and f_{0q} is the resonant frequency of a particular mode.

3.3.2 Comb-line Filter

Comb-line filters are arguably the most commonly used type of coaxial filters, for frequencies below 10 GHz or so [20]. A representation of a comb-line band pass filter is shown in Figure 3.4. The resonators are metallic cylindrical rods[2], which are grounded to the bottom of the cavity, and opened at the other end. The length of the resonators is less than a quarter wavelength long, typically 30 to 70 electrical degrees [13].

The resonators may be arranged in a linear array as shown in Figure 3.4 between the parallel top and bottom ground planes[3]. The cylindrical rods are brought into resonance with various type of capacitive gap loading between the top ground and the open end of the rods. The tuning screws are used to adjust the capacitive loading, and hence tune the resonance frequency. The screws are also used to tune the coupling between the resonating rods. Figure 3.4 shows that the filter is fed by a tapping scheme, there are other schemes available and will be discussed later.

The bandwidth is the main driver in the design of the comb-line filter [22]. The bandwidth determines the spacing or coupling scheme required between the rods and the type of input/output coupling scheme [22]. An important fact to understand regarding the design of a comb-line filter is that they can behave like an evanescent waveguide filter. This happens when the ratio between the ground plane spacing (W) in Figure 3.4 and the free space wavelength becomes larger than 0.083 [20], and when the bandwidth is such that the spacing between any two rods (S) is less than 1.5 times the diameter of any of the rods. When this happens, the waveguide modes become the predominant form of coupling, and the propagation is no longer considered as pure TEM [20]. The computation of the coupling between the rods must include the effects of at least the cutoff dominant waveguide modes (due to large ground spacing) [20]. For bandwidths typically in excess of 40 % or less than 2 %, the effects of other cutoff modes must be included as well [20]. Some examples of coaxial comb-line filters are shown in Figure 3.5.

[2] Rods of different shapes may be used, like bars.
[3] The resonating rods may also be located in individual cavities which may be coupled and separated by irises

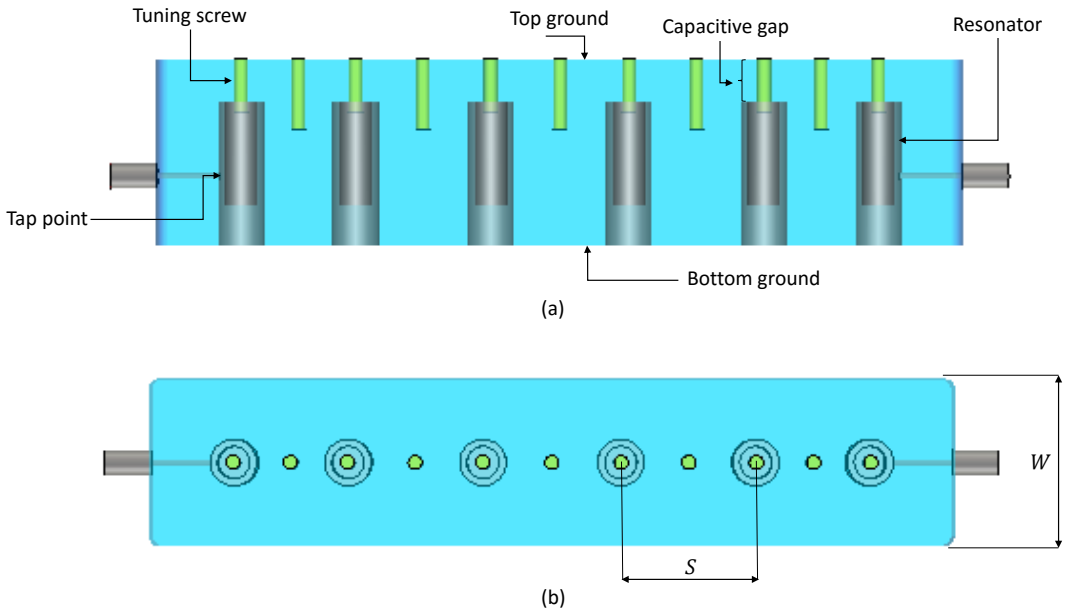

Figure 3.4: Comb-line band pass filter. (a) Front view. (b) Top view. CST [7]

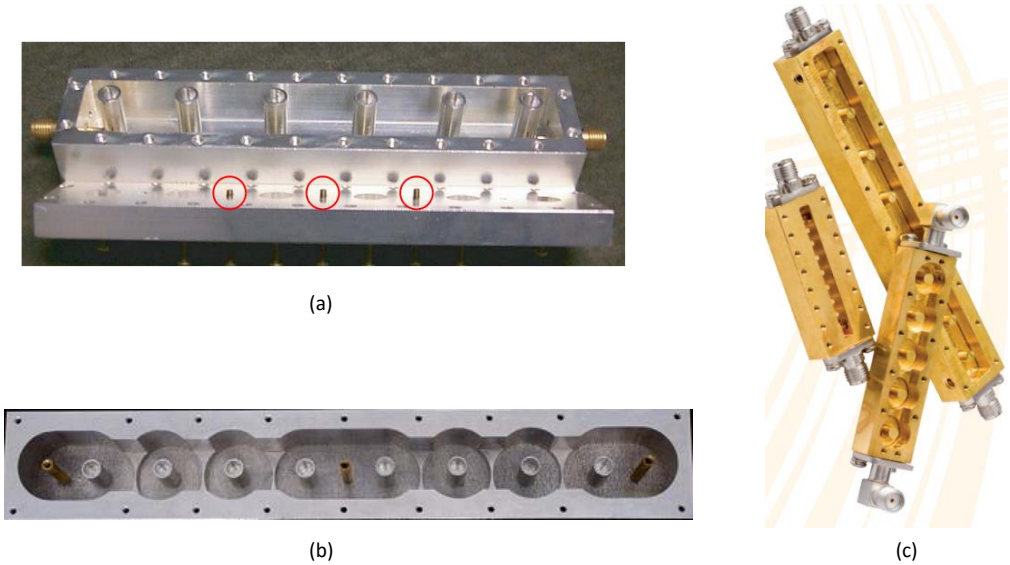

Figure 3.5: (a) Cover loaded comb-line filter from [22]. (b) Narrow band duplexer from [23]. (c) Comb-line filter from [24].

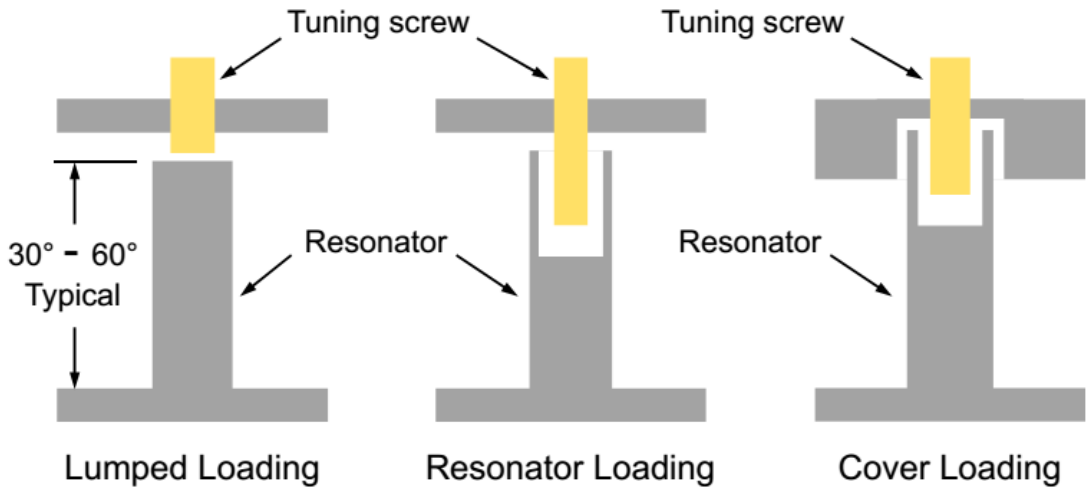

Figure 3.6: Comb-line resonator design schemes [26]

Advantage of comb-line filter

Comb-line filters are compact and have broad spurious-free stop band compared to interdigital filters. They are easier to manufacture than interdigital filters because all the tuning screws are located on the same top ground plane of the filter [25]. Additionally, The insertion loss of the comb-line filter can be reduced by increasing the size of the filter cavity [19].

Disadvantage of comb-line filter

A drawback of comb-line filters lies in the asymmetry or skewing of the insertion loss curve, which is practically much weaker on the lower frequency side of the pass band, especially for broad bandwidth filters [20].

Comb-line resonator loading and input/output coupling options

Figure 3.6 presents different ways to load a comb-line resonator. The length of the lumped loading rod is typically 30 to 60 degrees in electrical length. In this configuration neither the rod nor the cover is loaded, that is, there is no change done to the cylindrical rod or cover of the filter. This configuration is used at higher frequencies [26]. In the resonator loading set-up, the rods are modified by creating pockets in them. The tuning screws can extend into these pockets to change the capacitance of the resonating rods. The cover loading configuration is achieved by creating the pocket on the cover of the filter. The resonating rods can then extend into these pockets, and hence, the capacitance of the resonators can be modified in this way.

The options for feeding comb-line filters are shown in Figure 3.7. Direct tapping to the end res-

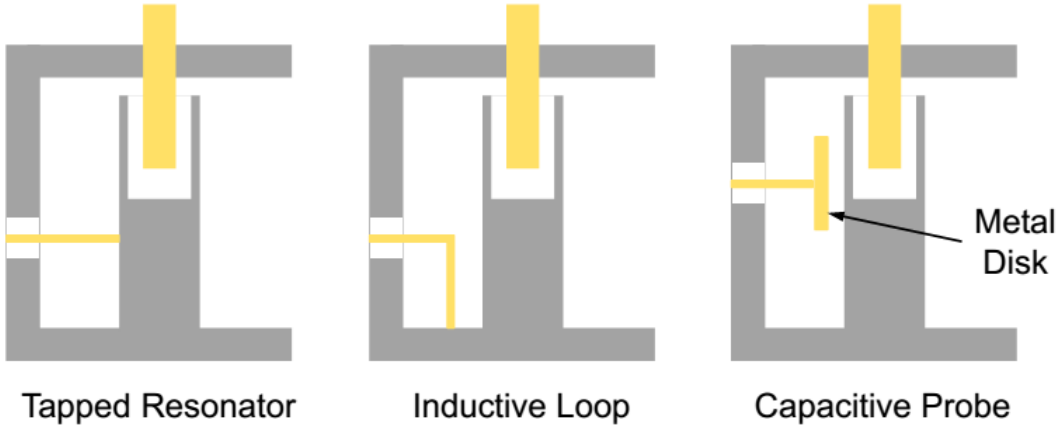

Figure 3.7: Comb-line input/output feeding options [26]

onator is a commonly used scheme. This method works well over a broad range of bandwidths [26] and [20]. This form of coupling is not suitable for narrow bandwidths at high frequencies because the tapping point is too close to the shorted end of the input/output resonators [20]. A good alternative is the inductive or magnetic loop coupling, which may be adjusted externally [20] and [26]. Capacitive loop coupling is another option. This alternative uses a disc to increase the strength of the coupling to the input/output resonators, resulting in broad bandwidth coupling.

Another useful coupling technique is to use the same-sided transformer. These transformers look like extra resonators at each end of the filter. These transformers only transform the impedance level of the input/output feed but do not contribute to the insertion loss function of the filter [20]. At low frequencies, this approach lengthens the filter compared to the direct tapping [20]. Figure 3.8 shows some examples where these resonator loading and feeding techniques were used.

3.4 The Design and Analysis of the Comb-line Filter

Before the comb-line filter was designed, all the design parameters were highlighted and the design technique to be used was selected. A perspective view of the desired filter configuration is shown in Figure 3.9a. This comb-line filter is a sixth order filter, employing the resonator loading technique of Figure 3.6. The tuning screws extend into the pockets created inside the resonator rods and are also placed between the rods inside the cavity. The filter is fed using the tapping technique of Figure 3.7. The spacing between the rods determines the interresonator coupling between the rods. For the comb-line filter in Figure 3.9a, the coupling between the rods is predominantly magnetic in nature [13].

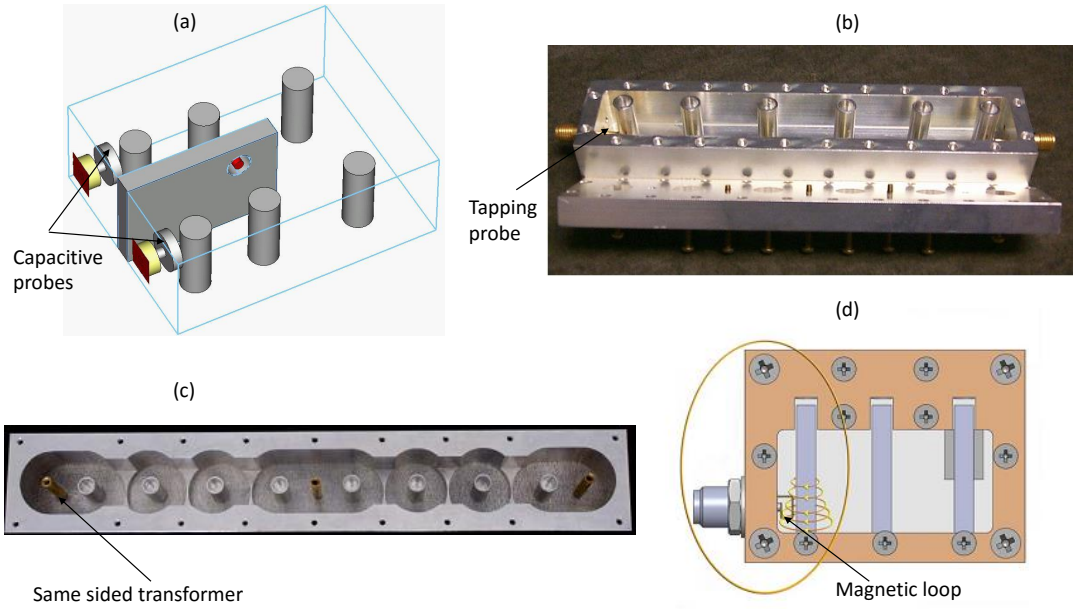

Figure 3.8: Different resonator loading and input/output feed options for comb-line filters. (a) Capacitive coupling from [27]. (b) Tapping probe from [26]. (c) Same sided transformer coupling from [23]. (d) Magnetic loop coupling from [3].

The desired centre frequency of the filter is 1300 MHz, with a fractional bandwidth of about 16.153 % and a return loss level of at least 20 dB. Figure 3.9b shows a cross section of the filter details. The physical lengths of the rods (H_{2_1}) to (H_{2_3}) will set the desired centre frequency of the filter. Only the lengths of three rods need to be determined since the filter is symmetrical about the T-T' line. The lengths of the tuning screws, (H_5), which extends into the resonator pockets, will tune the post manufactured centre frequency of the resonators. The height (H_3) of the SMA probe sets the return loss level of the filter. The height of the cavity (H_1), will determine the capacitance of the resonators.

Furthermore, the bandwidth is the main driver of the design of the comb-line filter, as stated earlier, as it determines the type of coupling scheme to be used and the way the filter should be fed. Here the bandwidth is set by the spacing (S_1) to (S_3) between the rods, as in Figure 3.9c. The coupling tuning screws of lengths (H_4) in Figure 3.9b are used to tune the post manufacturing couplings of the filter, and hence the bandwidth of the filter. The unloaded quality factor of the resonator is set by the ratio ($\frac{W}{D_3}$). The diameter of the tuning screws (D_1) will influence both the interresonator coupling and centre frequency. Finally, the corner radius (R) of the cavity and the inner diameter of the rods (D_2) were specified by the manufacturer.

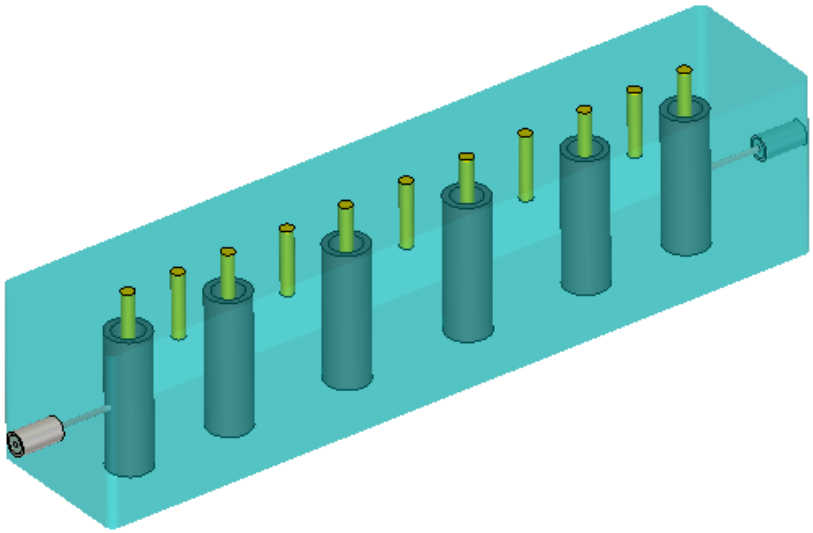

(a) Perspective view

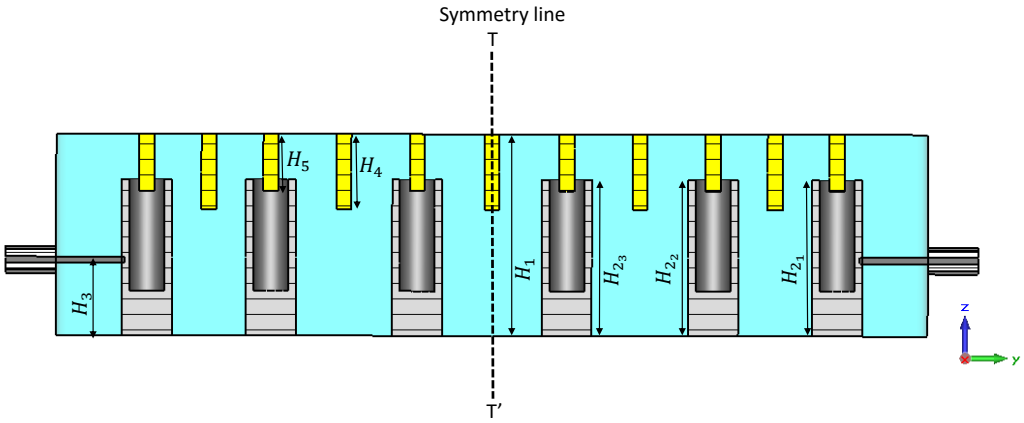

(b) X-plane view

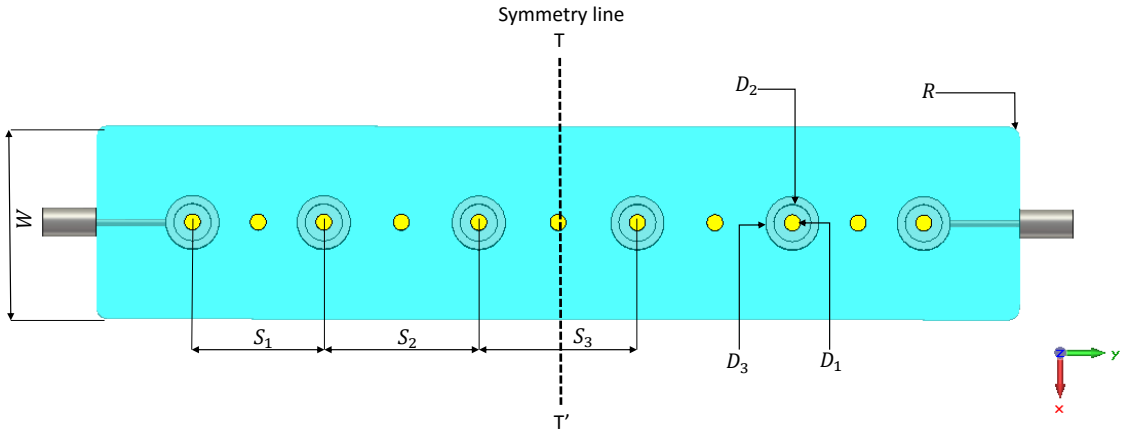

(c) Z-plane view

Figure 3.9: Field-solver model for the N = 6 comb-line filter: (a) perspective view of the complete filter; (b) X-plane view of the half model with design parameters; and (c) Z-plane view of the model with design parameters.CST [7]

3.4.1 Comb-line Filter Design Methods

A classical technique to determine the physical parameters of the comb-line filter is given in [13]. The dimensions of the filter are determined from the lumped capacitance and the normalized self and mutual capacitances. It has been reported in [28] that this theory, based on TEM mode coupling between the resonators, results in bandwidths which are too large in practice, for a ratio greater than 0.08 between the ground plane spacing (W) to the waveguide wavelength. There is also an increase in the unloaded quality factor of the resonator. This is because this method does not consider the higher order modes in the calculation of the self and mutual capacitances [28]. It seems that the interresonator coupling in a general comb-line filter is due to the evanescent waveguide modes, the TE_{10} and TM_{11} being the dominant modes [28]. For small values of ground plane spacing to wavelength ratio, these modes appear to be similar to the TEM mode [28].

Therefore, instead of working on the self and mutual capacitances, an alternative design approach is to determine the required dimensions of the filter in terms of another set of design parameters, the external quality factors, and the coupling coefficients. Milton Dashal [29] recognised as early as the 1951, that any narrow to moderate band (less than 20 % fractional bandwidth), lumped element or distributed element band pass filter could be described by three basic variables: the synchronous-resonant frequency of the cavities, the coupling between the adjacent resonators and the external quality factors. The resonant frequency determines the centre frequency of the filter, the coupling between adjacent resonators sets the bandwidth for the filter and the external quality factor sets the return loss level of the filter.

A possible design flow of a coupled resonator band pass filters may be as follows: create a model for the resonator that will give the desired unloaded quality factor, centre frequency, and spurious performance. Design curves for the interresonator coupling and the external quality factor can be built. Finally, build a model of the complete filter, apply a tuning technique, and check the result against the specifications. This design flow was followed in this section.

3.4.2 Comb-line Coaxial Resonator

This section deals with the determination of the physical parameters of the resonator that will give the desired electrical performance of the resonator. The electrical performance of the resonator will be measured in terms of the resonant frequency, the unloaded quality factor and the spurious-free window of the resonator.

Ground plane spacing and rod diameter for loss

As is well-known, the unloaded quality factor of a comb-line resonator is given as [28]

$$Q_u = AW\sqrt{f_0}, \tag{3.4}$$

where W is the ground plane spacing of the cavity in inches, f_0 is the resonant frequency in GHz and A is usually constant for any given type of resonator. For a comb-line filter with small values of W, that is when the ratio $\frac{W}{\lambda_0}$ is less than 0.08, A is considered constant. However, when the ratio $\frac{W}{\lambda_0}$ becomes greater than 0.08, the increase in Q_u with $\frac{W}{\lambda_0}$ is quite dramatic, and this has the effect of making A in (3.4) no longer constant [20] and [28]. The expression which relates A to $\frac{W}{\lambda_0}$ was derived by [30] from the scattered points in [28] and is given as

$$A = 14000\left(\frac{W}{\lambda_0}\right) + 200 \quad \text{for} \quad 0.1 < \left(\frac{W}{\lambda_0}\right) < 0.2. \tag{3.5}$$

Equation (3.5) assumes that the filter is silver plated. Figure 3.10 shows a cross-sectional view of a square coaxial transmission line, with the design parameters being W and D_3. The parameter D_3 was selected to be 10 mm, due to manufacturing constraints. W was calculated as 36 mm at a mid-band frequency of 1300 MHz. Therefore, $\frac{W}{\lambda_0}$ = 0.156, this value substituted in Equation (3.5) and then in Equation (3.4) results in a value of Q_u = 3852.53 approximately. Figure 3.11 shows that the characteristic impedance for the dimensions of W and D_3 is 81.24 Ω. This is close enough to 77 Ω required for maximum quality factor.

Rod and cavity dimensions for resonance

Initial dimensions for the rod height (H_2) and the cavity height (H_1) as shown in Figure 3.12 was obtained by using the lumped loading resonator topology in Figure 3.6. It is known that the height of the rod is less than a quarter wavelength long, typically 30 to 70 electrical degrees. The height of the cavity was selected to be H_1 = 40 mm, which corresponds to an electrical length of 62.4 degrees. The model in Figure 3.12 was built and simulated in CST [7].

It was found that the resonator resonated with a frequency of 1302.8 MHz and had a quality factor of approximately 3700.9 when the height of the rod H_2 = 38.65 mm. The quality factor is very close to the calculated value of 3852.53. This resonator has a spurious-free window of about 3042 MHz or the first spurious pass band happens at $2.33f_0$. Traditional analysis based on TEM mode transmission line theory predicts that the first spurious pass band of a comb line filter will happen at $3f_0$ for 90° resonators [17]. The simulated value of $2.33f_0$ is close enough

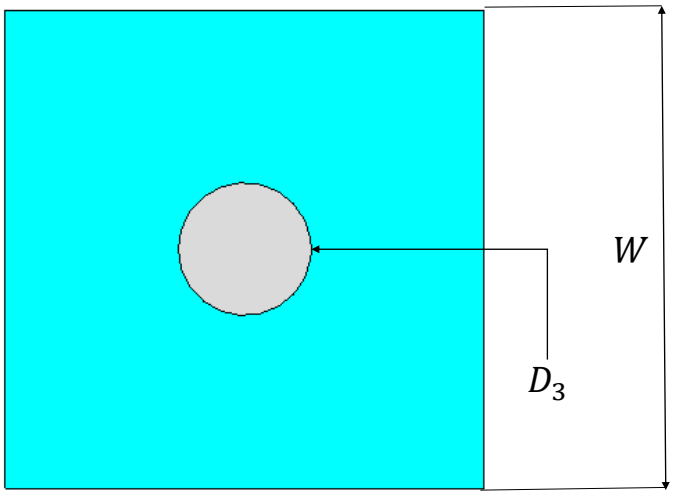

Figure 3.10: Cross section of a square coaxial transmission line: with the diameter D_3 of the rod and width W of the cavity. CST [7]

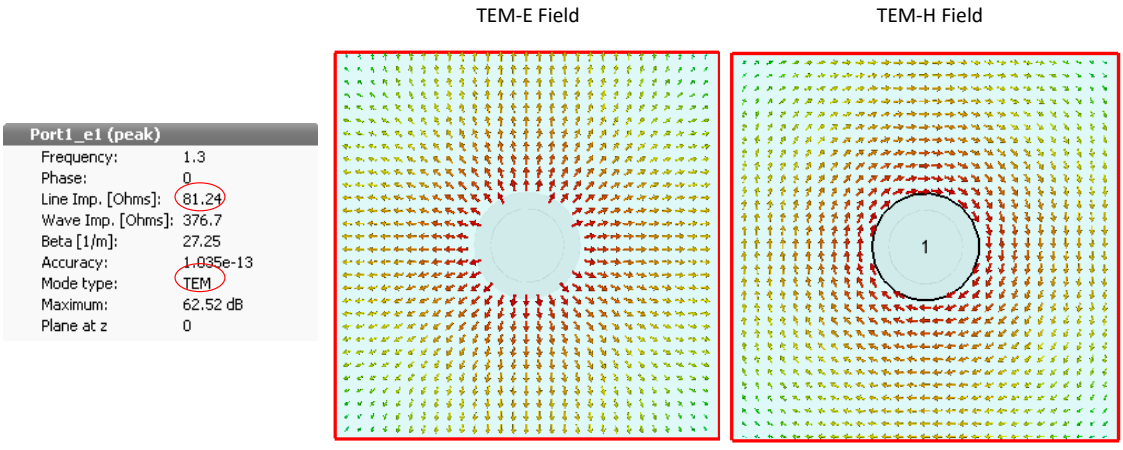

Figure 3.11: TEM electric and magnetic fields on the cross section of the coaxial transmission line, and the characteristic impedance of the coaxial transmission line. CST [7]

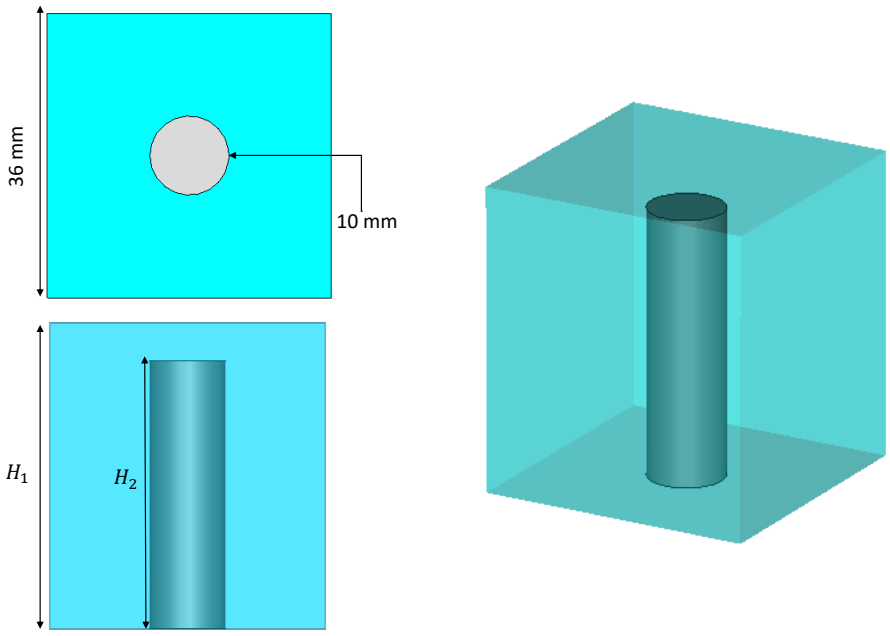

Figure 3.12: Parameter definition for lumped loading comb-line resonator topology. CST [7]

to the theoretical value.

Modified rod and cavity for manufacturing and tuning

The resonator in Figure 3.12 was modified to take into account post manufacturing tuning of the filter and unwanted electrical effects due to the sharp corners of the cavity. The modified model is that of a resonator loading model and is presented in Figure 3.13. The corner radius R is required to prevent any electrical spark that might be created by the sharp corners of the cavity if the filter is used for high power applications. These electrical sparks are caused by strong electric fields at the corner of the cavity. The value of R depends on the height of the cavity from the manufacturing point of view. For a 40 mm high cavity, Kline Engineering specified that R must be at least 4 mm for a good finish inside the filter. Therefore, R was selected to be 4 mm.

According to [8], perturbing a resonator with a screw has the effect of changing its resonant frequency. This idea can be used to tune the manufactured filter. The resonant frequency of the cavity will decrease as the screw is inserted into the cavity. Therefore, the resonator was made short, so as to resonate at a higher frequency, before inserting the tuning screw into the resonator. The tuning screw was inserted to decrease the resonant frequency back to the desired value. A standard D_1 = 3 mm M3 tuning screw, with a length H_5 = 11.3 mm was used. A pocket was created inside the rod to allow the tuning screw to extend into the rod.

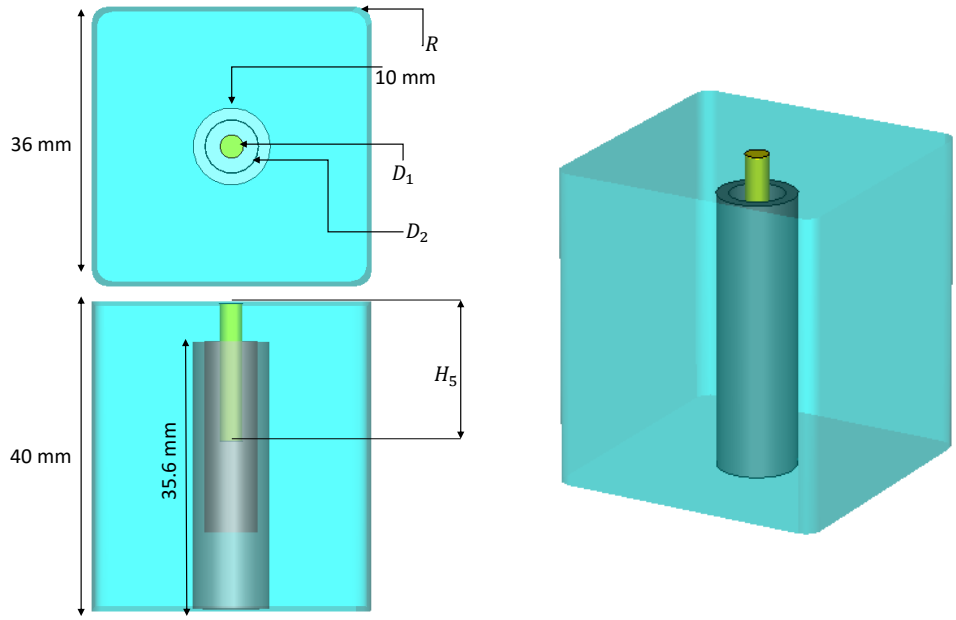

Figure 3.13: Parameter definition for resonator loading comb-line resonator topology. CST [7]

The inner diameter D_2 of the rod had to be at least 8.1 mm for a cutter to machine in between the rod. Therefore, D_2 = 8.2 mm was selected. The electrical performance of the resonator is summarised in Table 3.2. The physical parameters of the resonator in Figure 3.13 is presented in Table 3.3.

Table 3.2: Comparison of resonators with and without tuning screw

Dimensions	No Screw	Screw
Mode1 (MHz)	1302.8	1305
Mode 2 (MHz)	4344.01	4100
Q_u Mode1	3700.9	3815.49
Q_u Mode2	6375.93	5005.162
Spurious (MHz)	3042	2795

Note that in Table 3.2, the unloaded quality factor of mode 1 increases with the insertion of the tuning screw into the rod. This improves the loss of the filter, however, the size of the spurious-free window is reduced. What is also interesting is that unloaded quality factor of Mode 2 decreases as well with the insertion of the tuning screw.

3.4.3 **Interresonator Coupling**

The bandwidth of the filter is set by the type of coupling topology used. As stated before, the bandwidth of a comb-line filter is the main driver of the design. A fractional bandwidth of 16.153 % is required for the comb-line filter designed here. Table 3.4 presents the values

Table 3.3: Physical parameters of the loaded resonator. All units are in [mm]

Dimensions	Values
Width of Cavity: (W)	36
Height of Cavity: (H_1)	40
Height of Rod: (H_2)	35.6
Length of Screw: (H_5)	11.3
Diameter of Screw: (D_1)	3
Inner Diameter of Rod: (D_2)	8.2
Diameter of Rod: (D_3)	10
Corner Radius: (R)	4

of the desired coupling coefficients which will realize the required bandwidth. The coupling coefficients were calculated from Equations (2.19) or (2.20). The element values of the low pass prototype circuit were obtained from the table in Figure 2.5.

Table 3.4: Low pass prototype circuit element values and interresonator coupling coefficients for N = 6 Chebyshev band pass filter

g_i	g values	$\kappa_{j,j+1}$	κ values
g_1	0.996	$\kappa_{1,2}$	0.136
g_2	1.413	$\kappa_{2,3}$	0.099
g_3	1.895	$\kappa_{3,4}$	0.094
g_4	1.551	$\kappa_{4,5}$	0.099
g_5	1.727	$\kappa_{5,6}$	0.136
g_6	0.815	-	-
g_7	1.222	-	-

By inspecting Table 3.4, one can see that the coupling coefficients are reasonably large. This is not surprising since the bandwidth to be realized is quite moderate. A reasonable technique to realize such coupling coefficients is to place the rods close to each other, and by adjusting the separation between the resonator rods, one can obtain different values for the coupling coefficients. Figure 3.14 shows the set-up used to determine the coupling coefficients in CST [7].

An eigenmode analysis for the set-up in Figure 3.14 was carried out, and the eigenmode frequencies are presented in Figure 3.15. The curves show the even and odd eigenmode frequencies as a function of the spacing (S) between the rods, and the depth of the tuning screw (H_4). The separation between the curves of mode 1 and mode 2 determines the strength of the coupling between the rods. In Figure 3.15, the separation between the modes is much greater for low values of S, than for high values of S. This implies that the coupling coefficient will be much larger for lower values of S, than for higher values of S.

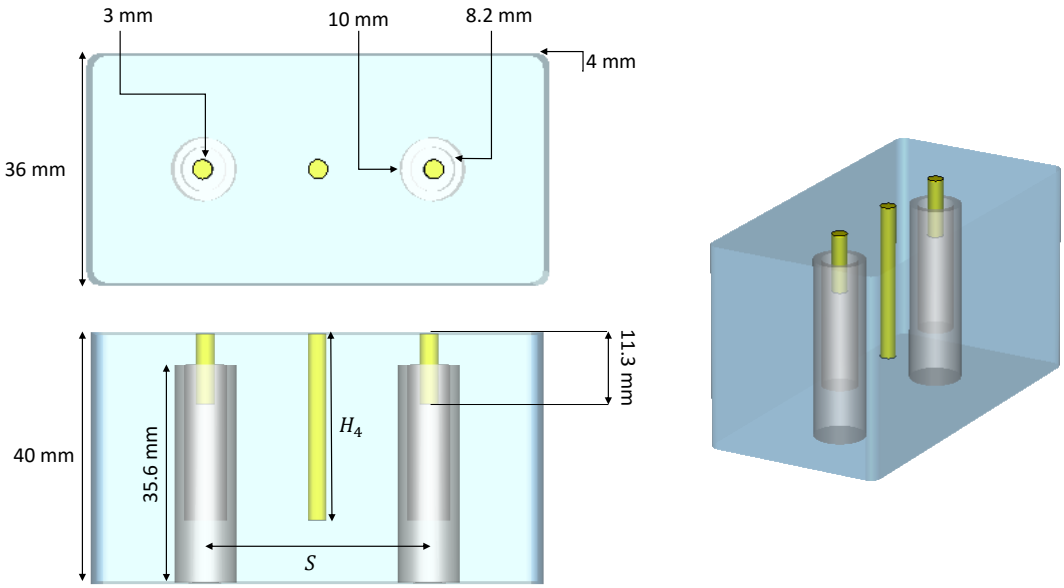

Figure 3.14: Configuration to determine the coupling coefficients for N = 6 Chebyshev band pass filter. CST [7]

The strength of the coupling is also influenced by the insertion of the tuning screw between the rods. Note, that there is an upper limit for $S < 28$ mm, where the insertion of the tuning screw has a significant effect on the modes. For $S \geq 28$ mm, the tuning screw hardly affects the modes. The insertion of the tuning screw by a depth of $H_4 = 15$ mm, results in the modes being separated further apart, and hence an increase in the coupling coefficient.

Mode 1 is influenced dramatically by the insertion of the tuning screw. But, mode 2 is hardly affected by the insertion of the tuning screw. The reason for this can be seen in Figure 3.16 and 3.17. Inspecting the fields around the tuning screw for mode 1 and mode 2, one sees that in Figure 3.16, the even electric field of mode 1 is greatly disturbed by the tuning screw, however, the odd magnetic field is hardly influenced. In Figure 3.16, the odd electric and even magnetic fields are hardly disturbed. Moreover, the influence of the tuning screw on mode 1 is much more dramatic for lower values of the rod separations S. A second look at Figure 3.16 and 3.17 shows that the strength of the magnetic fields is much greater than that of the electric fields. This means that the coupling between the rods is predominantly magnetic.

The coupling coefficient curves were obtained from Equation (2.23) or (2.26) and is shown in Figure 3.18. It is evident that the coupling coefficient increases with a decrease in S and an increase in H_4 as already observed from the eigenmode analysis. In order to select a nominal depth for the tuning screw, around which the coupling is to be tuned, two simulation depths of H_4 equals 15 mm and 20 mm were used. Figure 3.18 shows that the coupling for $H_4 = 20$ mm is

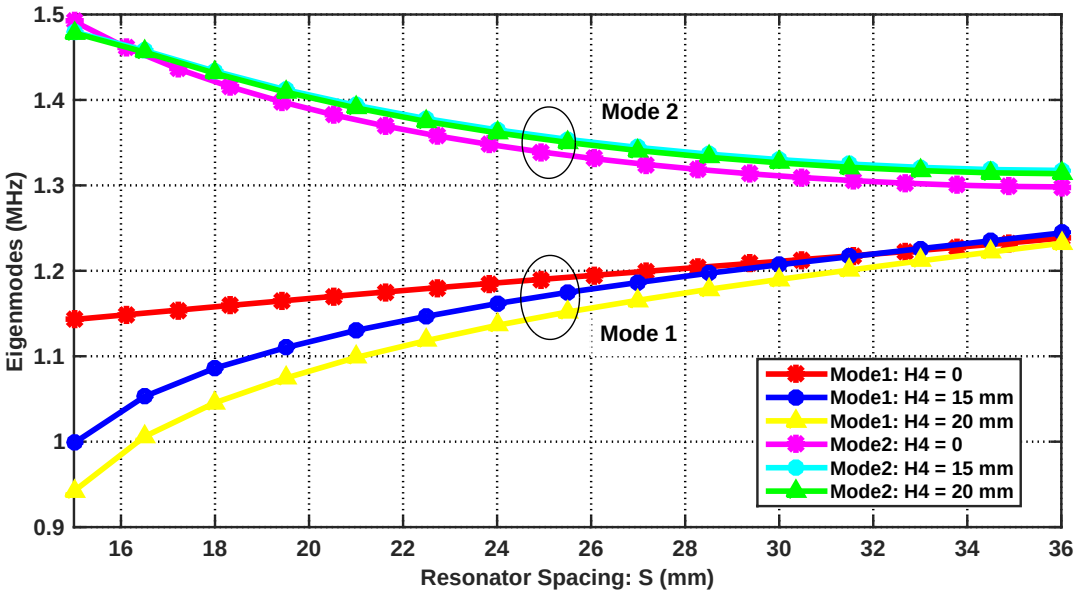

Figure 3.15: Eigenmode frequencies versus rod spacing (S) for the configuration in Figure 3.14

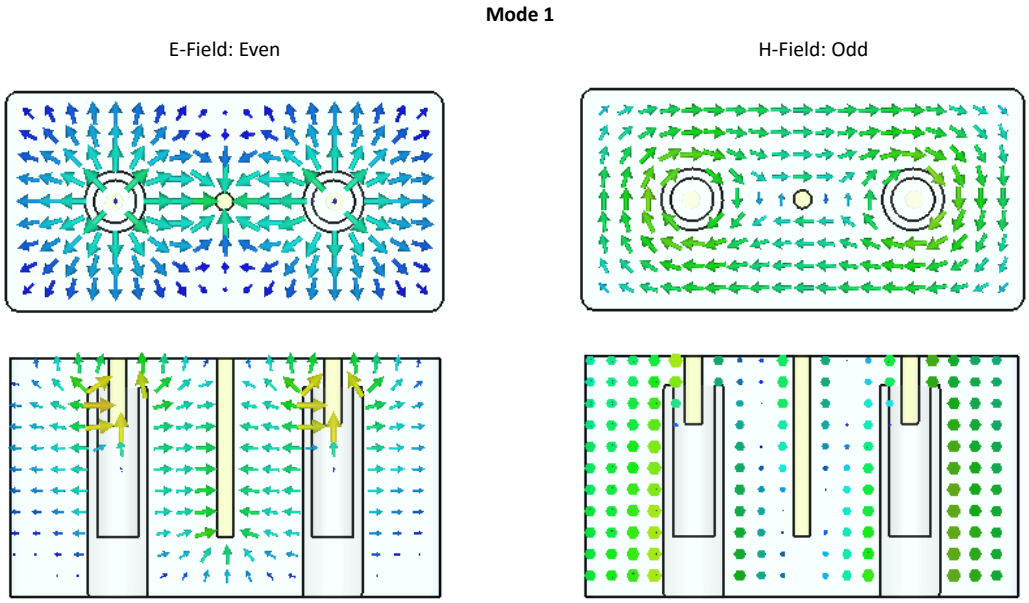

Figure 3.16: Mode 1 even electric field and odd magnetic field CST [7]

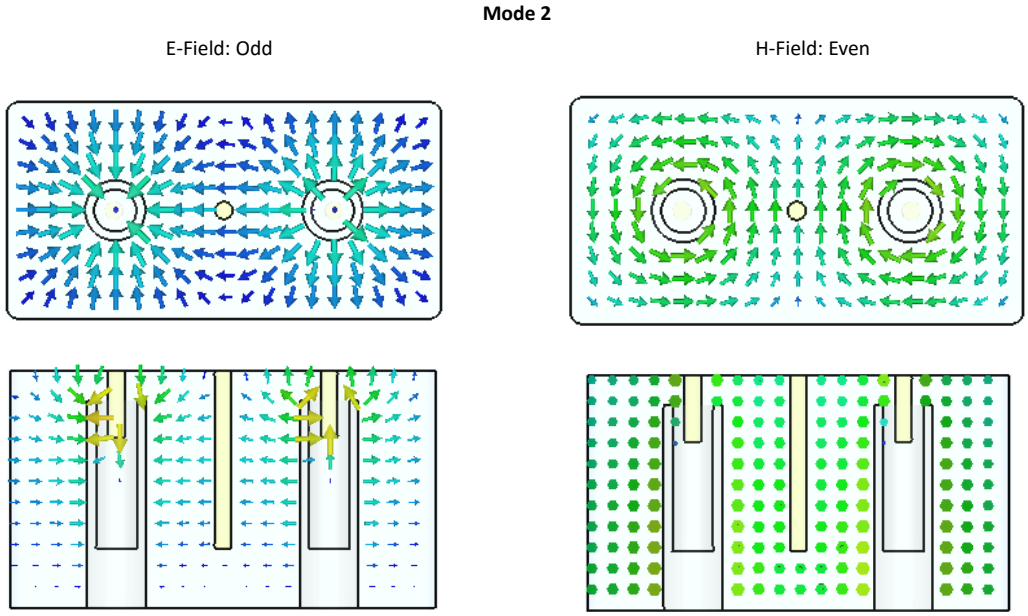

Figure 3.17: Mode 2 odd electric field and even magnetic field CST [7]

higher than that for the H_4 = 15 mm. A close inspection of the curves shows that by increasing the depth of the tuning screw, the desired coupling coefficients are achieved by using higher values of S. This means that the size of the filter will be larger. Therefore, a nominal depth of H_4 = 15 mm was considered good enough for the tuning. Table 3.5 was constructed from Figure 3.18, it presents the required rod separation (S) to give the desired coupling coefficients.

Table 3.5: Rod spacing (S) and coupling coefficients (κ) with H_4 = 15 mm

S_i	S values	$\kappa_{j,j+1}$	κ values
S_1	26 mm	$\kappa_{1,2}$	0.136
S_2	30 mm	$\kappa_{2,3}$	0.099
S_3	30.3 mm	$\kappa_{3,4}$	0.094
S_4	30 mm	$\kappa_{4,5}$	0.099
S_5	26 mm	$\kappa_{5,6}$	0.136

3.4.4 Input/output External Quality Factor

The input/output coupling coefficients set the return loss level of the filter. The tapped scheme was selected due to the required bandwidth. This scheme allows one to get a broadband matching. The set-up for this scheme is shown in Figure 3.19.

The resonator was fed using a straight square flange jack receptacle SMA feed. The centre probe of the SMA feed extended into the cavity until it made direct contact with the rod inside the cavity. The height H_3 will determine the required external quality factor. It is already

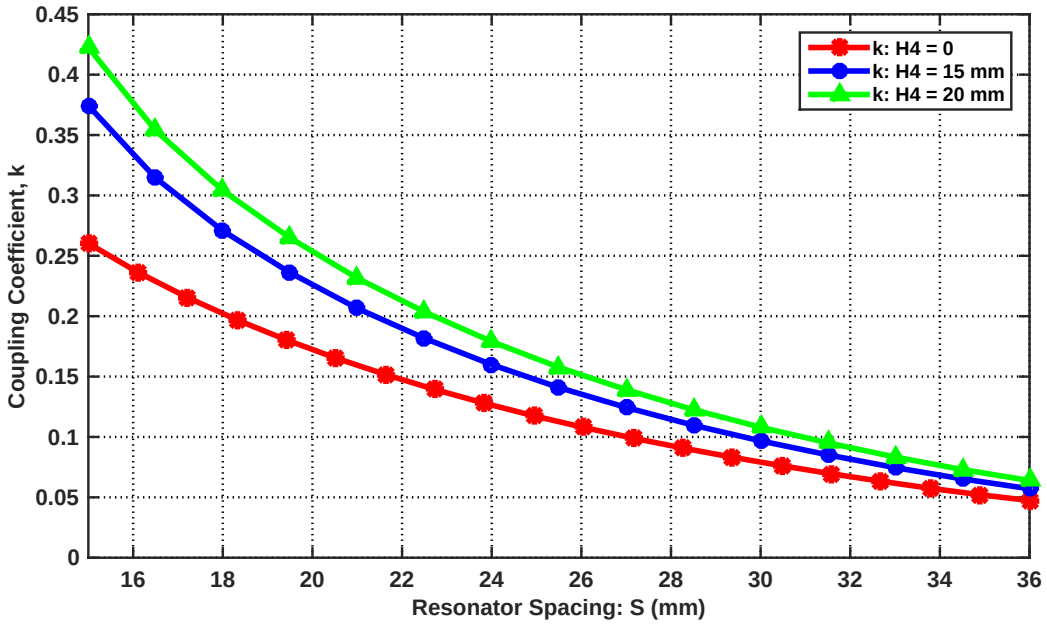

Figure 3.18: Interresonator coupling coefficient (κ), versus rod spacing (S)

known that the larger H_3, the larger the bandwidth. Therefore, for a bandwidth of 16.153 %, one expects H_3 to be large. Note that by inserting the probe into the cavity, the centre frequency is disturbed, for this reason, the height of the rod has to be adjusted slightly too. The reflected group delay method was used to determine the external quality factor. The desired external quality factor was calculated from Equations (2.19) or (2.20).

The height of the rod was adjusted and fixed to 38.3 mm. Thereafter, H_3 was varied. The curves for the reflected group delay and the external quality factor is shown in Figure 3.20. The external quality factor was calculated from the reflected group delay using Equation (2.30). The reflected group delay and external quality factor decrease, as H_3 increase from 20 mm to 26 mm. Table 3.6 provides the dimensions of H_3 that yields the desired external quality factor.

Table 3.6: Calculated versus simulated external quality factor, with rod height H_2 = 38.3 mm

Group Delay	Q_e Simulated	Q_e Calculated	H_3
3.02 ns	6.17	6.16	23.49 mm

3.4.5 **Initial Filter Response**

The physical parameters for an initial simulation of the comb-line filter in Figure 3.9 is given in Table 3.8. The filter was simulated in CST [7] and the response of the filter is shown in Figure 3.21. The filter is centred at 1159.97 MHz and has a bandwidth of about 194.7 MHz. The return

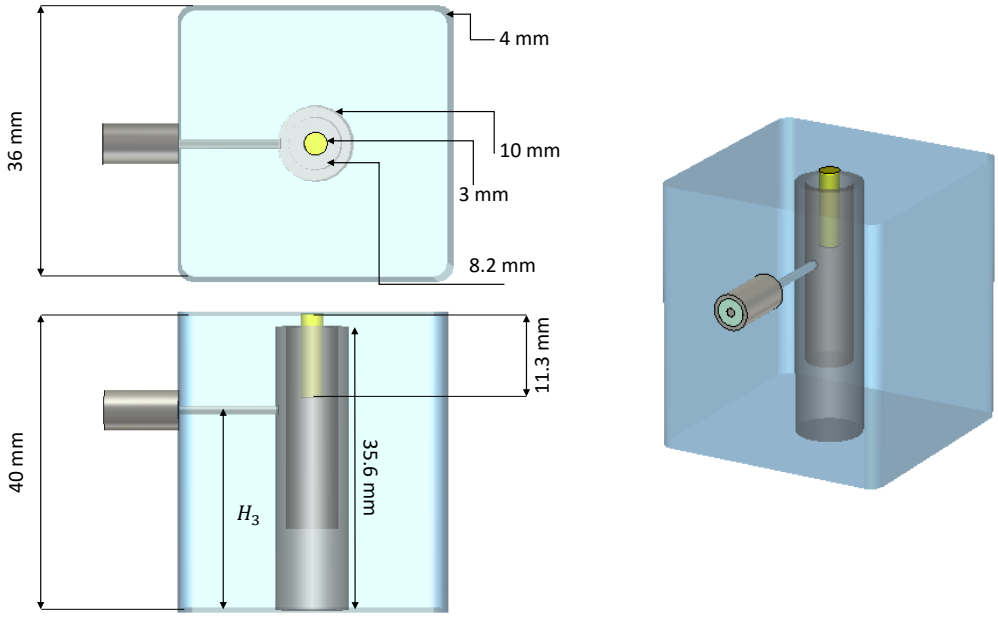

Figure 3.19: Configuration to determine the group delay and external quality factor CST [7]

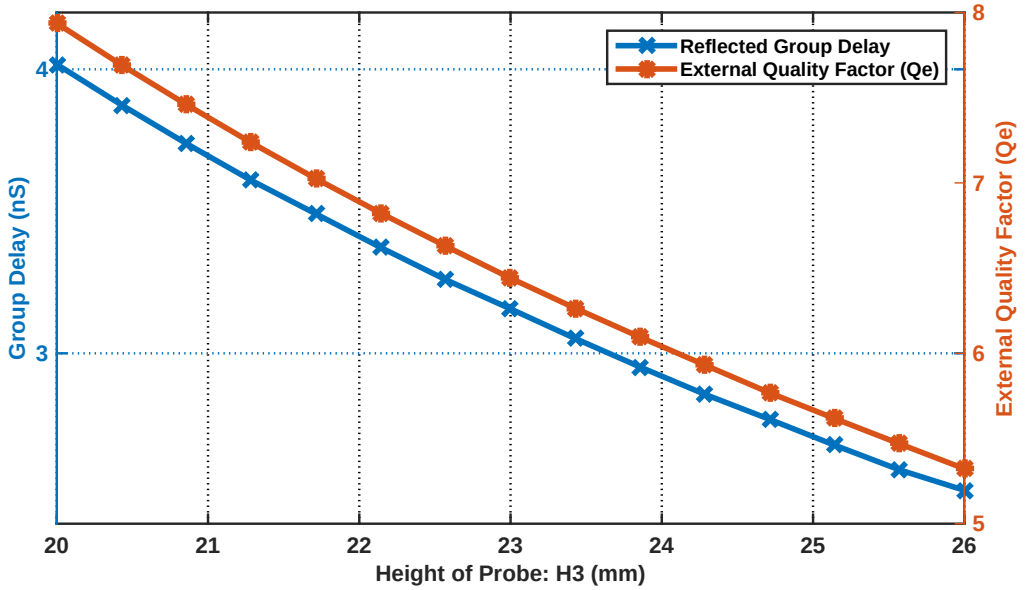

Figure 3.20: Group delay and external quality factor curves versus the height of the probe (H_3)

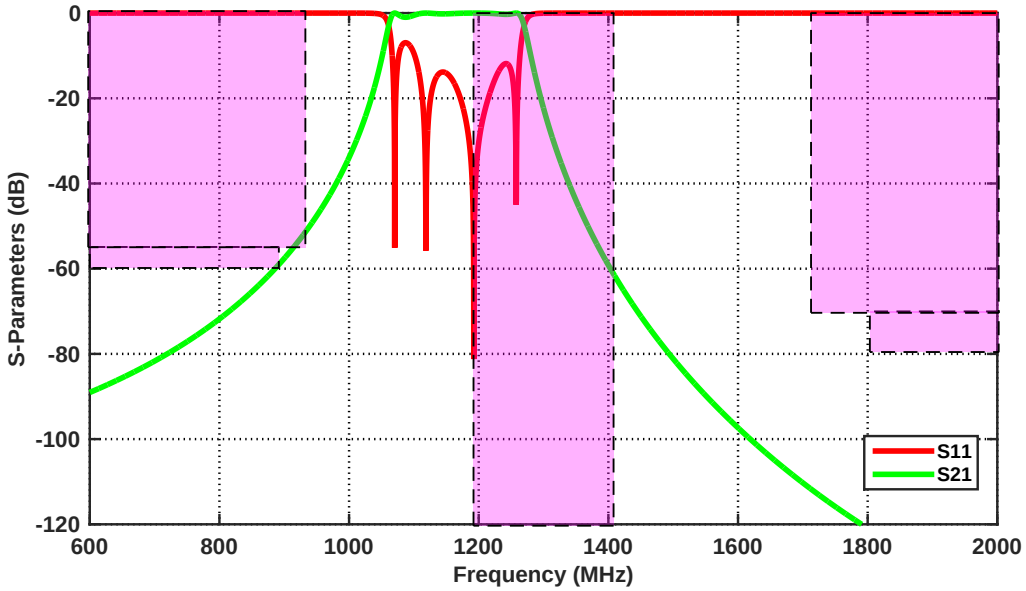

Figure 3.21: Simulation of initial response for Chebyshev comb-line band pass filter (N = 6, RL = 20, $f_0 = 1300\,\text{MHz}$, $\Delta = 16.153\,\%$)

loss of the filter is at least 6.5 dB. The asymmetric nature of the insertion loss of the comb-line filter is also apparent in this response. The insertion loss is lower on the upper side of the pass band than the lower side of the pass band which agrees with what is expected practically.

However, the initial response in Figure 3.21 is not the desired response. The desired response requires that the filter operates at 1300 MHz centre frequency, with a bandwidth of 210 MHz and a return loss of at least 20 dB. Therefore, the above response must be tuned. It is clear that the filter in Figure 3.21 has to be shifted to the right for it to operate at the desired frequency. The shift can be accomplished by tuning the height of the rods H_2. The bandwidth of the filter must be increased, this can be achieved by tuning the spacing S between the rods. The return loss level (S11) must be reduced, and this is done by adjusting the height H_3 of the SMA probe.

3.4.6 Optimised Comb-line Filter Response

The response in Figure 3.21 was tuned using the group delay technique[4], and then optimized using the Nelder-Mead Simplex Algorithm[5] in CST [7]. The optimized filter is compared with the ideal filter in Figure 3.22. Table 3.7 summarizes the result of the comparison. Notice that the stop band performance of the ideal filter and optimized filter differs, but the filters are

[4] The group delay technique is explained in great deal in [5].

[5] The Nelder-Mead Simplex Algorithm was selected simply because it gave a better response much quicker than the others algorithms such as the CMA Evolution Strategy and the Trust Region Framework

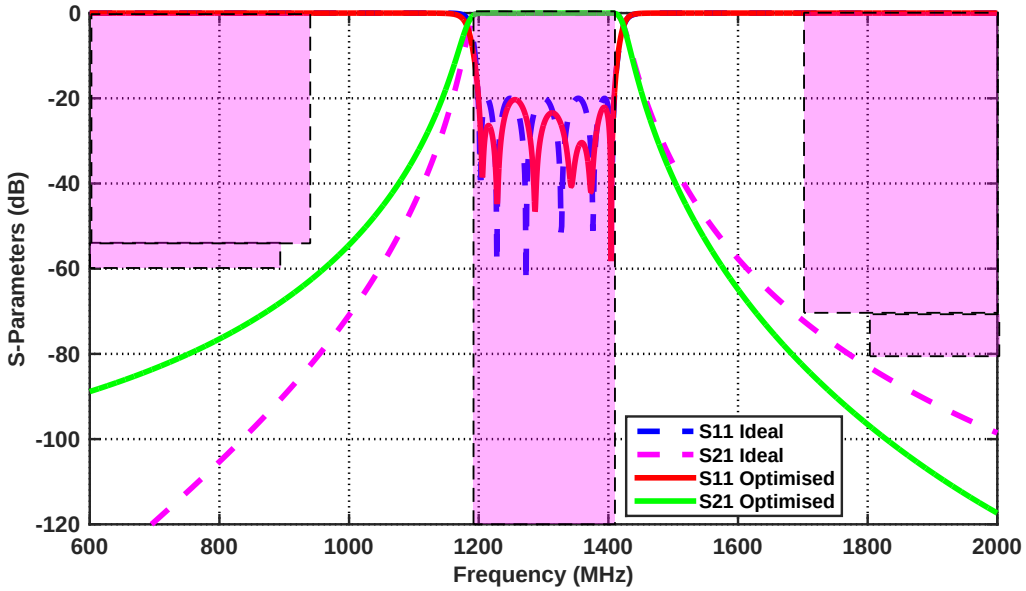

Figure 3.22: Narrow band optimised response compared with ideal response for Chebyshev comb-line band pass filter (N= 6, RL =20, $f_0 = 1300\,\mathrm{MHz}$, $\Delta = 16.153\,\%$)

well matched in the pass band. This is because the circuit model used to implement the ideal filter uses impedance inverters, and impedance inverters only operate well over a very narrow bandwidth. Also, the ideal model used does not represent the comb-line filter above and below the pass band. Notice also that the insertion loss of the optimized filter increases below the pass band and decreases above the pass band. This justifies the choice of a sixth order filter, rather than a fifth order filter in Section 3.2.

A wide band simulation of the optimized response in Figure 3.23 shows that the filter has a spurious-free window of about 2208 MHz at -60 dB. From literature, the first harmonic of a comb-line filter happens at 3 times the operating frequency for a rod of 90° electrical length [17] and [31] . The wide band response shows that the first harmonics for this comb-line filter happens at 2.98 times the operating frequency, this is very close to the ideal case.

3.5 FABRICATION OF COMB-LINE FILTER

CST [7] was used to simulate and optimize the L- band comb-line band pass filter. Thereafter, the filter was exported to Solid Works, where the filter was drawn and dimensioned. Figures 3.24 and 3.25 shows the drawing of the filter body and cover sent to the manufacturer, Kline Engineering. An assembly view was also sent to the manufacturer. The assembly view is shown in Figure 3.26. The drawing of the filter body and cover provides the manufacturer with the

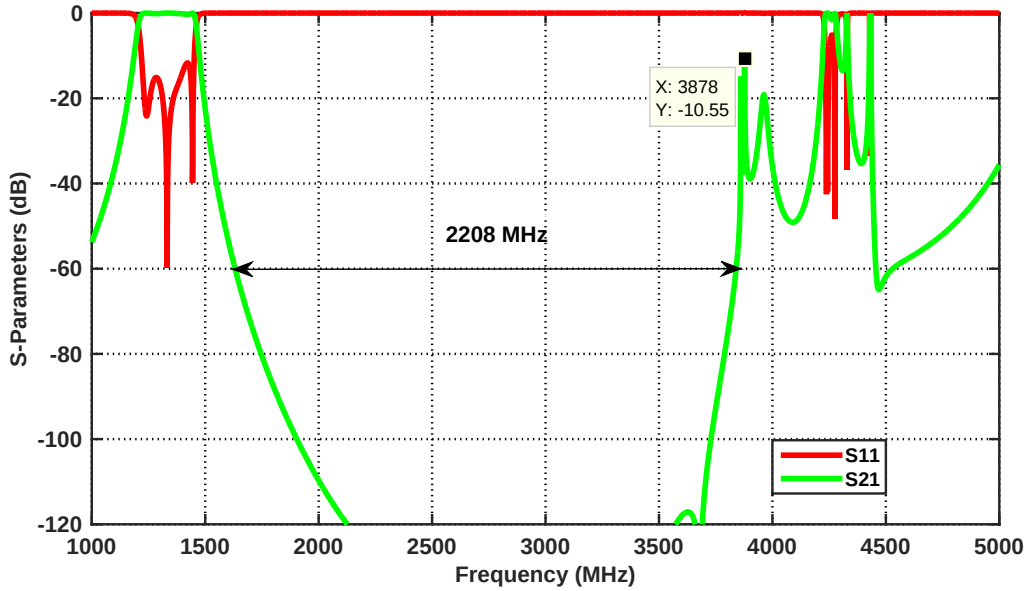

Figure 3.23: Wide band response of the optimised Chebyshev comb-line band pass filter (N= 6, RL =20, $f_0 = 1300\,\text{MHz}$, $\Delta = 16.153\,\%$)

Table 3.7: Comparison of NeXtRAD modified specifications with ideal and simulated filter responses

Dimensions	Specifications	Ideal	Simulated (Optimised)
Centre Frequency (MHz)	1300	1300	1300
Equal ripple bandwidth (MHz)	210	210	210.15
Insertion loss (dB)	0.5	0.043	0.135
Return loss (dB)	20	20	more 20.32
Spurious free window (MHz)	-	-	2208

dimensions of the filter, while the assembly view shows the manufacturer how the components of the filter fit together. Kline Engineering was also provided with the instruction sheet given in Appendix A, Figure A.2.

The manufactured filter is shown in Figures 3.27 and 3.28. The filter will operate near the ocean, this can lead to corrosion of the filter. Aluminum alloy 6082 T6 has excellent corrosion resistance. It was used as the base material to construct the filter. This material was proposed by the manufacturer[6]. According to the investigation conducted in [3], silver plating gives resonator with lower insertion loss. Therefore, the body and cover of the filter were both silver plated.

[6] All simulations in CST [7] were carried out using Aluminum alloy 6082 T6 as the base material.

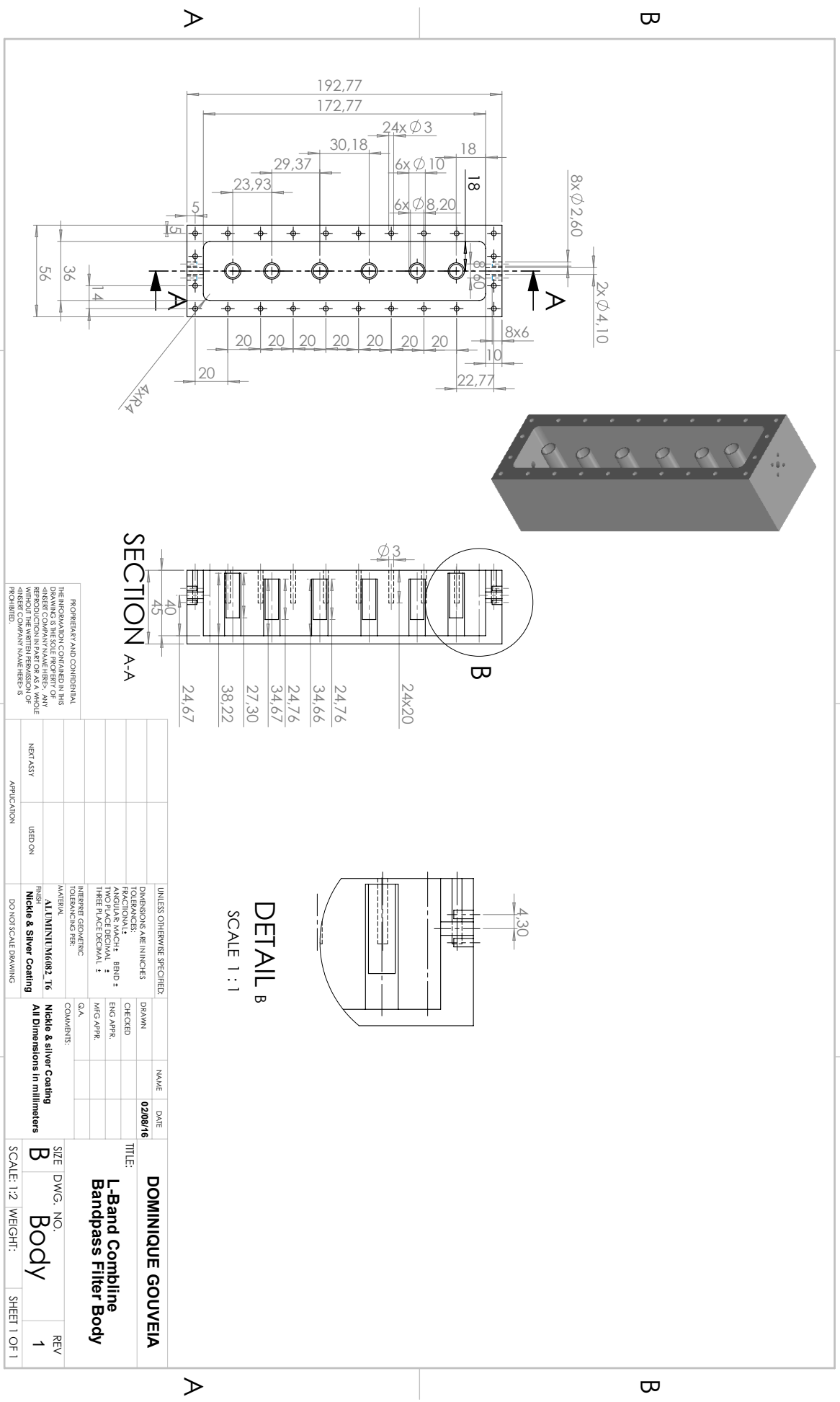

Figure 3.24: Drawing of the comb-line filter body

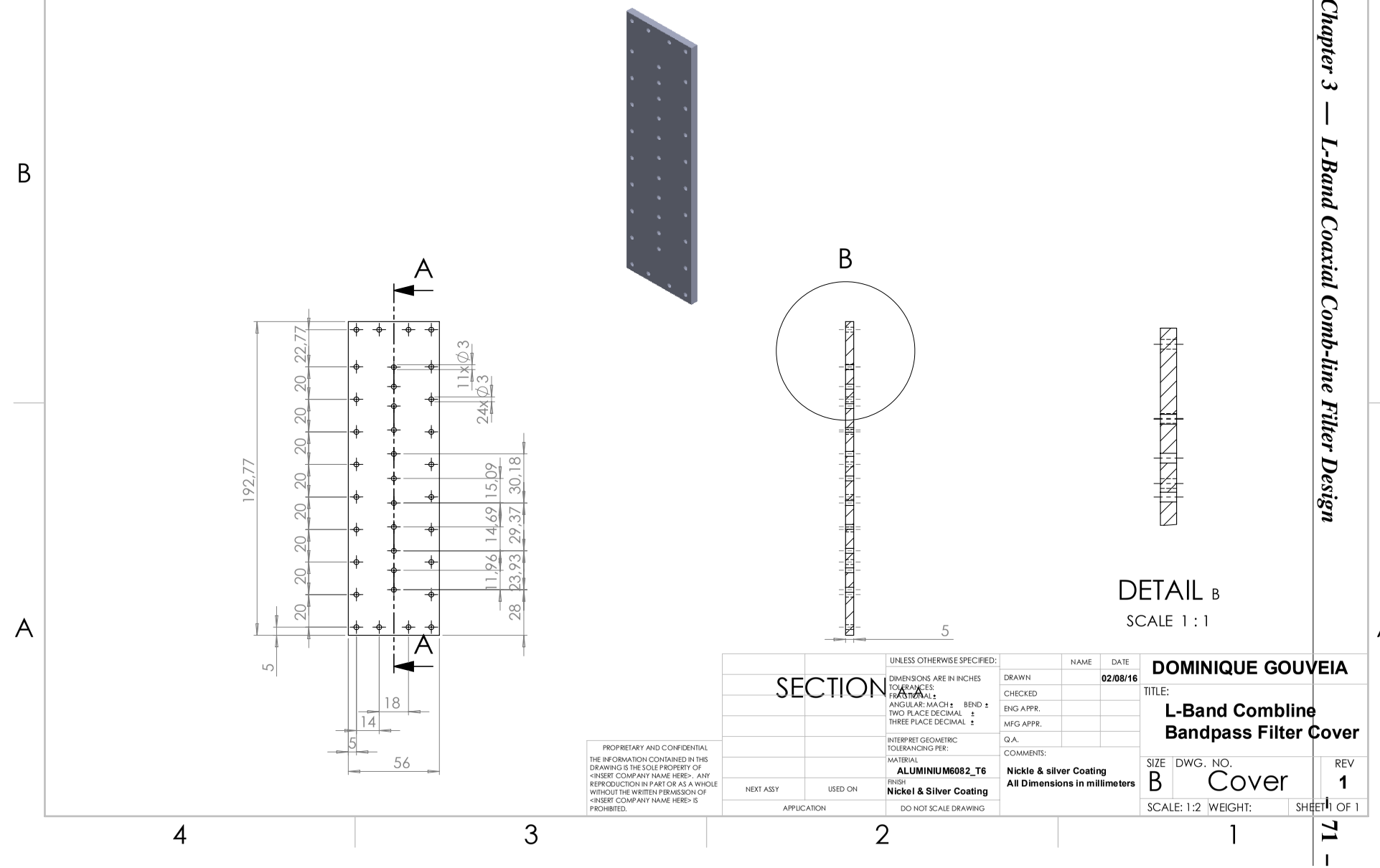

Figure 3.25: Drawing of the comb-line filter cover

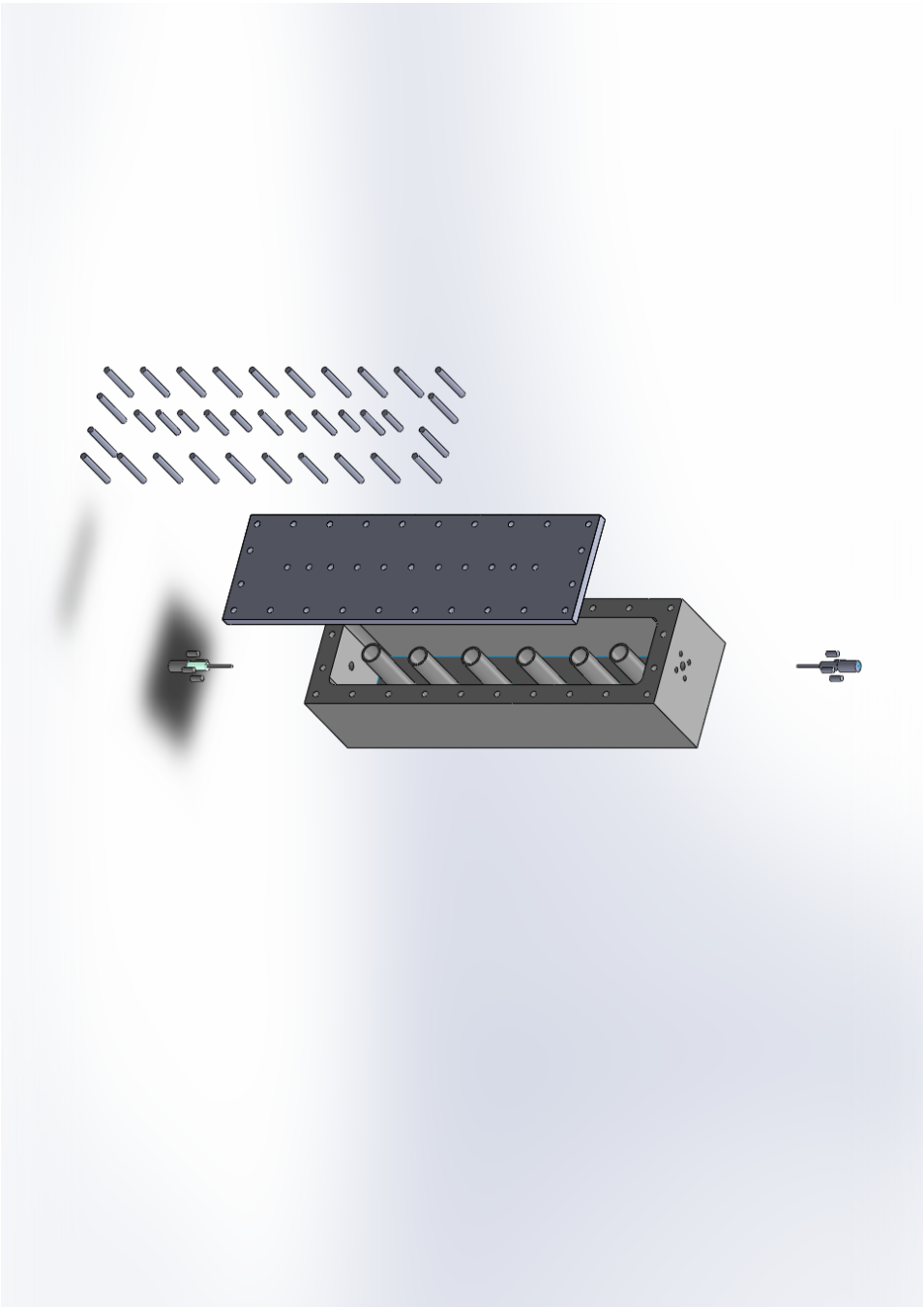

Figure 3.26: Assembly of the comb-line filter

Table 3.8: Dimensions of the designed sixth order Chebyshev comb-line filter. Width of Cavity: (W = 36), Height of Cavity: (H_1 = 40), Diameter of Rods: (D_3 = 10), Inner Diameter of Rods: (D_2 = 8.2), Diameter of Screws: (D_1 = 3), Length of Rod Screw (H_5 = 11.3), Length of Coupling Screw (H_4 = 15). All dimensions are in [mm]

Parameters	Initial Values	Optimised Values
Height of rod (H_2): 1 and 6	38.3	38.22
Height of rod (H_2): 2 and 5	35.6	34.67
Height of rod (H_2): 3 and 4	35.6	34.66
Rod Spacing (S): 1 and 5	26	23.93
Rod Spacing (S): 2 and 4	30	29.37
Rod Spacing (S): 3	30.3	30.18
Probe Height (H_3): Input/output	23.49	24.6723

The tuning screws were also silver plated. The tuning screws used were M3 50 mm long screws. These screws were locked to the cover of the filter with M3 hexagon nuts. The cover was connected to the body of the filter with M2 cheese head screws. The filter was fed from the sides with an SMA straight square flange jack receptacle connector which was screwed to the filter body with M2 screws. The SMA probe was extended by soldering an additional piece of metal at the end of the SMA probe so that the SMA probe would make direct contact with the first/last rods. The filter was then measured.

3.6 TEST RESULTS

The manufactured filter in Figure 3.27 was tested using the PNA-X 4 port N5247A network analyzer. The network analyzer operates in a frequency range from 10 MHz to 67 GHz and is a product of Agilent Technologies. The N4697-60200 1.85 mm flexicable was used to connect the filter to the network analyzer. The cable was connected to the filter through the 11901A 2.4-3.5 mm male to male adapter. These components are all products of Agilent Technologies. The calibration kit used was from Maury Microwave and it was the 3.5 mm SOLT cal KIT, with model number 8050CK and serial number 3267. The measurement set-up is shown in Figure 3.29. Calibration was done in order to remove the influence of the cables from the response of the measured filter, the red circles in Figure 3.29 indicate the reference point.

Figure 3.30 is a comparison of the narrow band response of the measured and simulated comb-line filter, while Figure 3.31 shows the comparison the wide band response. The insertion loss and group delay of both filters are presented in Figure 3.32 and 3.33 respectively. An adjacent comparison of the specifications, measurement, and simulation is presented in Table 3.9.

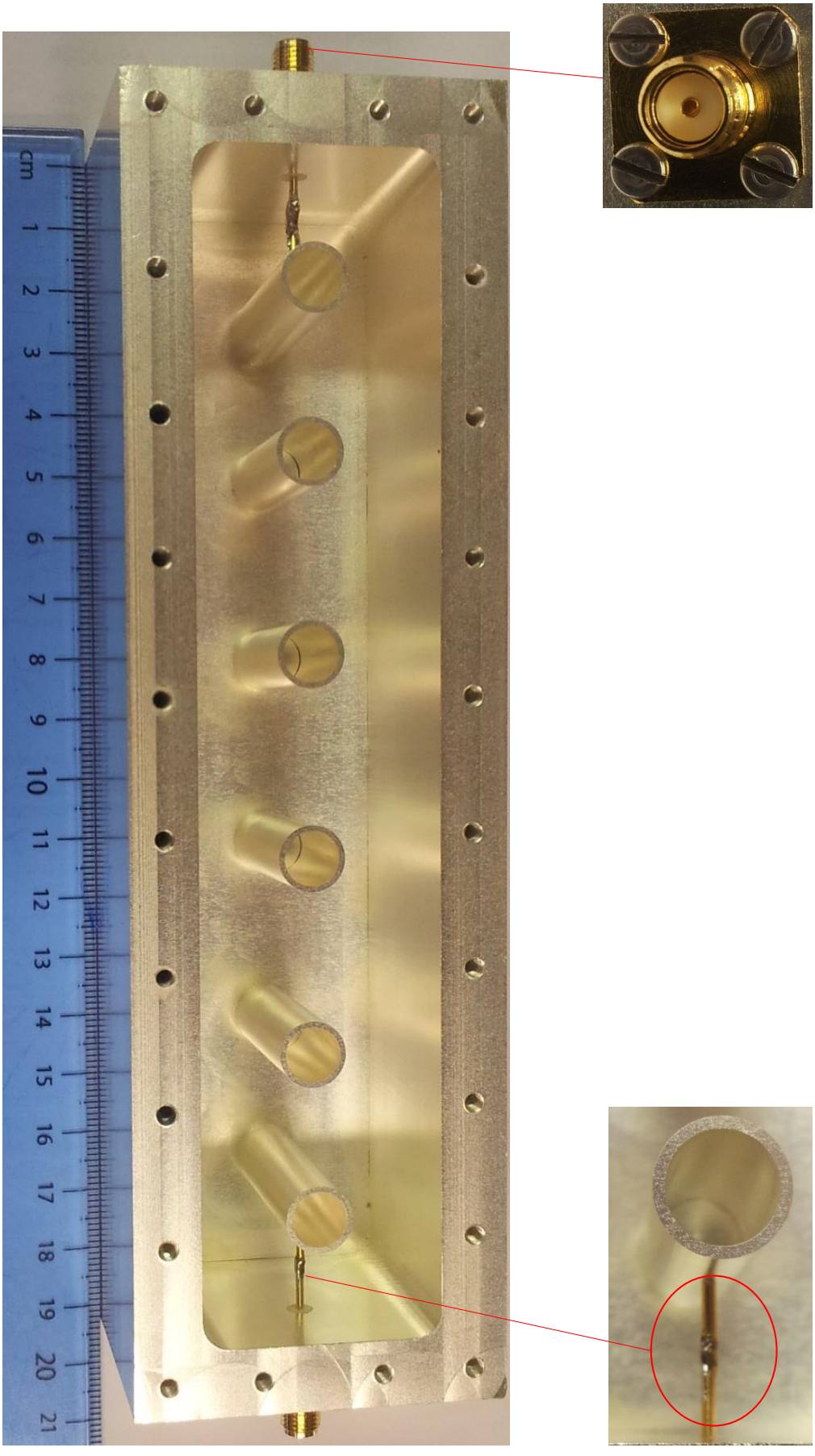

Figure 3.27: Manufactured comb-line filter by Kline Engineering

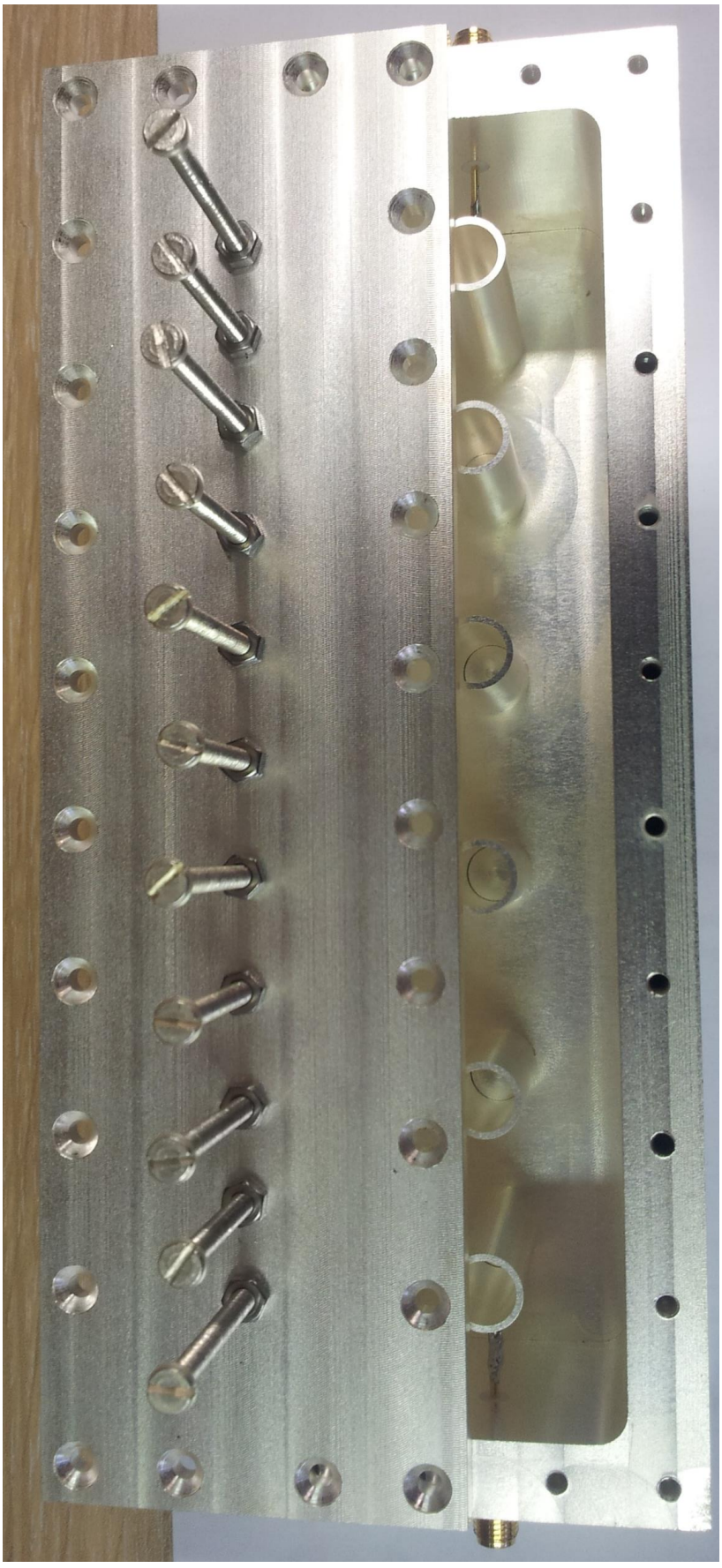

Figure 3.28: Manufactured comb-line filter by Kline Engineering with cover

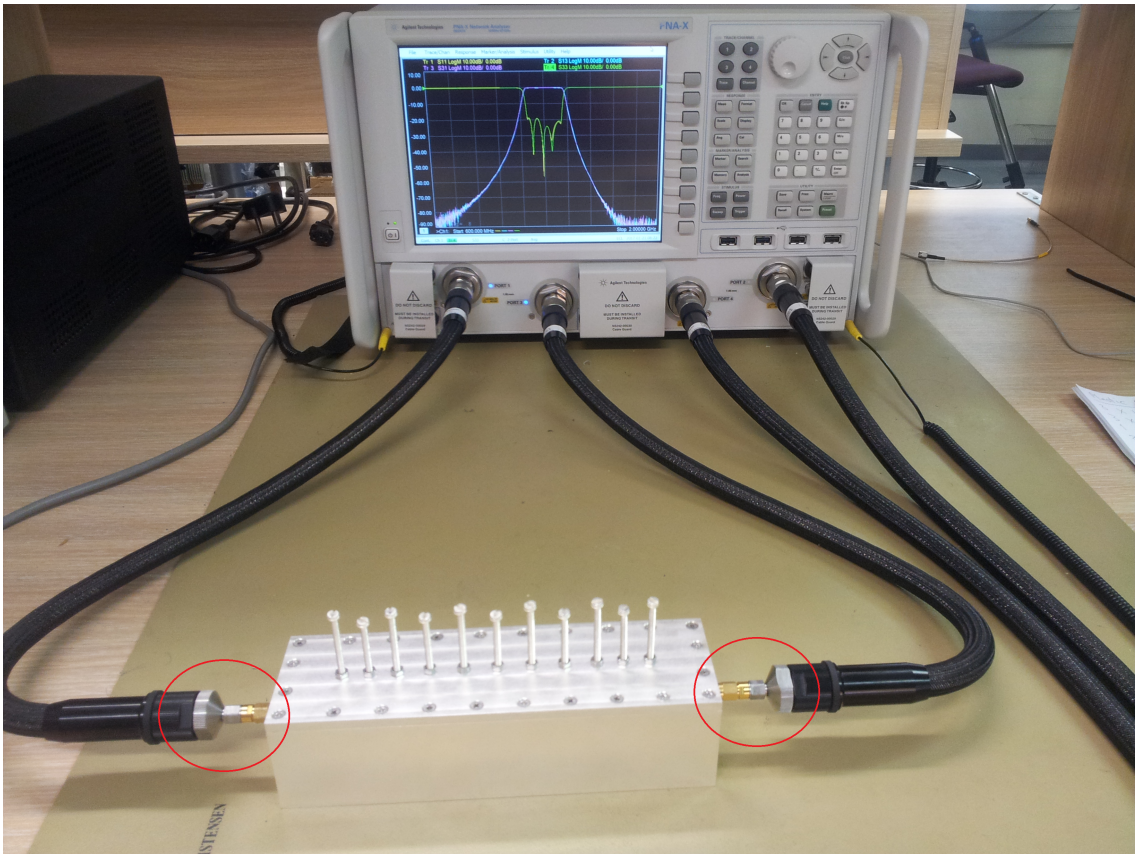

Figure 3.29: Measurement set-up for the L-band comb-line filter

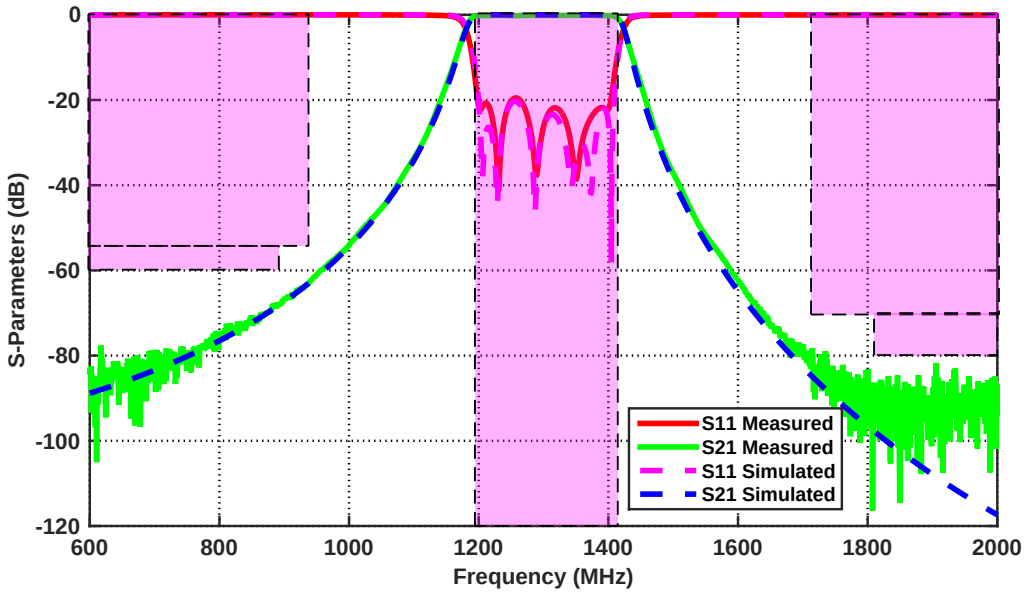

Figure 3.30: Narrow band measured response compared with optimised response for Chebyshev comb-line band pass filter (N= 6, RL =20, $f_0 = 1300\,\mathrm{MHz}$, $\Delta = 16.153\,\%$)

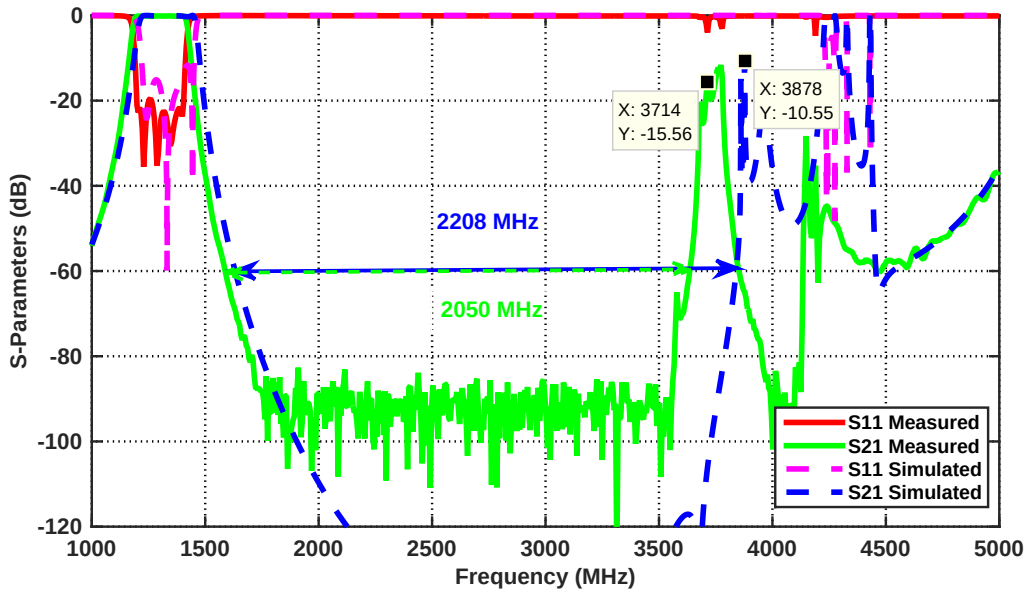

Figure 3.31: Wide band response of the measured and optimised Chebyshev comb-line band pass filter (N= 6, RL =20, $f_0 = 1300\,\text{MHz}$, $\Delta = 16.153\,\%$)

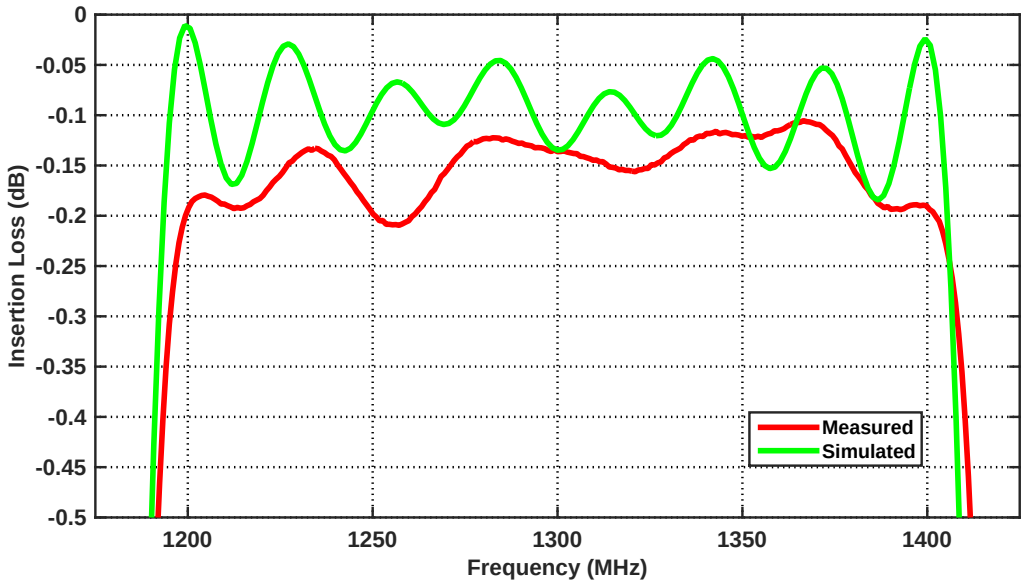

Figure 3.32: Insertion loss response of the measured and simulated Chebyshev comb-line band pass filter (N= 6, RL =20, $f_0 = 1300\,\text{MHz}$, $\Delta = 16.153\,\%$)

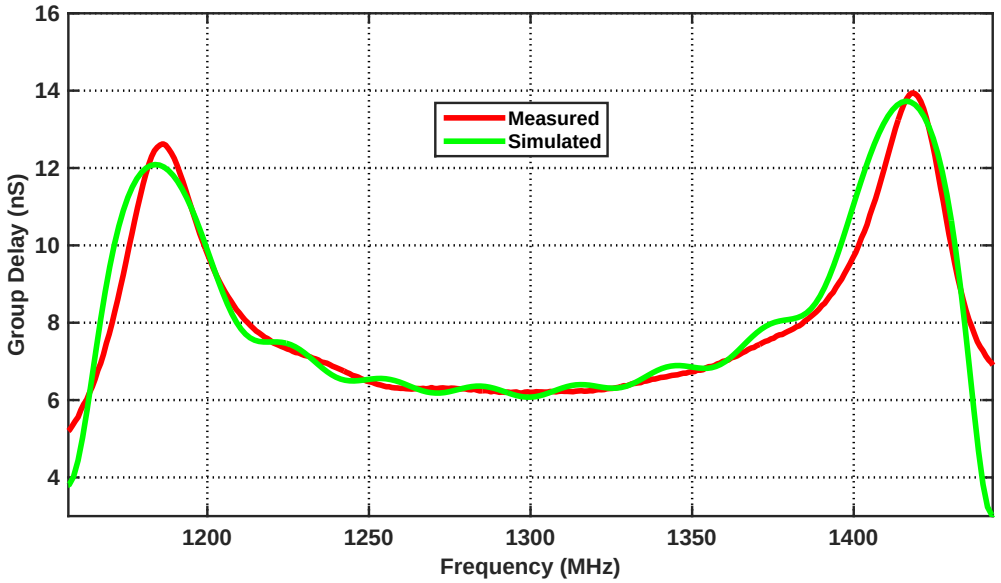

Figure 3.33: Group delay response of the measured and simulated Chebyshev comb-line band pass filter (N= 6, RL =20, $f_0 = 1300\,\mathrm{MHz}$, $\Delta = 16.153\,\%$)

Table 3.9: Comparison of specifications, simulated and measured filter responses

Dimensions	Specification	Simulated	Measured
Centre Frequency (MHz)	1300	1300	1300
Equal ripple bandwidth (MHz)	210	210.15	210
Insertion loss (dB)	0.5	0.135	0.14
Return loss (dB)	20	more 20.32	more 19.52
Group Delay (nS)	-	6.13	6.19
Spurious free window (MHz)	-	2208	2050

3.7 CONCLUSION

The L-band Coaxial comb-line filter was designed, manufactured and measured. The narrow band measurement results showed that the filter was centred at 1300 MHz, with an equal ripple bandwidth of 210 MHz. The spurious-free window at - 60 dB was measured to be 2050 MHz, with the first spurious at 2.86 times the operating frequency. The return loss of the filter was measured to be more than 19.52 dB, and the insertion loss at mid-band was 0.14 dB. It is interesting to note that the bandwidth of the measured filter did not increase above the specified value. An increase in bandwidth would be expected if the classical method to design the comb-line filter was used. However, here the filter was designed using the external quality factor and coupling coefficients parameters, instead of the self and mutual capacitance used in the classical

technique.

Moreover, the filter has very low insertion loss. This may be attributed to the large ground plane spacing used to design the filter. When the ground plane spacing become an appreciable fraction of the wavelength, the comb-line filter behaves like an evanescent mode filter, as stated before, and these filters have very low loss. Furthermore, the spurious performance of the filter agrees well with the theory. The second pass band occurs at 2.86 times the operating frequency. Figure 3.34 shows the manufactured filter being used at the RF Front End of the NeXtRAD system.

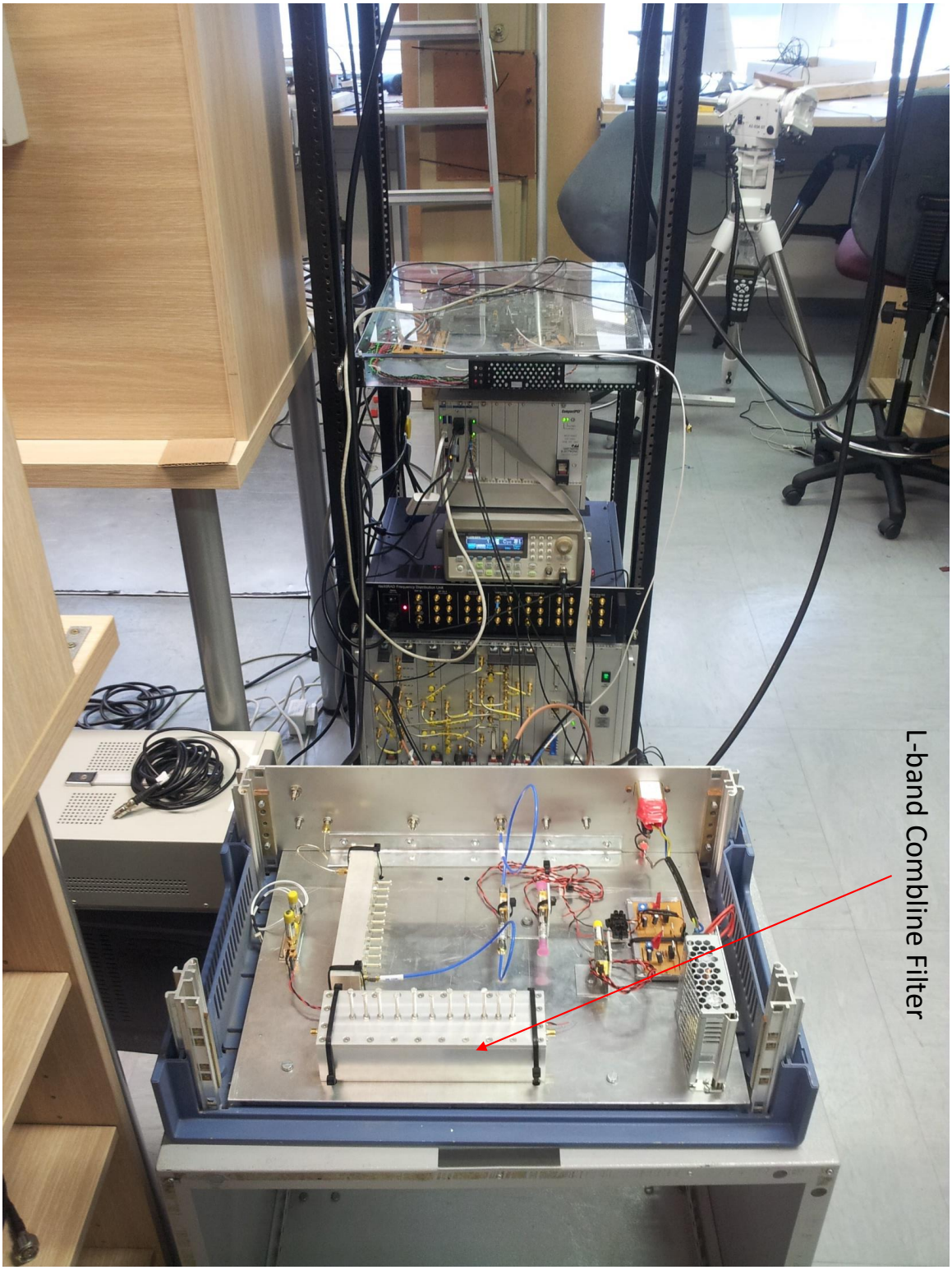

Figure 3.34: The L-band comb-line filter used at the RF front end of the NeXtRAD System

CHAPTER 4

X-BAND WAVEGUIDE INDUCTIVE IRIS COUPLED FILTER DESIGN

4.1 INTRODUCTION

Waveguide band pass filters perform valuable functions in microwave systems used in radar and other applications. Despite more recent technologies, waveguide band pass filters operating above 8 GHz are still used in microwave systems for precision design, high power levels, low insertion loss and adequate stop band selectivity [32].

This chapter follows a similar layout as Chapter 3. Section 4.2 deals with the estimation of the order of the iris coupled waveguide filter that will give the desired stop band rejection performance. A concise review of the special properties of the rectangular waveguide, inductive iris coupled waveguide filter and coaxial to waveguide transition are presented in Section 4.3. The design and analysis of the inductive iris coupled waveguide filter are discussed in Section 4.4. The fabrication process of the filter is discussed in Section 4.5. Section 4.6 presents the measured results of the filter. Finally, the results are discussed in Section 4.7 to conclude this chapter.

4.2 ESTIMATION OF X-BAND FILTER ORDER AND STOP BAND REJECTION

The NeXtRAD X-band synthesizer operates from 8.5 GHz to 10.5 GHz. Initially, the X-band filter was to be designed for this frequency range. That is, a 2 GHz wide band filter, with a fractional bandwidth of about 21.2 %, was required by NeXtRAD. However, the high power amplifier of the NeXtRAD system operates in a frequency range below the X-band synthesizer. The high power amplifier operates from 8.4 GHz to 8.5 GHz. Signals with frequencies above

8.5 GHz will be distorted by the high power amplifier. Due to this, the bandwidth of the filter was limited to 50 MHz, a narrow band filter, with a fractional bandwidth of about 0.588 % at a centre frequency of 8.5 GHz as presented in Table 1.2.

The bandwidth specification in Table 1.2 was modified by adding a 100 MHz margin, to compensate for any drift in the centre frequency due to temperature changes and manufacturing tolerances. The X-band filter order and stop band performance were estimated from the modified specifications in Table 4.1. For a Chebyshev response, a fifth order filter was estimated from Equation (2.7). The admittance circuit model in Figure 4.1 was used to simulate an ideal filter response, as shown in Figure 4.2. Table 4.1 compares the ideal filter response with the modified specifications of NeXtRAD.

Table 4.1: Modified NeXtRAD specifications versus ideal 5^{th} order circuit theory filter response

Parameters	Specifications	Ideal circuit model
Pass band	8.425 GHz to 8.575 GHz	8.425 GHz to 8.575 GHz
Centre Frequency	8.5 GHz	8.5 GHz
Return Loss	20 dB (min)	25 dB
Equal Ripple Bandwidth	150 MHz	150 MHz
Fractional Bandwidth	1.764 %	1.764 %
Stop band		
Frequency/GHz	Attenuation/dB (min)	Attenuation/dB (min)
8.2	45	59.15
8.8	45	58.27
Input/output Impedance	50 Ω	50 Ω

4.3 THE PROPERTIES OF WAVEGUIDES

Waveguides are hollow metallic[1] pipes that confine and guide electromagnetic waves above a certain cutoff frequency with minimal loss from one point to another in a system [8] and [13]. Figure 4.3 shows pictures of some commercially available waveguides. Waveguides are able to propagate an infinite number of modes; these modes are denoted as $\mathrm{TE}_{m,n}$ (transverse-electric) and $\mathrm{TM}_{m,n}$ (transverse-magnetic) that satisfy the Maxwell equations [33] and [13]. For $\mathrm{TE}_{m,n}$ modes, the electric field in the direction of propagation is zero ($\mathrm{E_z} = 0$), while in the case of the $\mathrm{TM}_{m,n}$ modes, the magnetic field in the direction of propagation is zero ($\mathrm{H_z} = 0$) [33]. Usually, waveguides are operated to propagate energy in a single mode, the mode which is selected to carry the energy is termed the dominant mode [13].

[1] Not all waveguides are metallic

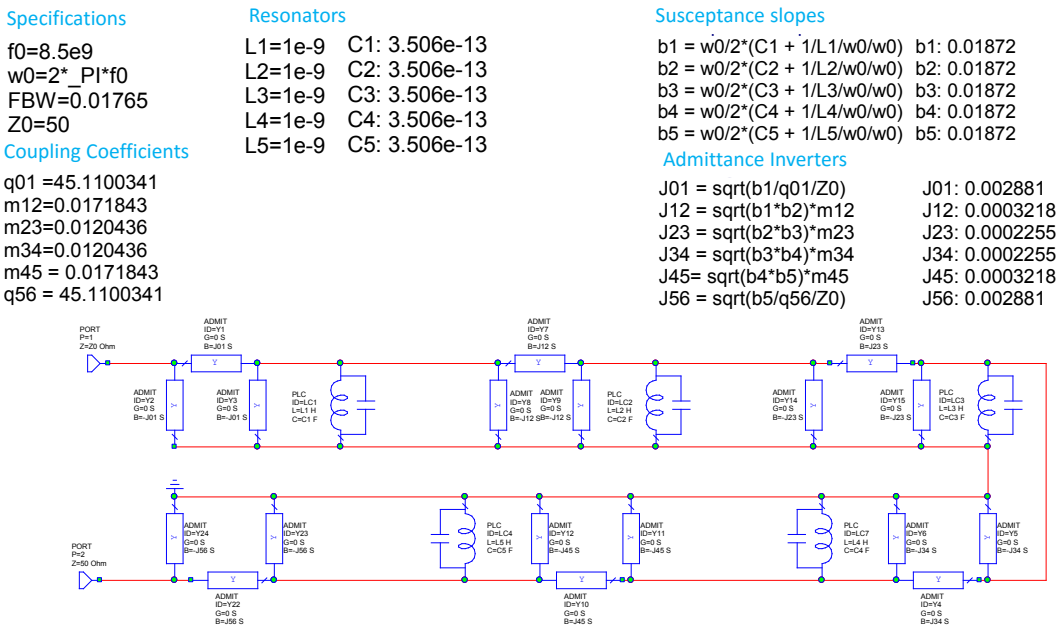

Figure 4.1: J-inverter circuit model for a 5^{th} order Chebyshev band pass filter

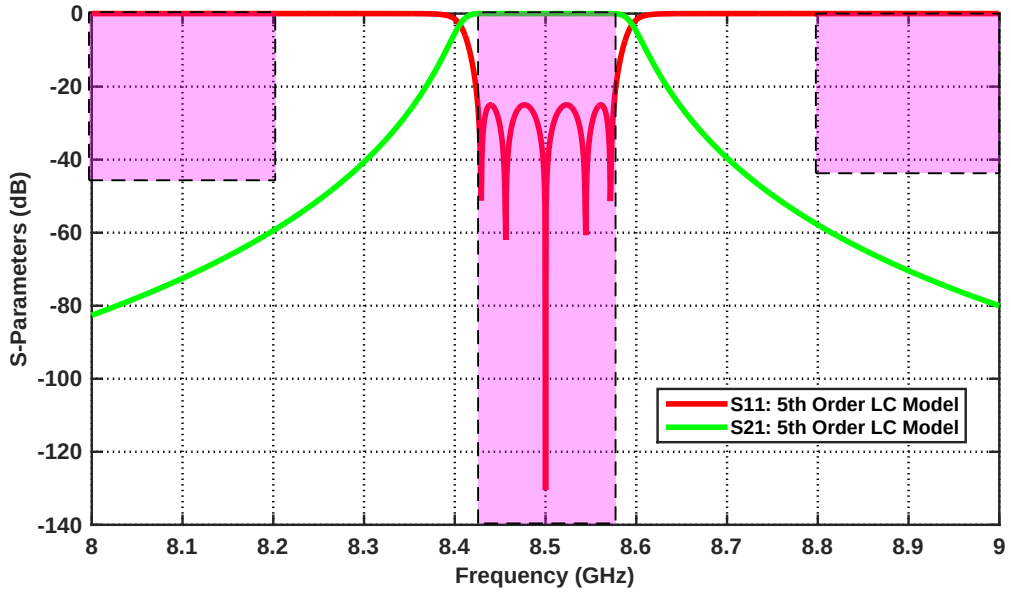

Figure 4.2: Circuit theory model response for Chebyshev filter (N= 5, RL =25, $f_0 = 8.5\,\text{GHz}$, $\Delta = 1.764\,\%$)

Figure 4.3: Pictures of waveguides used regularly in practice. Moving clockwise from top right, a circular waveguide, a magic tee waveguide, a flexiguide and rectangular waveguide from [34]

4.3.1 **Rectangular Waveguide**

The rectangular waveguide is the most popular and most often used waveguide [13]. This is because the rectangular waveguide is easier to manufacture as opposed to the circular waveguide [33] and [13]. The rectangular waveguide has low loss and good power handling capability. But, it is very bulky and difficult to integrate with active components [33]. Figure 4.4 shows a rectangular waveguide. The $\mathrm{TE}_{1,0}$ mode is the fundamental mode in a rectangular waveguide. Figure 4.5 shows the electric and magnetic fields distribution inside the waveguide of the fundamental $\mathrm{TE}_{1,0}$ mode.

The guide wavelength of a rectangular waveguide operating in $\mathrm{TE}_{1,0}$ mode is given as

$$\lambda_{g_0} = \frac{\lambda_0}{\sqrt{1 - \left(\frac{\lambda_0}{2a}\right)^2}}, \tag{4.1}$$

where λ_{g_0} is the guide wavelength and λ_0 is the free space wavelength.

The cutoff frequency, f_c of the waveguide is given as

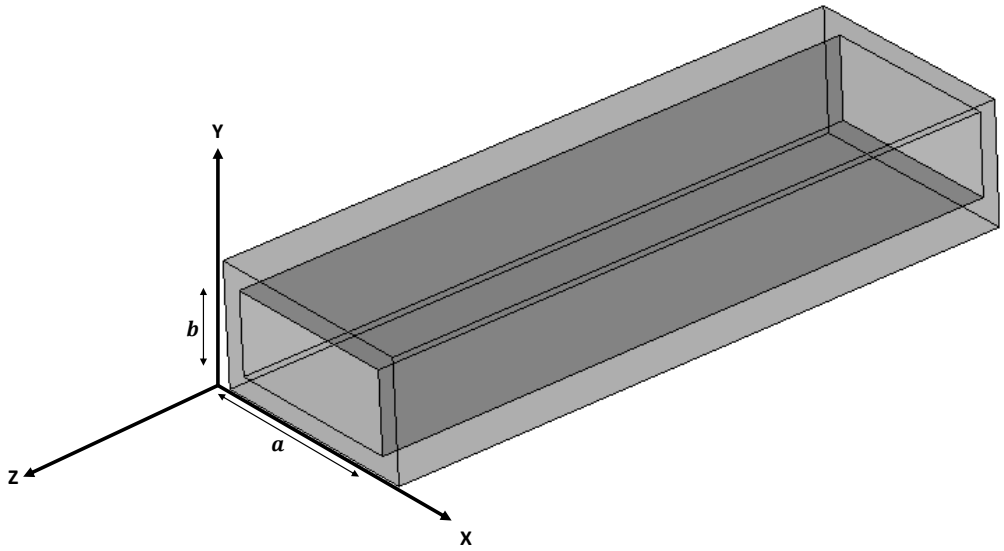

Figure 4.4: A rectangular waveguide consisting of arbitrary lateral dimensions a and b, and outer metallic plates (conducting walls) CST [7]

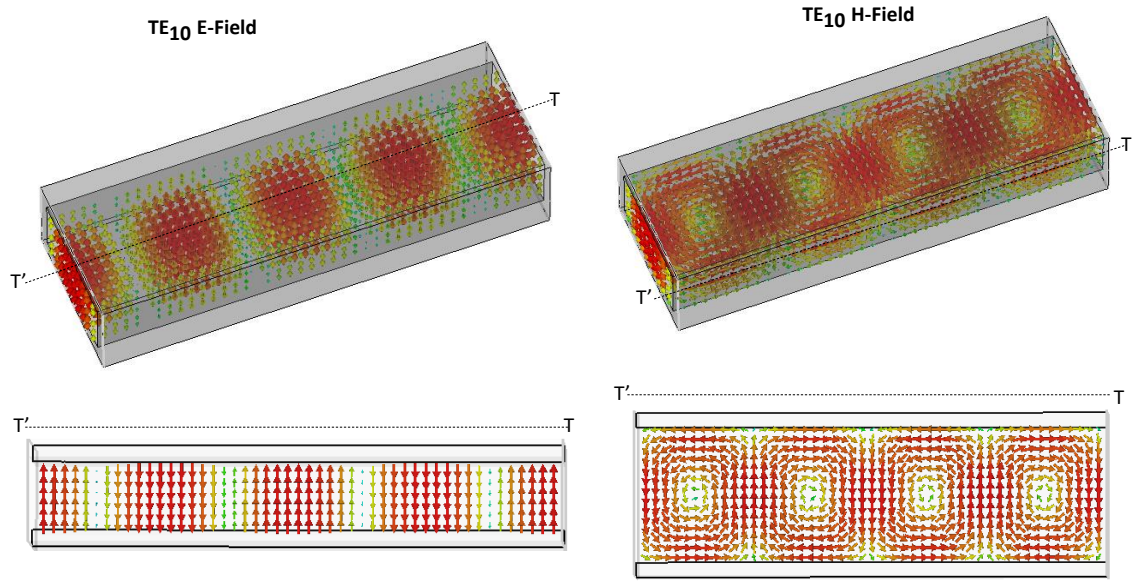

Figure 4.5: The electric and magnetic fields of the fundamental $\mathrm{TE}_{1,0}$ mode inside a rectangular waveguide CST [7]

$$f_c = \frac{c_0}{2a}, \tag{4.2}$$

where c_0 is the speed of light.

4.3.2 Rectangular Cavities

The rectangular waveguide is often used as cavity resonators in band pass filters, due to their extremely high unloaded quality factor, which ranges from 5000 to 10 000 [35]. The resonant frequency of the fundamental $\mathrm{TE}_{1,0}$ mode of a rectangular waveguide is [5]

$$f_0 = \frac{c_0}{2\pi}\sqrt{\left(\frac{\pi}{a}\right)^2 + \left(\frac{\pi}{d}\right)^2}, \tag{4.3}$$

where a is as defined in Figure 4.4, d is the length of the rectangular cavity along the direction of propagation (z).

4.3.3 Inductive Iris Coupled Waveguide Band pass Filter

A waveguide band pass filter can be built from uniform lengths of waveguide sections, loaded with shunt discontinuities. A shunt inductive iris coupled waveguide filter is shown in Figure 4.6. The filter is made up of series connected uniform waveguide cavities. The cavities are a half a guide wavelength long and are used to store the fundamental TE_{101} mode.

The cavities are coupled by symmetrical inductive[2] irises[3] placed transversely across the broad wall of the filter. These irises offer inductive reactance across the rectangular waveguide when the waveguide is excited in dominant mode [36].

An incident TE_{10} mode on the iris junction will excite higher order evanescent TE and TM modes near the junction, so as to satisfy the boundary condition of zero total tangential electric fields on the irises [36]. This fact is seen in Figure 4.7, which shows that the electric field across the iris junction is predominantly perpendicular to the junction, and the magnetic field is tangential to the junction.

The higher order modes do not propagate, but decay within a distance of a quarter wavelength from the junction [36]. These higher order modes perform the function of storing reactive energy at the junction. The irises in Figure 4.6 affect mainly the magnetic field of the fundamental

[2] Capacitive reactance can be offered too, depending on the obstacle used across the narrow or broad wall of the waveguide.

[3] Also called windows or diaphragms

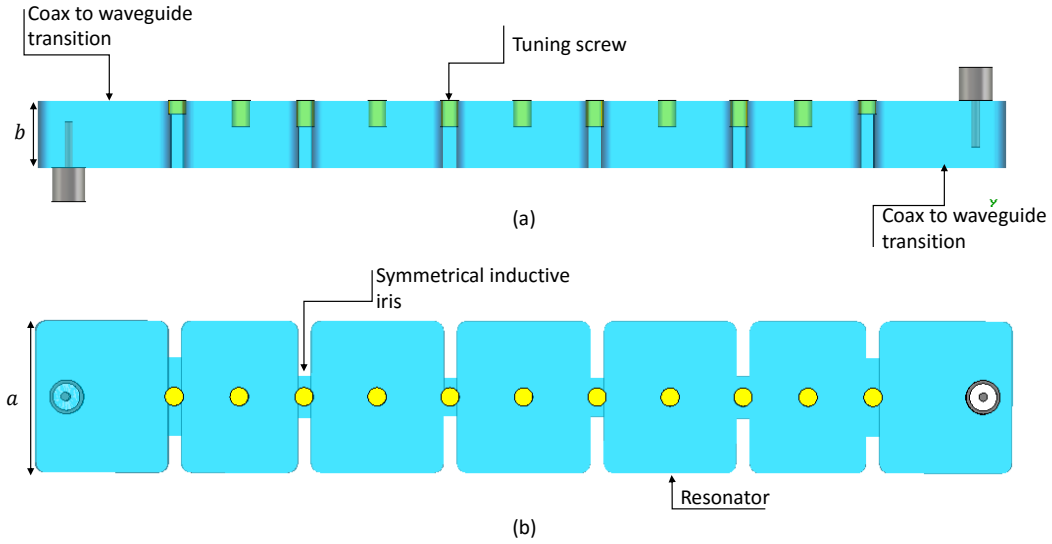

Figure 4.6: Shunt inductive iris coupled waveguide filter CST [7]

TE_{10} mode, and therefore, stores predominantly magnetic energy [36].

Tuning screws are used to tune the centre frequency and the bandwidth of the filter. The screws are inserted perpendicularly into the cavities, through the centre of the guide broad wall. They provide reactance across the broad side of the waveguide, which may be varied from capacitive to inductive, by changing the penetration depth of the screw into the cavity [36]. The filter is fed by a coaxial to waveguide transition positioned on opposite sides of the broad wall of the filter. Figure 4.8 shows examples of practical waveguide filters.

4.3.4 Coaxial to Rectangular Waveguide Transition

The principle to excite or detect a desired waveguide mode should maximize the energy exchange or transfer between the source and the waveguide or the waveguide and the receiver [35]. The energy exchange could be between two waveguides, a linear electrical probe (monopole antenna) to a waveguide, or a magnetic loop (loop antenna) to a waveguide and so on [35]. Figure 4.9 (a) shows a transition from a coaxial electrical probe to a waveguide. The electrical probe excitation is the simplest technique and is commonly found in literature [35]. The centre probe of the coaxial connector is inserted into the waveguide through the broad wall of the guide and is oriented to be parallel to the electric field of the TE_{10} mode in the waveguide. To ensure maximum energy transfer, the probe is placed near the maximum of the electric field of the TE_{10} mode. This scheme only excites the electric field of the TE_{10} mode, a magnetic loop can be used to excite the magnetic field of the TE_{10} mode.

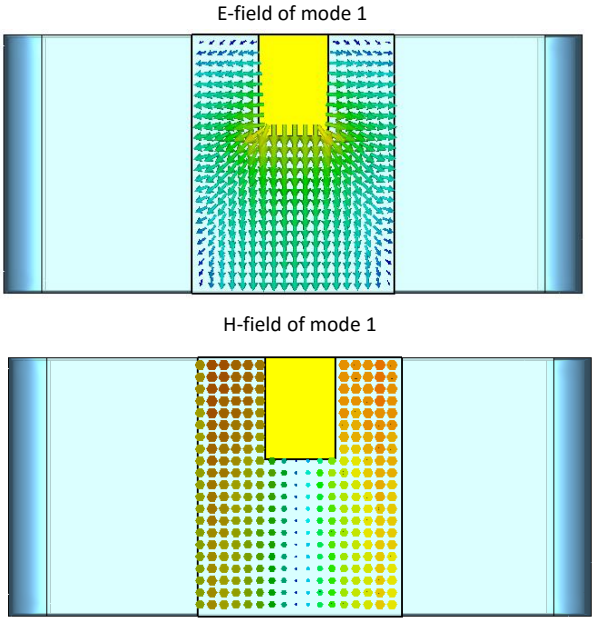

Figure 4.7: E-field and H-field of mode 1 at the iris junction CST [7]

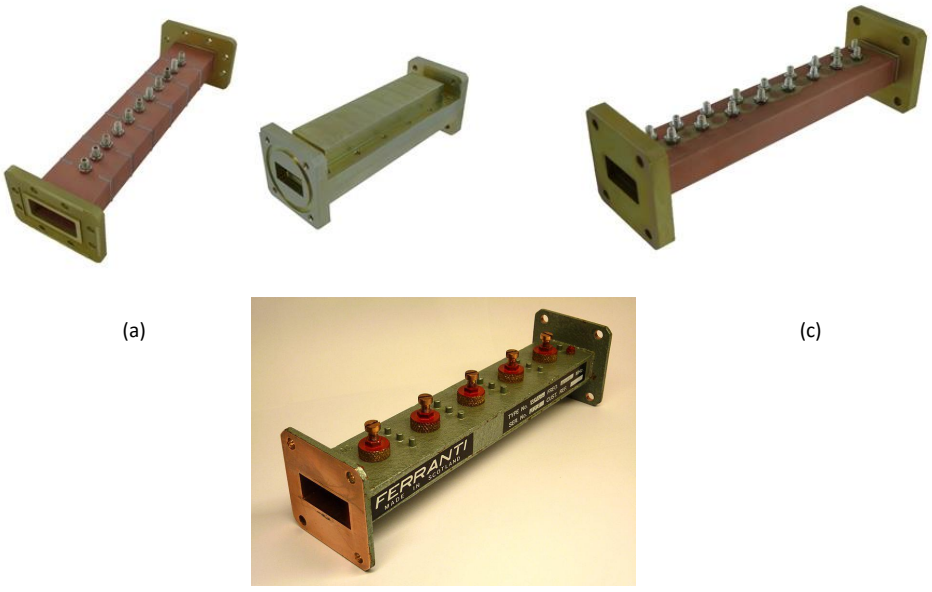

Figure 4.8: (a) Waveguide receive reject filter from [37]. (b) Waveguide band pass filter from [38]. (c) WG15 triple post waveguide bandpass filter from [39]

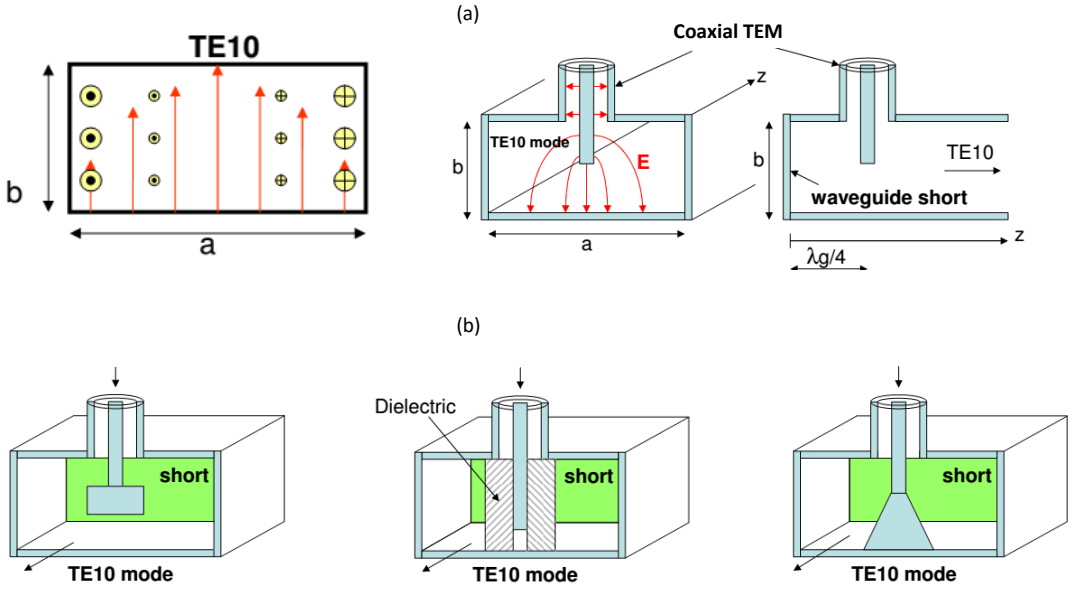

Figure 4.9: Coaxial to rectangular waveguide transition using an electrical probe to excite the electric field of the TE_{01} mode. (a) Coaxial to waveguide transition for narrow band matching. (b) Modifications done to (a) for broadband matching from [41]

The electrical probe inside the waveguide acts as an impedance transformer, transforming the low impedance of the coaxial connector, typically 50 Ω, to the high impedance of the waveguide, which is typically greater than the impedance of free space, which is 377 Ω [40]. A longer probe will produce a lower impedance in the waveguide. In Figure 4.9 (a) the probe is positioned approximately a quarter of the guide wavelength away from the waveguide short. Ideally, the waveguide short at the position of the probe should act like an open circuit and adds no reactance to the probe. However, in practice, the waveguide short must be varied along with the length of the probe to tune out the reactance of the probe, so as to match the probe to the waveguide. The impedance matching technique in Figure 4.9 (a) is used for narrow band matching. Modifications can the done to the transition network of Figure 4.9 (a) for broadband matching. These modifications are shown in Figure 4.9 (b). Examples of practical coaxial to waveguide transitions are shown in Figure 4.10.

4.4 Design and Analysis Iris coupled Waveguide Filter

The desired filter is shown in Figure 4.11, along with all the design parameters considered in this chapter. A perspective view of the filter in Figure 4.11a shows that the iris coupled filter is made up of five resonators, hence a fifth order filter. Tuning screws are placed into the waveguide cavities through the centre of the broad wall of the waveguide. The cavities are coupled together by means of irises. Irises are also used to couple the input/output cavities to

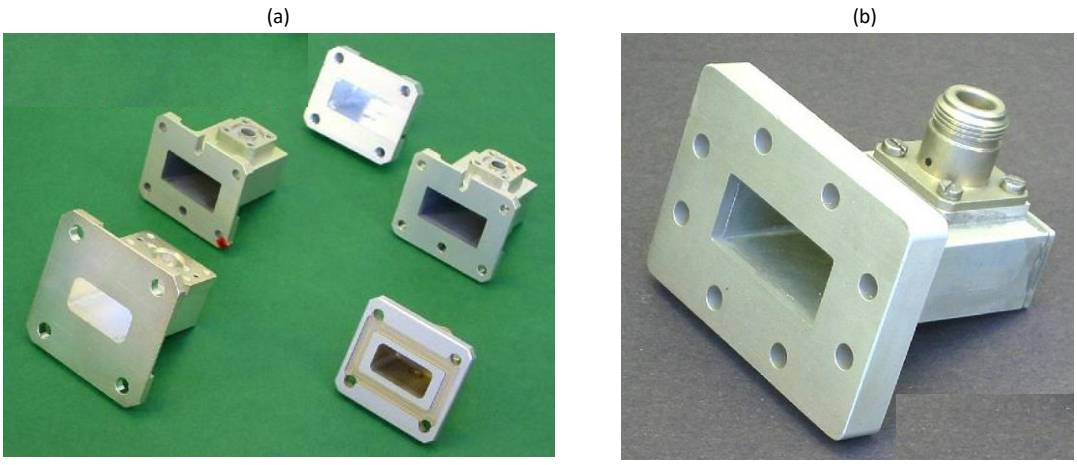

Figure 4.10: Examples of coaxial to rectangular waveguide transitions from [42]

the coaxial to waveguide transition. Tuning screws are also inserted through the iris junctions as shown in Figure 4.11a. The filter is fed with a coaxial to waveguide transition using the electrical probe technique in Figure 4.9 (a).

The filter operates at 8.5 GHz, with a fractional bandwidth of 1.76 % and a return loss of at least 20 dB. A cross-sectional view of the filter detail is shown in Figure 4.11b. The impedance matching of the coaxial to waveguide transition is determined by the parameters P_1 and P_2, which determine the return loss level of the filter. The parameters S_1, S_2 and S_3 are used for post-manufacture tuning of the input/output coupling, the interresonator coupling and the centre frequencies of the cavities respectively. The centre frequency of the filter is set by the parameters L_1 to L_4 as shown in Figure 4.11c. The interresonator coupling is achieved by designing for the parameters A_1 to A_3. Finally, the corner radius R is specified by the manufacturer.

4.4.1 Waveguide Filter Design Methods

The physical parameters of the iris coupled waveguide filter in Figure 4.11 can be determined by using the impedance inverter model in Figure 2.15. An example of this technique is shown in [5]. The technique assumes that the irises embedded in the waveguide can behave like an impedance inverter. An equivalent T network is then used to represent the irises. The S-parameters of the irises is related to the T network. By performing a full-wave simulation of the coupling iris between to cavities, the S-parameters of the dominant TE_{10} mode can be obtained.

The S-parameters are then used to calculate the parameters of the T network, which are in turn related to the impedance K of the inverters. Therefore, by varying the width of the iris, a plot can be made of K versus the iris width. The equations for this technique is provided in [5].

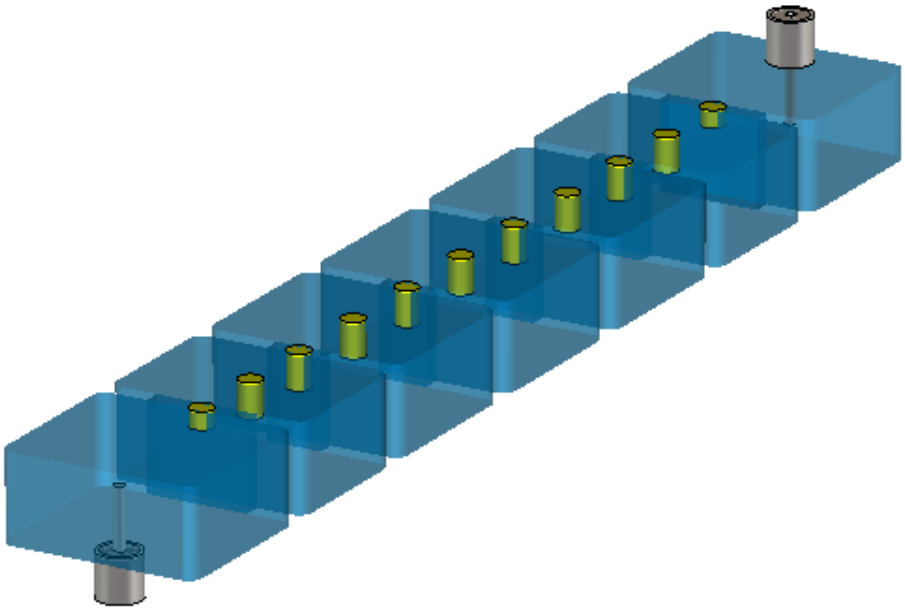

(a) Perspective view

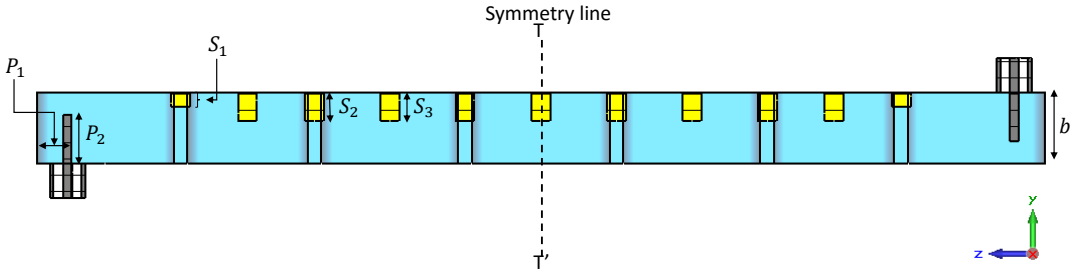

(b) X-plane view

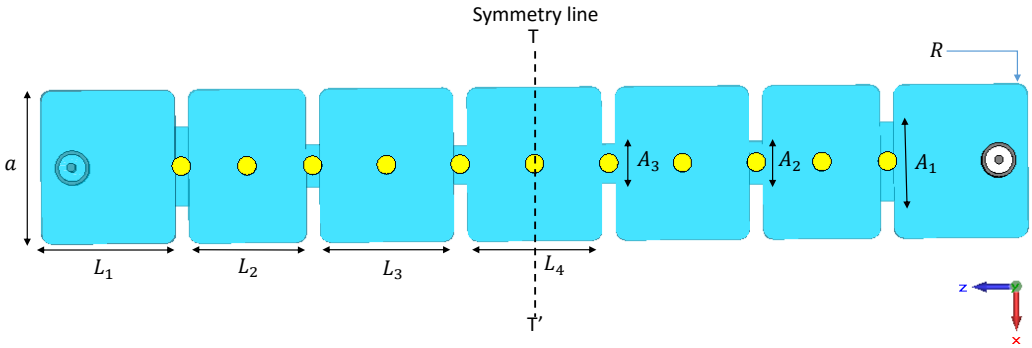

(c) Z-plane view

Figure 4.11: Field-solver model for the N = 5 Iris coupled waveguide filter: (a) perspective view of the complete filter; (b) X-plane view of the half model with design parameters; and (c) Y-plane view of the model with design parameters. The tuning screws are inserted through the broad wall of the resonators. Note: the filter is symmetrical excluding the probes. Also, the mirrored type feed configuration was requested by NeXtRAD. CST [7]

This technique yield a good initial response because the K-impedance inverter model makes it possible to accurately include the effects of the iris loading on the resonators [5]. However, this technique takes more time to calculate the desired filter parameters, compared to using the coupling coefficients and the external quality factor. This is due to the equations involved in calculating K, and also the construction of the curves are usually done using a different program than that used to calculate the S-parameters. However, it provides a very good initial solution as opposed to the coupling coefficients and the external quality factor method using an eigenmode solver, hence saving on optimization time. Nevertheless, the coupling coefficients and the external quality factor method was used, as done in Chapter 3, because the design parameters could be obtained very quickly from one software, instead of using an additional software such as Matlab to plot the K versus Iris width graphs.

4.4.2 Waveguide Resonator Design

The design of the rectangular cavity, unlike the coaxial cavity, is much simpler. The physical parameters which determine the electrical characteristics of the rectangular cavity are shown in Figure 4.12. The standard X-band WR90 RG-52/U rectangular waveguide was chosen for the design of the cavity. This waveguide has a cutoff frequency of 6.557 GHz for the TE_{10} mode, and dimensions $a = 22.86$ mm and $b = 10.16$ mm. The length L = 27.57 mm of the resonator was calculated from Equation (4.1) as half the guide wavelength.

The bend radius R = 2 mm of the cavity was specified by Kline Engineering for a cavity height b= 10.16 mm. A standard M3 tuning screw of length S_3 = 4 mm was used. The length (L) of the resonator was reduced to L = 21 mm, to compensate for the shift in the resonant frequency due to the insertion of the tuning screw. The results of a full-wave simulation and the physical parameters of the cavity are shown in Tables 4.2 and 4.3.

Table 4.2: Comparison of rectangular waveguide cavity with and without tuning screw

Dimensions	No Screw	Screw
Mode1 (GHz)	8.5	8.5202
Mode 2 (GHz)	12.629	15.064
Q Mode1	5247	4570.300
Q Mode2	6516.6	6351.85
Spurious (GHz)	4.129	6.544

Table 4.2 shows that the unloaded quality factor of mode 1 decreases with the insertion of the tuning screw into the cavity. That is the insertion loss of the filter increases. The screws are required for post-manufacture tuning of the filter. The unloaded quality factor is still reasonably high, even after the insertion of the screw. Therefore, there was no need to remove the screw

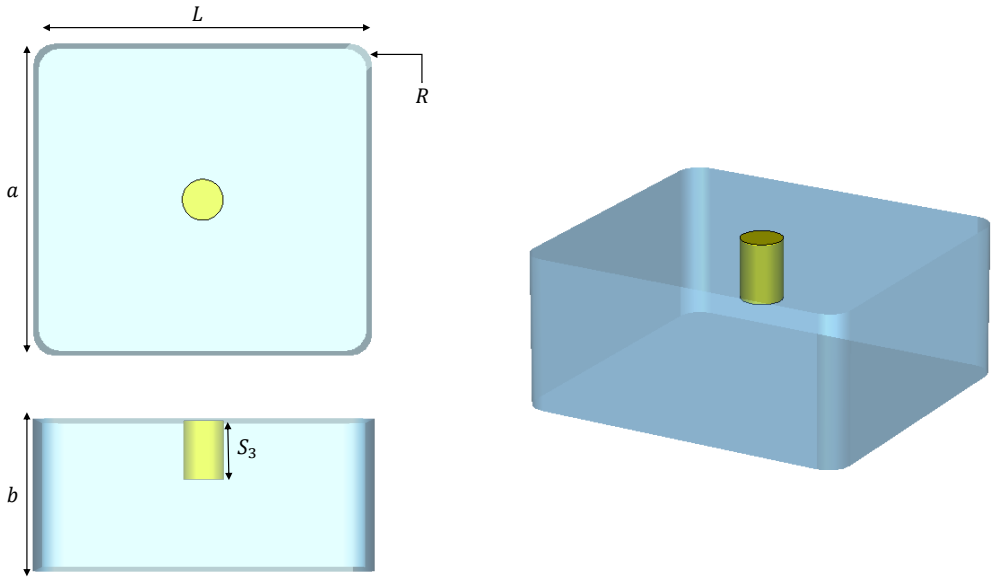

Figure 4.12: Parameter definition for rectangular waveguide cavity CST [7]

Table 4.3: Physical parameters of rectangular waveguide cavity. All dimensions are in [mm]

Dimensions	Values
Width of Cavity: (a)	22.86
Height of Cavity: (b)	10.16
Length of Cavity: (L)	21
Length of Screw: (S_3)	4
Corner Radius: (R)	2

from the design of the cavity. The insertion of the screw increases the spurious-free window of the cavity as seen in Table 4.2.

4.4.3 **Interresonator Coupling**

Table 4.4 presents the coupling coefficients and the low pass element values for the desired bandwidth. The values in Table 4.4 were obtained by selecting the return loss level of the filter to be 25 dB, then the pass band ripple was calculated from Equation 2.8. Thereafter, the low pass element values were obtained from a table in ([5], page 505). The desired coupling coefficients were calculated from Equations 2.19 or 2.20.

Figure 4.13 shows the set-up used to determine the coupling coefficient in CST [7]. The iris is 2 mm thick. The coupling coefficients can be realized by adjusting the aperture A of the iris. An eigenmode analysis for the set-up in Figure 4.13 was carried out, and the eigenmode frequencies are presented in Figure 4.14. The curves show the even and odd eigenmode frequencies as a

Table 4.4: Low pass circuit element values and interresonator coupling coefficients for N = 5 Chebyshev band pass filter

g_i	g values	$\kappa_{j,j+1}$	κ values
g_1	0.796	$\kappa_{1,2}$	0.017
g_2	1.325	$\kappa_{2,3}$	0.012
g_3	1.621	$\kappa_{3,4}$	0.012
g_4	1.325	$\kappa_{4,5}$	0.017
g_5	0.796	-	-
g_6	1	-	-

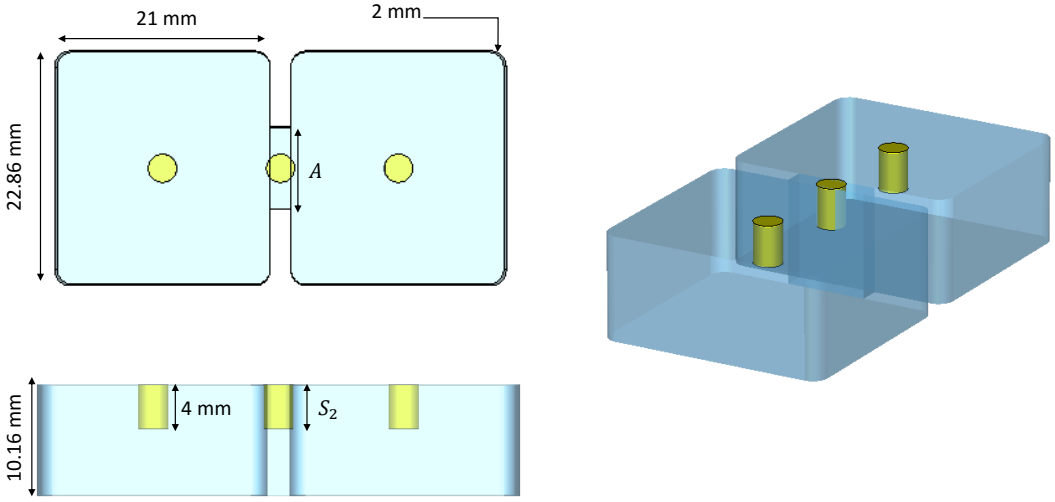

Figure 4.13: Configuration to determine the coupling coefficients of N= 5 Chebyshev band pass filter CST [7]

function of the aperture width (A) and the depth of the tuning screw (S_2). Figure 4.14 shows that the modes are separated more for higher values of A. Therefore, the coupling coefficients will be larger for higher values of A.

The modes are shifted further apart by the insertion of a tuning screw at the iris junction between the cavities, which causes the coupling coefficient to increase. The insertion depth of S_2 = 4 mm of the tuning screw into the iris junction affects both mode 1 and mode 2 over the range of A = 55 mm to A = 8 mm. Mode 1 is affected more dramatically for higher values of A, while the effect of the tuning screw on mode 2 in approximately uniform over the swept range of A. Figure 4.15 and 4.16 show why the tuning screw affects the modes in different ways. From Figure 4.15, it can be seen that the even E-field of mode 1 couples strongly to the tuning screw in various directions. As the aperture width is changed, the tuning screw will influence the E-field in a non-uniform way. That is, in some directions, it will affect it more strongly than

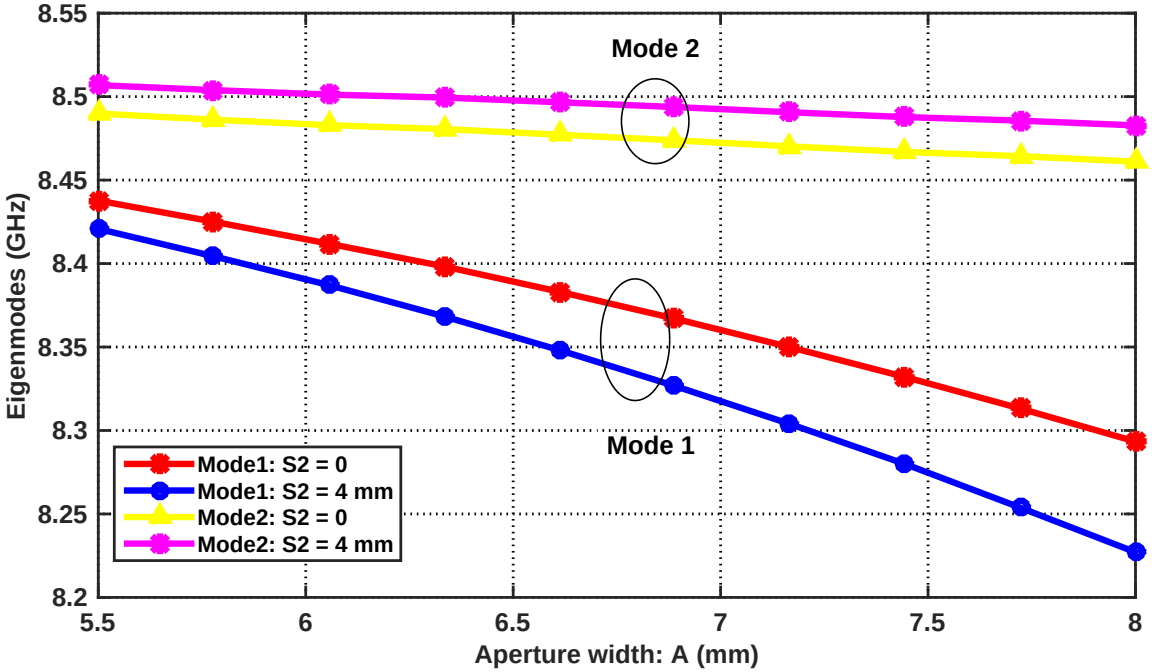

Figure 4.14: Eigenmode frequencies versus aperture width (A) for the configuration in Figure 4.13

in other directions. The tuning screw hardly affects the odd H-field of mode 1. In Figure 4.16 it is easy to see that the odd E-field of mode 2 is not affected by the tuning screw. The even H-field of mode 2 is affected approximately in a uniform way. Figure 4.15 and 4.16 also shows that the strength of the H-fields across the iris junction for both modes is much stronger than that of the E-field, implying that the coupling is predominantly magnetic in nature, as expected.

The coupling coefficient curves for the set-up in Figure 4.13 were calculated from Equations 2.19 or 2.20 and is shown in Figure 4.16. The coupling coefficients increase with increasing aperture width A. A nominal length of S_2 = 4 mm for the tuning screw was selected around which the tuning was to be done. The depth of the tuning screw was limited by the height of the narrow wall of the waveguide to b =10.16 mm. Therefore, S_2 = 4 mm is a reasonable base value for the tuning screw to be used to tune the filter. Table 4.5 was constructed from Figure 4.16 and it presents the required aperture width (A) to give the desired coupling coefficients, and hence the bandwidth of the filter.

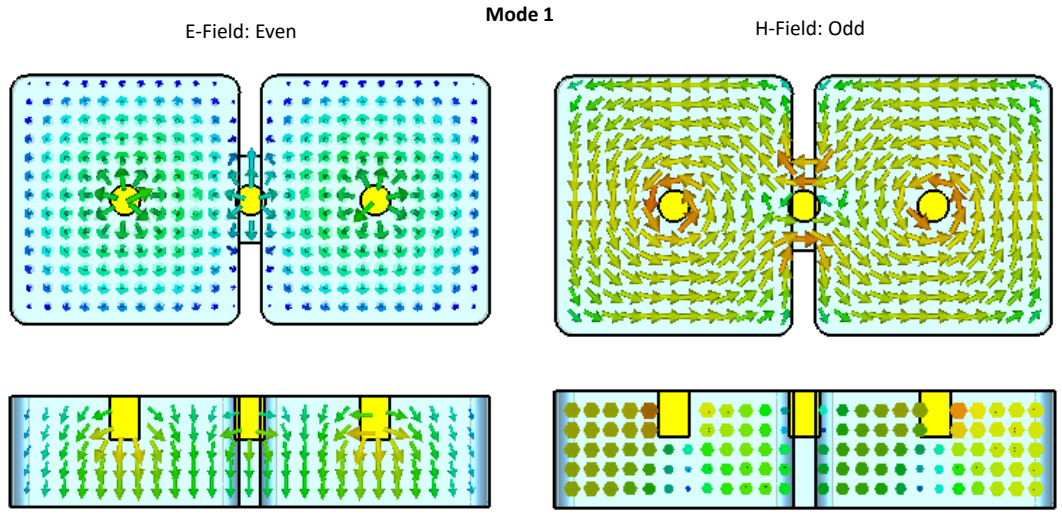

Figure 4.15: Mode 1 even electric field and odd magnetic field CST [7]

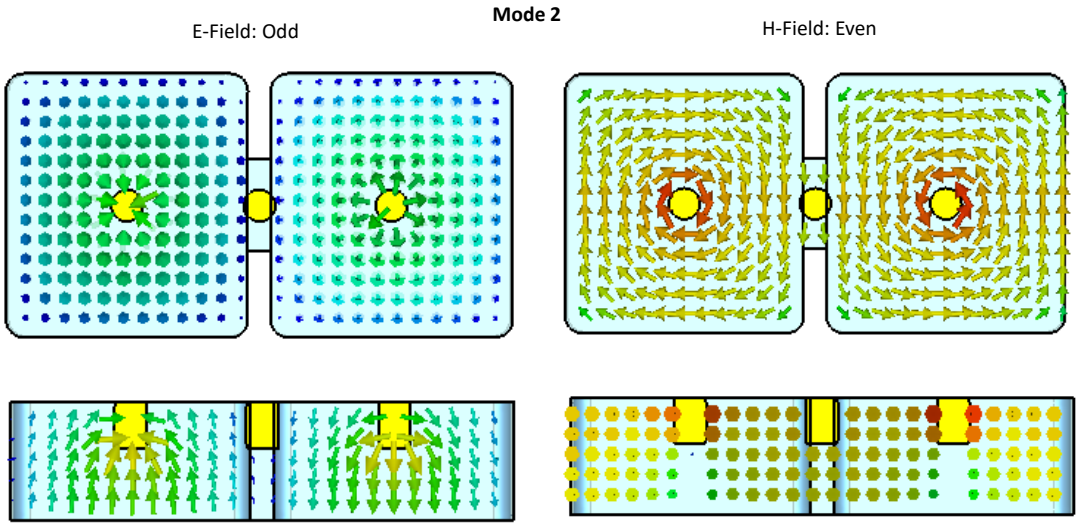

Figure 4.16: Mode 2 odd electric field and even magnetic field CST [7]

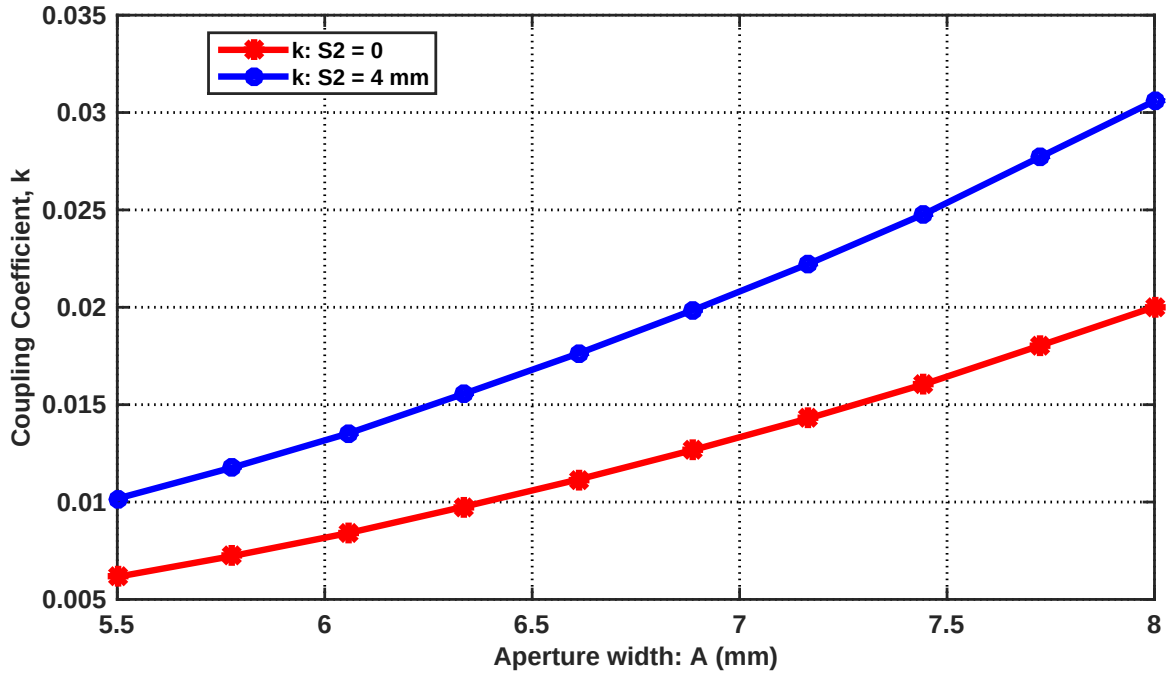

Figure 4.17: Interresonator coupling coefficients (κ) versus aperture width (A)

Table 4.5: Aperture width (A) and coupling coefficients (κ) with S_2 = 4 mm

A_i	A values	$\kappa_{j,j+1}$	κ values
A_2	6.553 mm	$\kappa_{1,2}$	0.017
A_3	5.8214 mm	$\kappa_{2,3}$	0.012
A_4	5.8214 mm	$\kappa_{3,4}$	0.012
A_5	6.553 mm	$\kappa_{4,5}$	0.017

4.4.4 **Input/output External Quality Factor**

The network configuration to determine input/output external quality factor is shown in Figure 4.18. The first and last cavities of the filter are coupled to a waveguide section through an iris. This technique is fine for the required fractional bandwidth of 1.76 %. A tuning screw is inserted through the iris, for post-manufacture tuning of the feed.

Opening the aperture between the cavity and feed waveguide will disturb the centre frequency of the resonant cavity. Therefore, the length of the cavity L has to be varied along with the aperture width A_1 so that this effect can be taken into account. The desired external quality factor was calculated from Equations 2.19 or 2.20. After that, the group delay method was used to determine the simulated external quality factor, and the resulting curves of the group delay

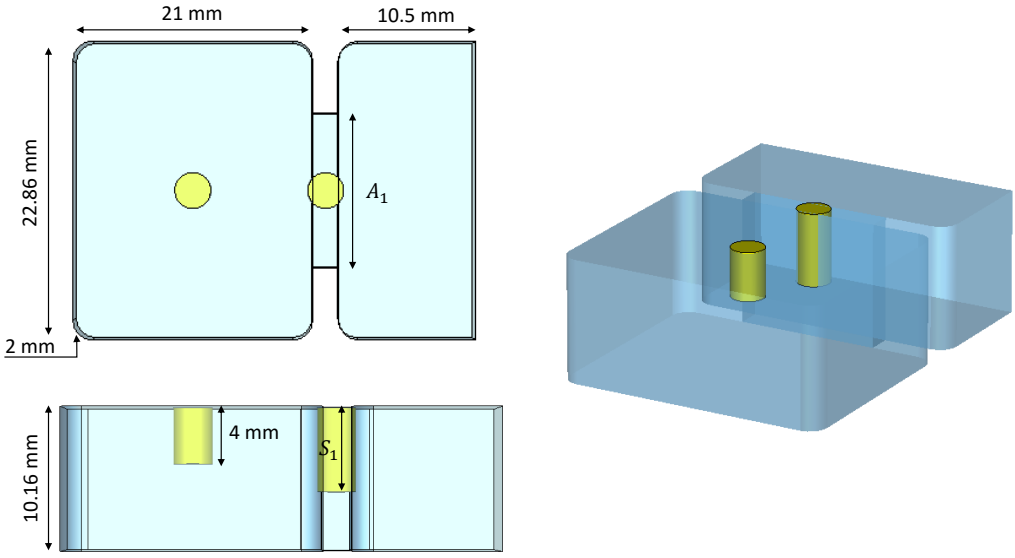

Figure 4.18: Set-up to calculate the group delay and external quality factor, The 10.5 mm long waveguide is fed with a waveguide port on the right hand side, while the 21 mm is shorted on the left hand side CST [7]

and the external quality factor are shown in Figure 4.19.

The external quality factor was calculated from the reflected group delay using Equation 2.30. The length (L) of the cavity was adjusted and fixed to 18.4 mm and the tuning screw was fixed at a nominal length of 2 mm. Thereafter, A_1 was varied. Figure 4.19, shows that the reflected group delay and external quality factor decreases, as A_1 increases from 10 mm to 13 mm. Table 4.6 gives the dimension of A_1 which corresponds to the desired external quality factor.

The method that is shown in Figure **??** for feeding the input/output cavities with a waveguide section and a waveguide port is not practical. In practice, most measurements systems use a coaxial cable to transfer power to a device. Therefore a transition from a coaxial to waveguide was designed to feed the filter. The set-up of the coaxial to waveguide transition is shown in Figure 4.20. The relevant parameters are the P_1 and P_2, the distance of the probe to the waveguide short, and the length of the probe respectively. The length of the waveguide is not important. The response of the transition is shown in Figure 4.21. The return loss is more than 20 dB over the frequency range from 8.1 GHz to 8.9 GHz. Table 4.6 shows the dimensions of the probe required for impedance matching.

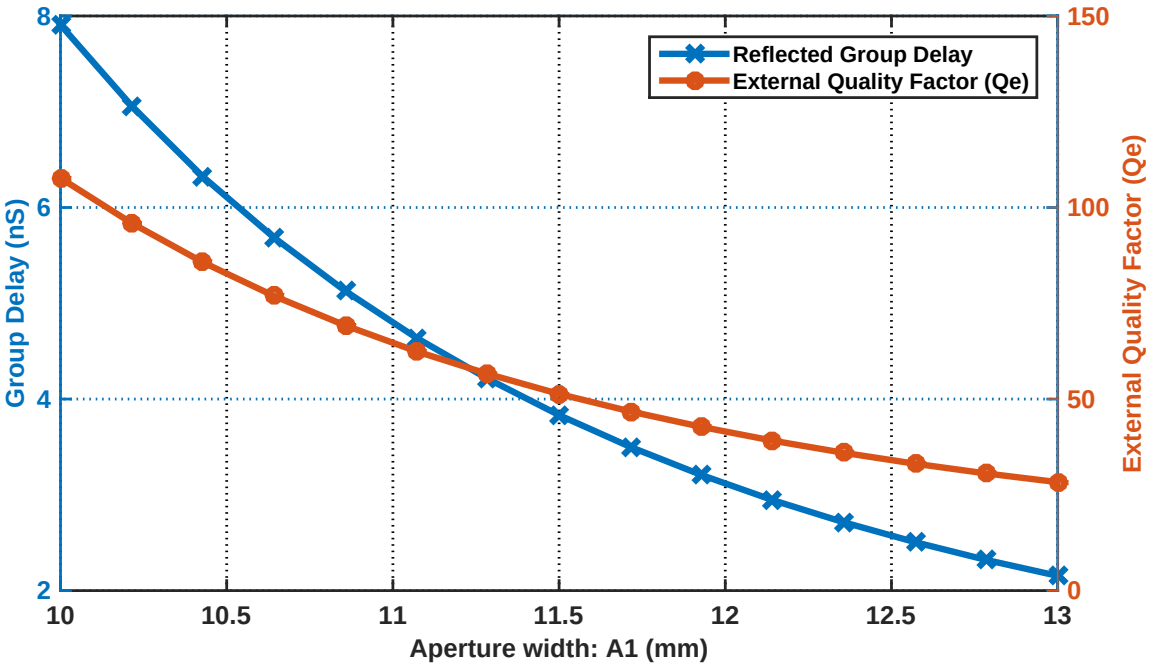

Figure 4.19: Group delay and external quality factor curves versus the aperture width fo the feed cavity (A_1)

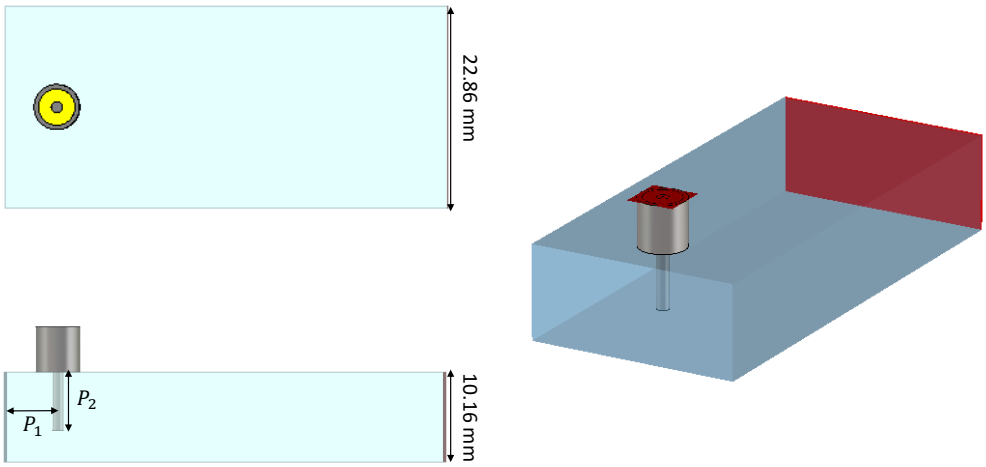

Figure 4.20: Coaxial to rectangular waveguide transition configuration CST [7]

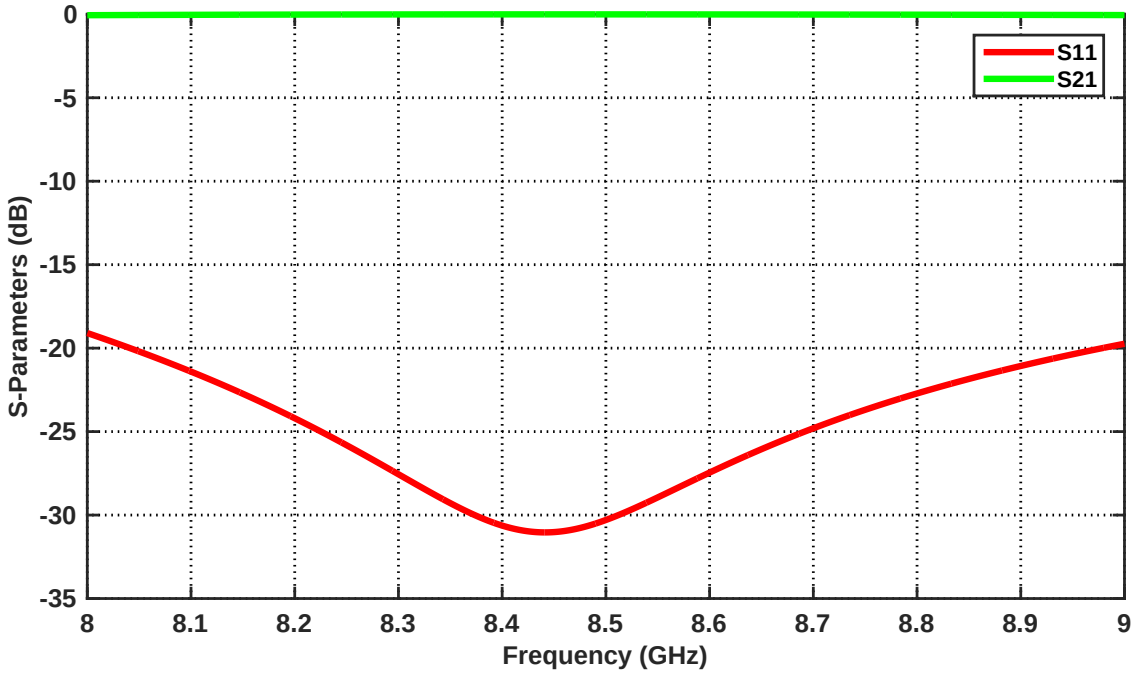

Figure 4.21: Simulated return loss and transmission coefficient of the coaxial to waveguide transition

Table 4.6: Calculated versus simulated external quality factor with the length of the input/output cavities L = 18.4 mm and tuning screw length S_1 = 2 mm. This table also provides the dimensions of the coaxial to waveguide transition

Group Delay	Q_e Simulated	Q_e Calculated	Aperture width: (A_1)
3.37 ns	45	45.11	11.81 mm
Waveguide short: P_1	Probe length: P_2	-	-
6 mm	6.604 mm	-	-

4.4.5 Initial Filter Response

The physical parameters for an initial simulation of the iris coupled waveguide filter in Figure 4.11 are presented in Table 4.8. The response for an initial simulation of the iris coupled filter done in CST [7] is shown in Figure 4.22. The response shows that the filter is centred at 8.37 GHz, with an equal ripple bandwidth of 172.19 MHz. The return loss of the filter is at least 5.16 dB.

The desired response, however, must be centred at 8.5 GHz, with a bandwidth of 150 MHz and a return loss of at least 25 dB. To accomplish the desired response, the centre frequency of the initial filter response must be shifted to the right by adjusting the lengths of the cavities L_2 to L_4. The bandwidth of the initial response can be reduced by adjusting the aperture width A_2 to A_3 between the cavities. The return loss level can be reduced by adjusting the aperture width A_1.

4.4.6 Optimised Iris Coupled Filter Response

The group delay technique was used to tune the response of Figure 4.22. The response was then optimized using the Trust Region Framework in CST [7]. The response of the tuned filter is compared to the ideal filter response in Figure 4.23. Table 4.7 summarizes the results of the comparison. The responses agree fairly well, even though the bandwidth of the optimized response is slightly wider.

A wide band response of the optimized response in Figure 4.24 shows that the filter has a spurious-free window of about 3502 MHz at -60 dB. According to [13] the second pass band for this filter will happen at a value a bit less than 2 times the operating frequency. The wide band response shows that the first harmonic for iris couple filter happens at 1.5 times the operating frequency.

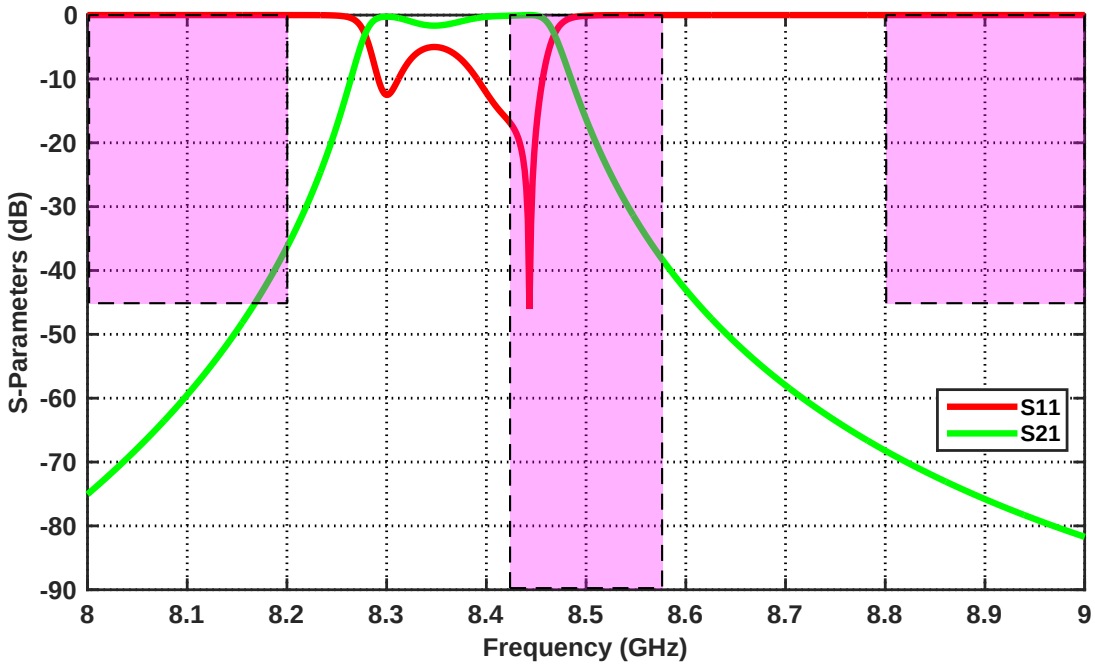

Figure 4.22: Simulation of initial response for Chebyshev iris coupled band pass filter (N= 5, RL =25, $f_0 = 8.5\,\mathrm{GHz}$, $\Delta = 1.764\,\%$)

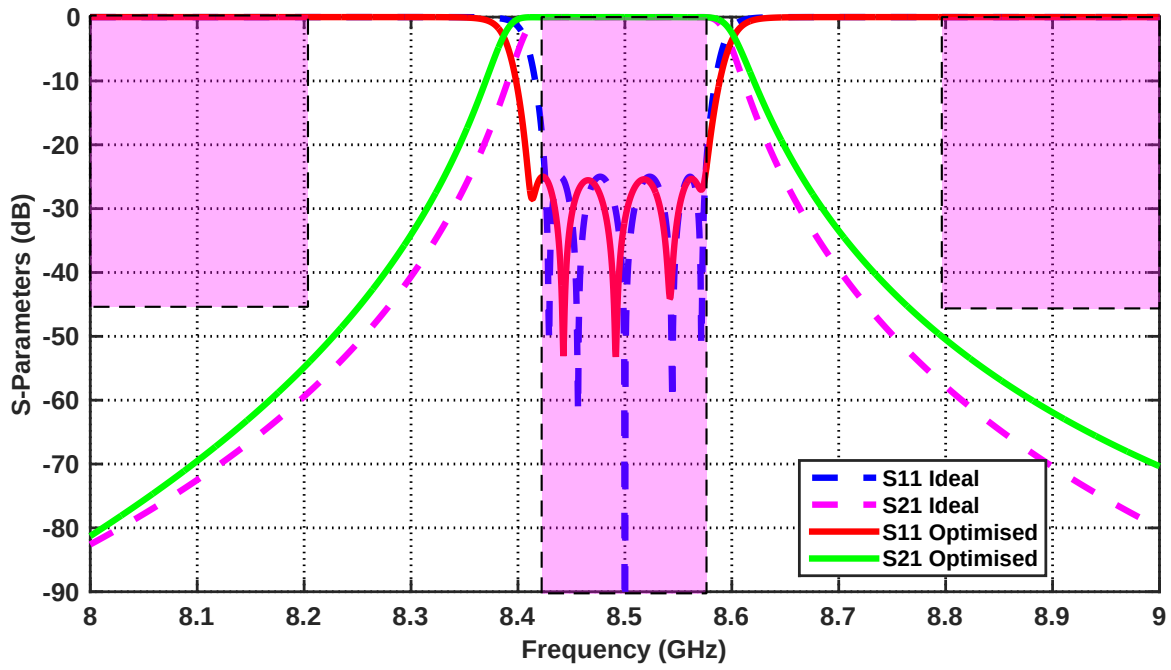

Figure 4.23: Narrow band optimised response compared with ideal response for Chebyshev iris coupled band pass filter (N= 5, RL =25, $f_0 = 8.5\,\mathrm{GHz}$, $\Delta = 1.764\,\%$)

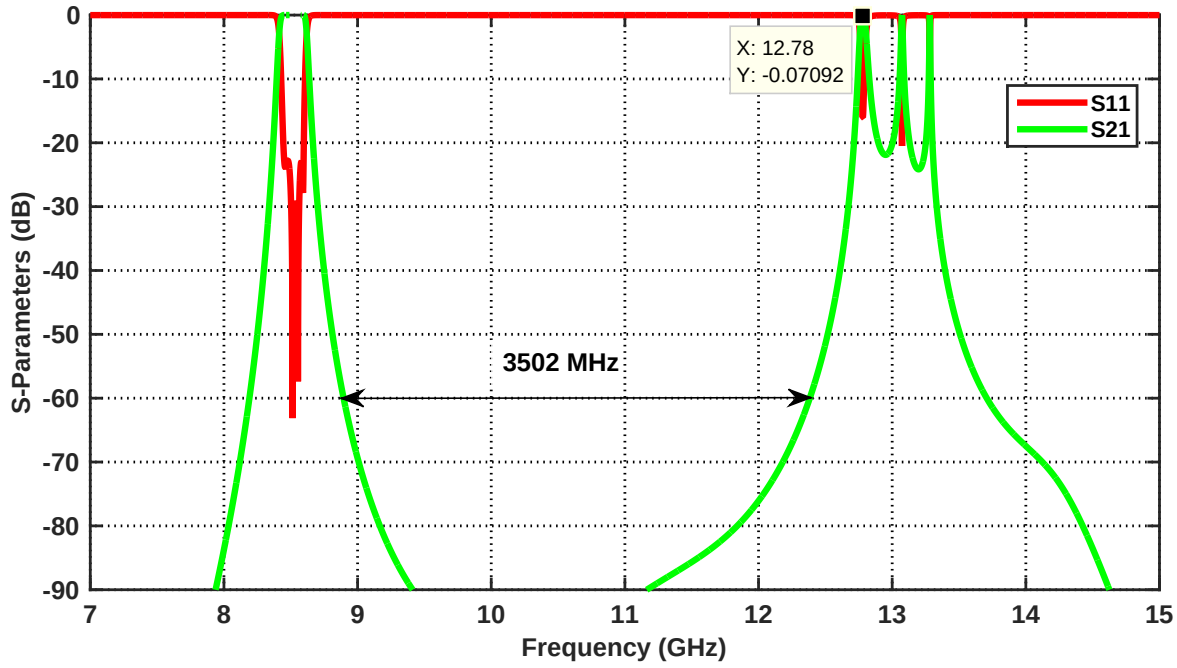

Figure 4.24: Wide band response of the optimised Chebyshev iris coupled band pass filter (N= 5, RL =25, $f_0 = 8.5\,\mathrm{GHz}$, $\Delta = 1.764\,\%$)

Table 4.7: Comparison of specifications, ideal and simulated filter responses

Dimensions	Specifications	Ideal	Simulated
Centre frequency (GHz)	8.5	8.5	8.49
Equal ripple bandwidth (MHz)	150	150	165
Insertion loss (dB)	-	0.013	0.33
Return loss (dB)	more 20	25	more 25
Spurious performance (GHz)	-	-	3.502

Table 4.8: Dimensions of designed fifth order iris coupled filter. WR 90: a = 22.86 mm , b = 10.16 mm. All tuning screws are M3, Waveguide Short: (P_1 = 6), Probe Length: (P_2 = 6.604), Feed Screw length: (S_1 = 2), Coupling Screw length: (S_2 = 4), Cavity Screw length: (S_3 = 4), Corner Radius: (R = 2), Transition Cavity length (L_1 = 20). All Parameters are in [mm]

Parameters	Initial Values	Optimised Values
Length of cavity (L): 2 and 6	18.4	17.47
Length of cavity (L): 3 and 4	21	19.96
Length of cavity (L): 5	21	20.10
Aperture width (A): 1 and 6	11.8	11.88
Aperture width (A): 2 and 5	6.55	6.45
Aperture width (A): 3	5.82	5.79

4.5 FABRICATION PROCESS

The drawings and dimensions of the Iris coupled waveguide filter were created using Solid Works. Figure 4.25 and 4.26 shows the drawing and dimensions of the filter body and cover sent to Kline Engineering. An assembly view of the filter is shown in Figure 4.27 along with an instruction sheet in Appendix A, Figure A.3 were sent to the manufacturer.

The manufactured filter is shown in Figure 4.28 and 4.29. The filter was made with the same base material as the comb-line filter and is silver plated too. The tuning screws were M3 25 mm long silver plated screws. The screws were locked to the cover with M3 hexagon nuts. The cover was screwed to the body by means of M2 cheese head screws. The filter is fed from the top of the cover and the bottom of the filter body by a coaxial to waveguide transition. The transition is made of a waveguide section, fed with an SMA straight Square Flange Jack Receptacle, which were screwed to the filter cover and body with M2 screws. The SMA probe extends into the waveguide cavity, acting like a monopole antenna. The filter was then measured.

4.6 TEST RESULTS

The PNA-X 4 port N5247A vector network analyzer was used to measure the response of the manufactured filter in Figure 4.28. The Network analyzer operates in the frequency range from

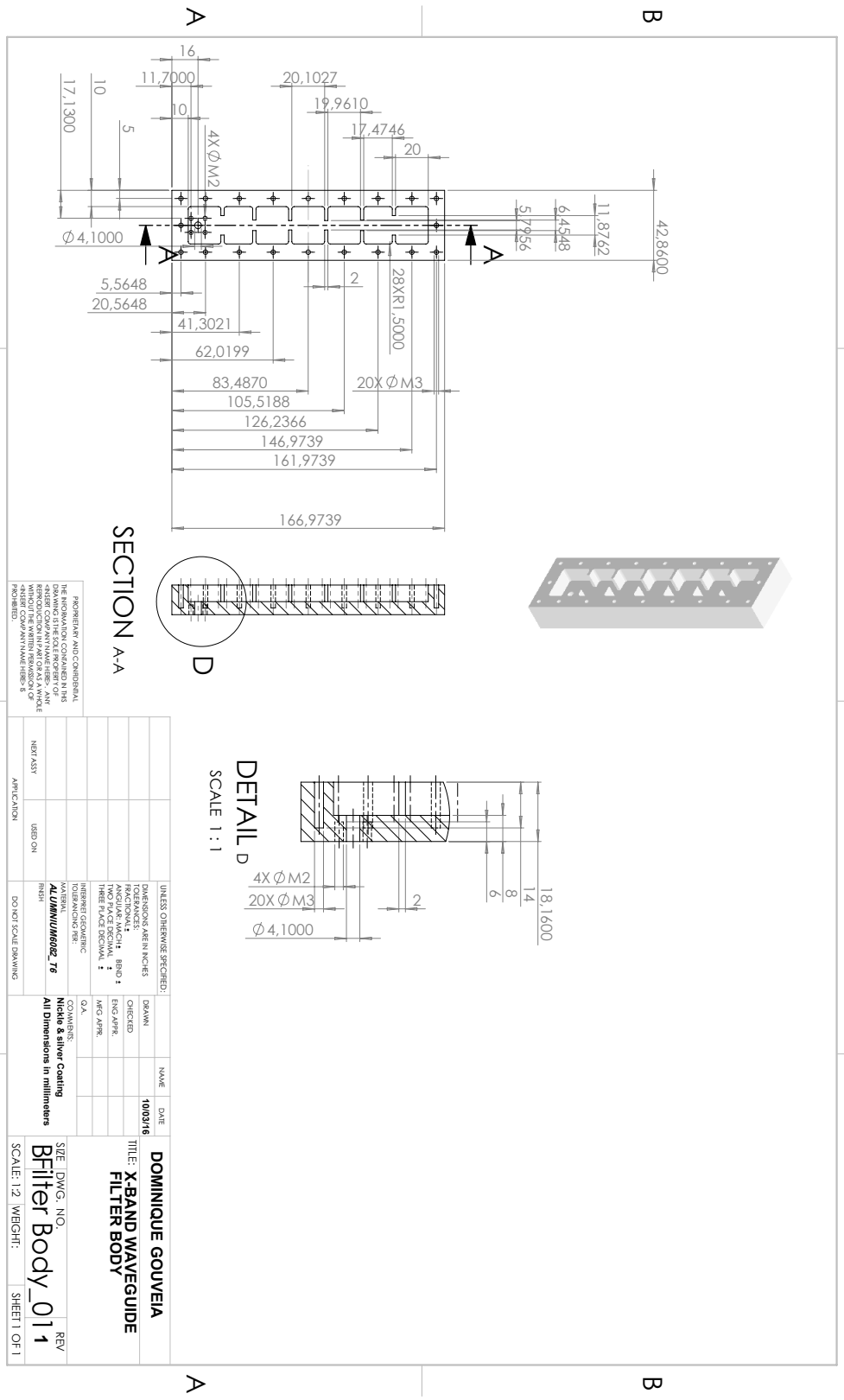

Figure 4.25: Drawing of the iris coupled coupled waveguide filter body

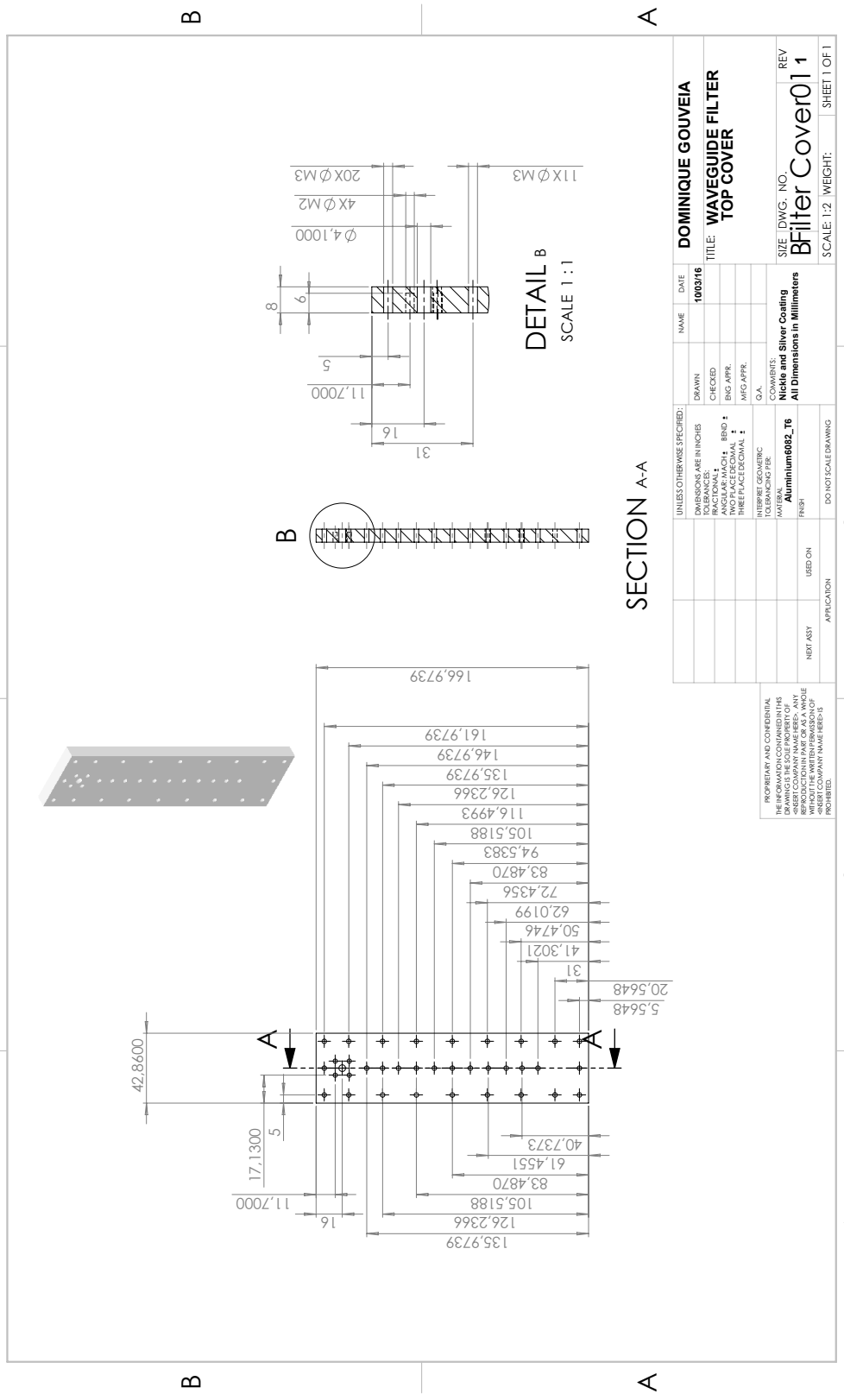

Figure 4.26: Drawing of the iris coupled coupled waveguide filter

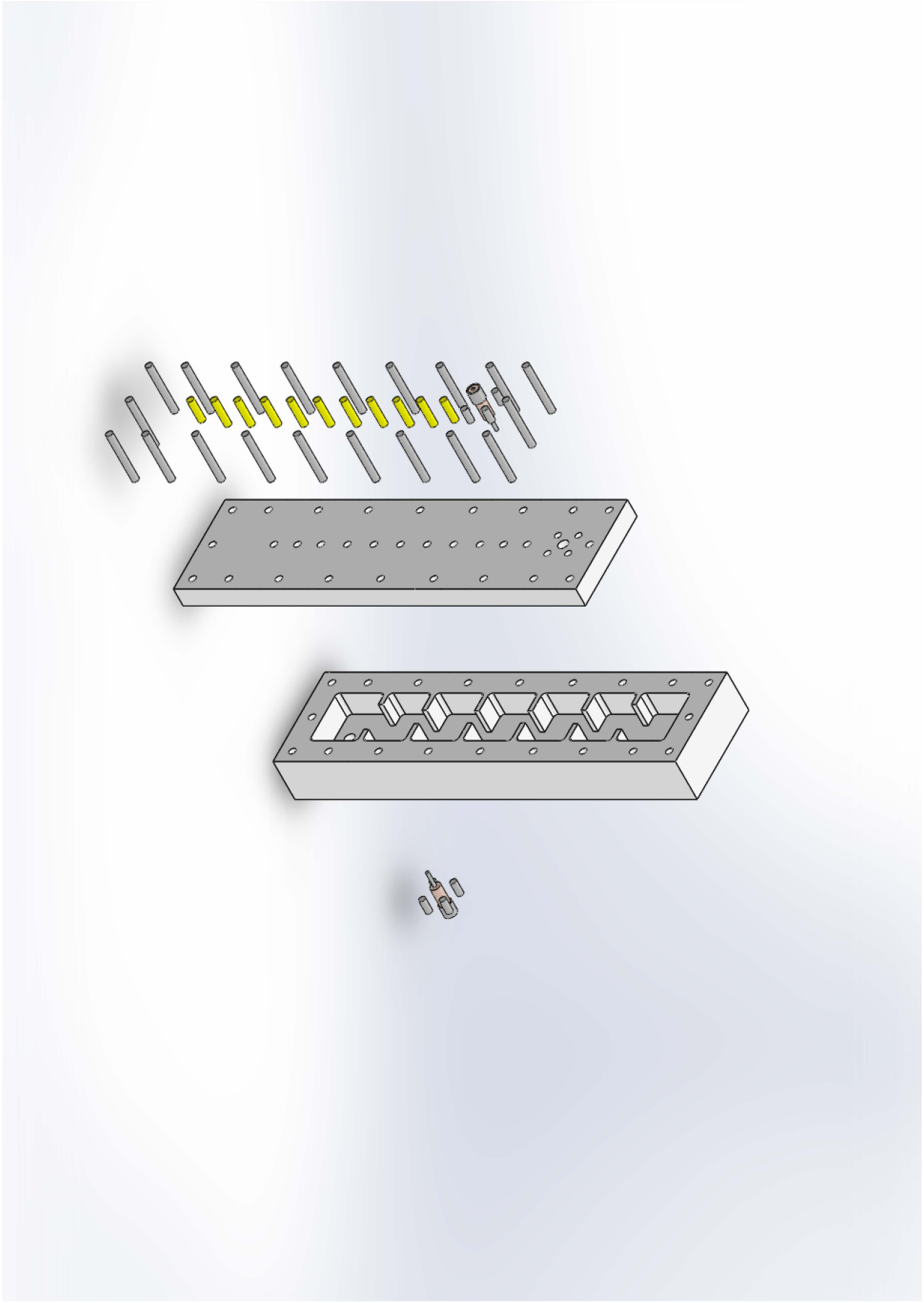

Figure 4.27: Assembly of the iris coupled waveguide filter

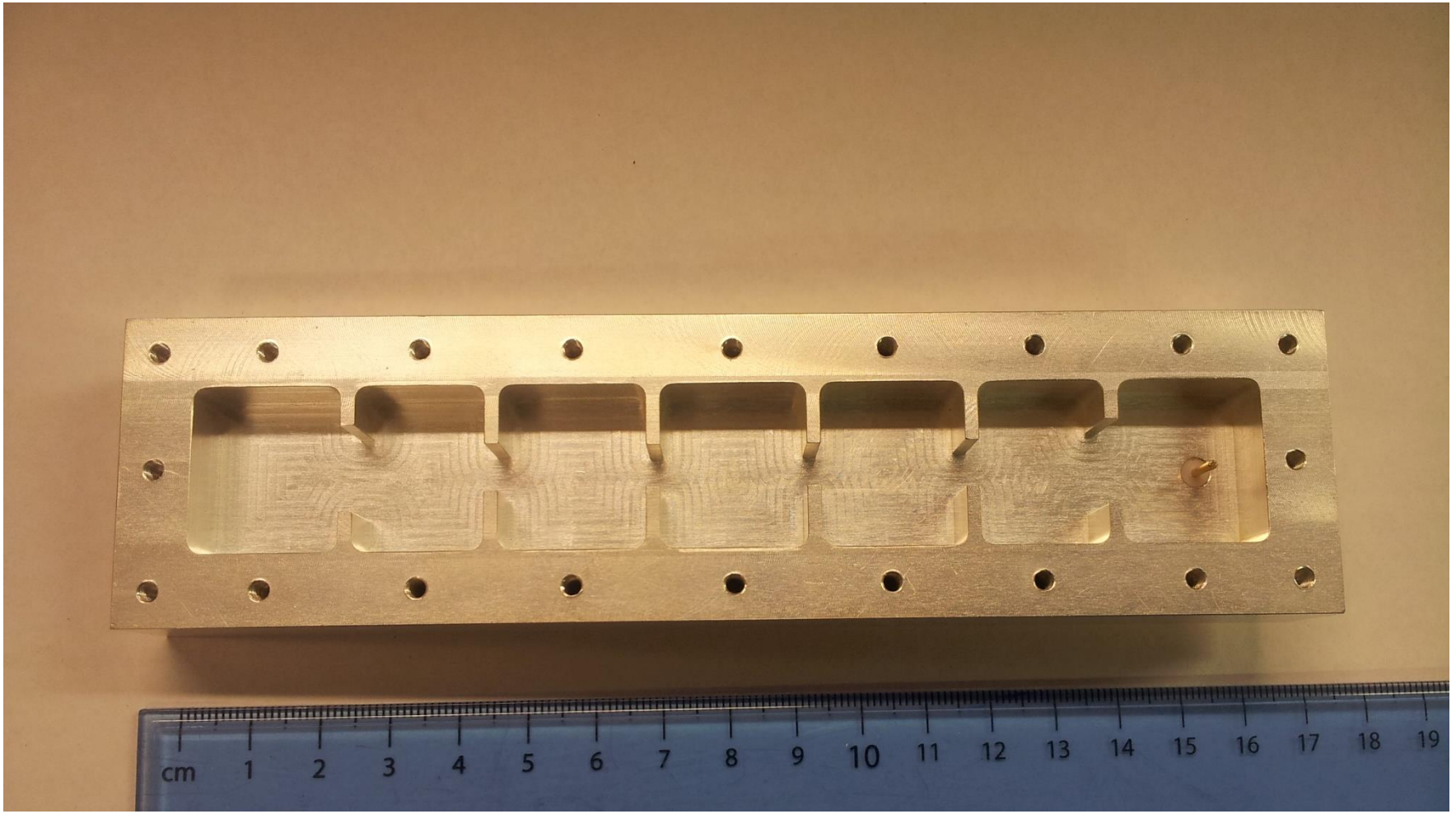

Figure 4.28: Manufactured iris coupled filter without the cover

Figure 4.29: Manufactured iris coupled filter with cover

10 MHz to 67 GHz. The filter was connected to the network analyzer through the N4697-60200 1.85 mm flexicable. The cable was then connected to the filter through an 11901A 2.4-3.5 mm male to male adapter. These devices are all a product of Agilent Technologies. The Maury Microwave 3.5 mm SOLT cal KIT with a model number of 8050CK and series of 3267 was used to calibrate the network analyzer. The measurement set-up is shown in figure 4.30. The system was calibrated up to the reference point indicated by the red circle so that the effect of the cable could be removed from the actual measurement of the filter.

Figure 4.31 is a comparison of the narrow band response of the measured and simulated iris coupled filter, while Figure 4.32 shows the wide band response comparison. The insertion loss and group delay are compared in Figure 4.33 and 4.34 respectively. An adjacent comparison of the specification, simulation, and measurement is presented in Table 4.9.

Table 4.9: Comparison of specified, simulated and measured filter responses

Dimensions	Specification	Simulated	Measured
Centre frequency (GHz)	8.5	8.49	8.5
Equal ripple bandwidth (MHz)	150	165	121
Insertion loss (dB)	low	0.33	2
Return loss (dB)	20	25	18.58 (at mid-band)
Group Delay (nS)	-	5.95	5.82
Spurious free window (GHz)	-	3.502	6.571

4.7 CONCLUSION

The X-band iris coupled waveguide filter was designed, manufactured and simulated. The narrow band measurement results showed that the filter was centred at 8.5 GHz, with an equal ripple bandwidth of 121 MHz. The spurious-free window of the measured filter at -60 dB was 6.571 GHz, with the first spurious at 1.82 times the operating frequency. The insertion loss of the filter was measured to be 2 dB at mid-band and the return loss of the filter was measured to be 18.58 dB at mid-band.

The measured equal ripple bandwidth of the filter is 29 MHz less than the specified value. However, this is not a problem, since a margin was added to the bandwidth earlier in the design to compensate for manufacturing tolerances and temperature changes. Also, the measured insertion loss is quite high. This might be due to the use of the tuning screws. It was observed during the design of the cavity, that inserting a tuning screw into the cavity had the effect of reducing the unloaded quality factor of the cavity. This might be the reason for the high insertion loss. The filter is well matched at the centre frequency, where the return loss is fairly good. The matching becomes worst below and above the centre frequency. NeXtRAD desired a filter with

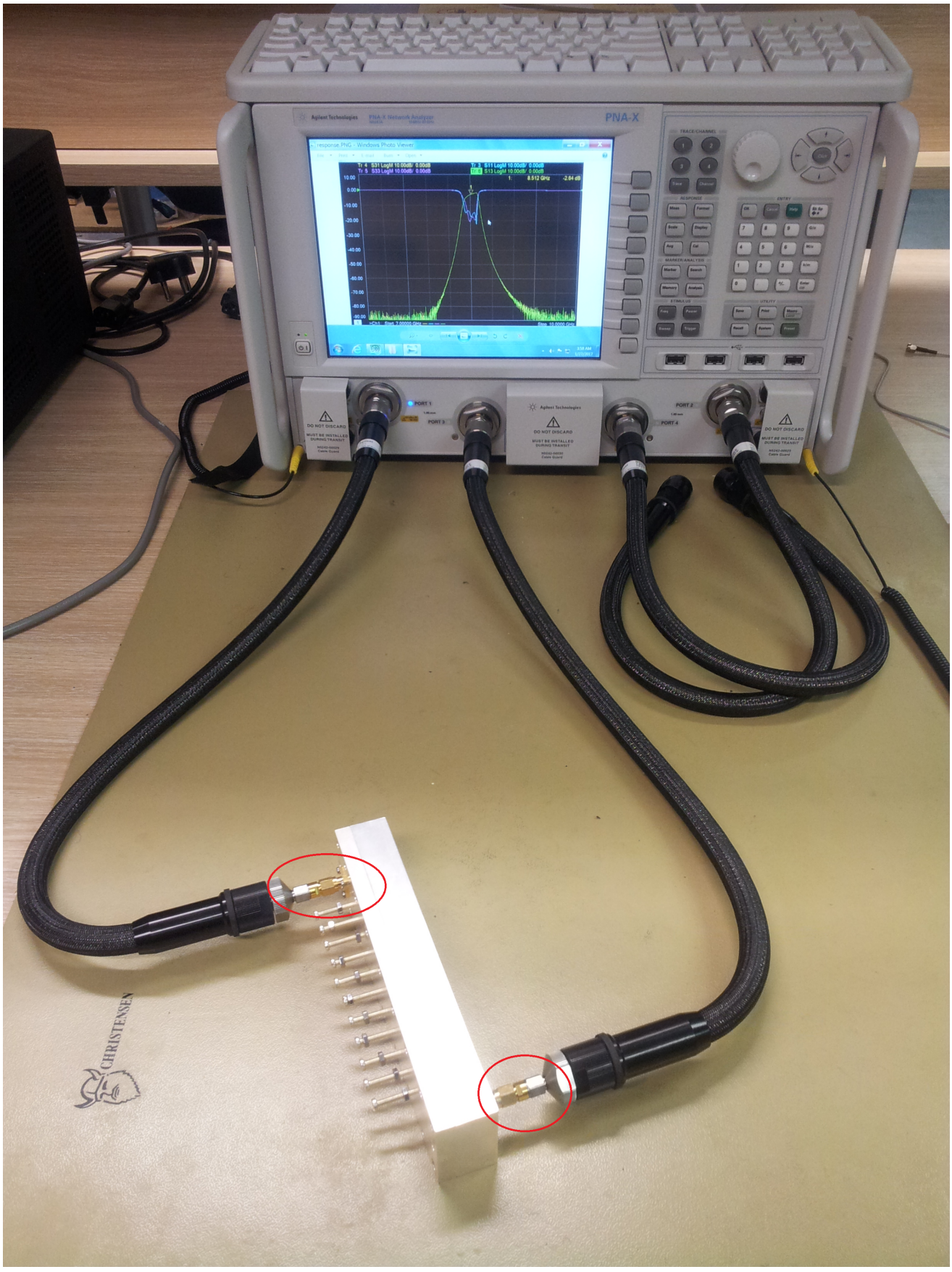

Figure 4.30: The measurement set-up for the iris coupled waveguide filter

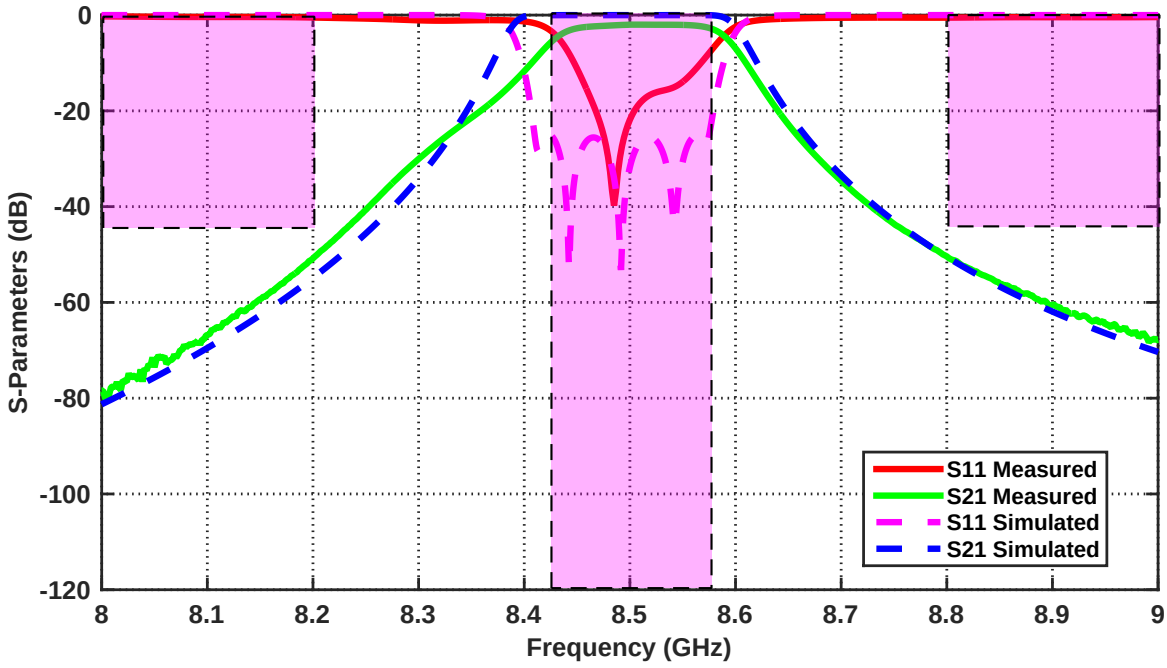

Figure 4.31: Narrow band measured response compared with optimised response for Chebyshev Iris coupled band pass filter (N= 5, RL =25, $f_0 = 8.5\,\mathrm{GHz}$, $\Delta = 1.764\,\%$)

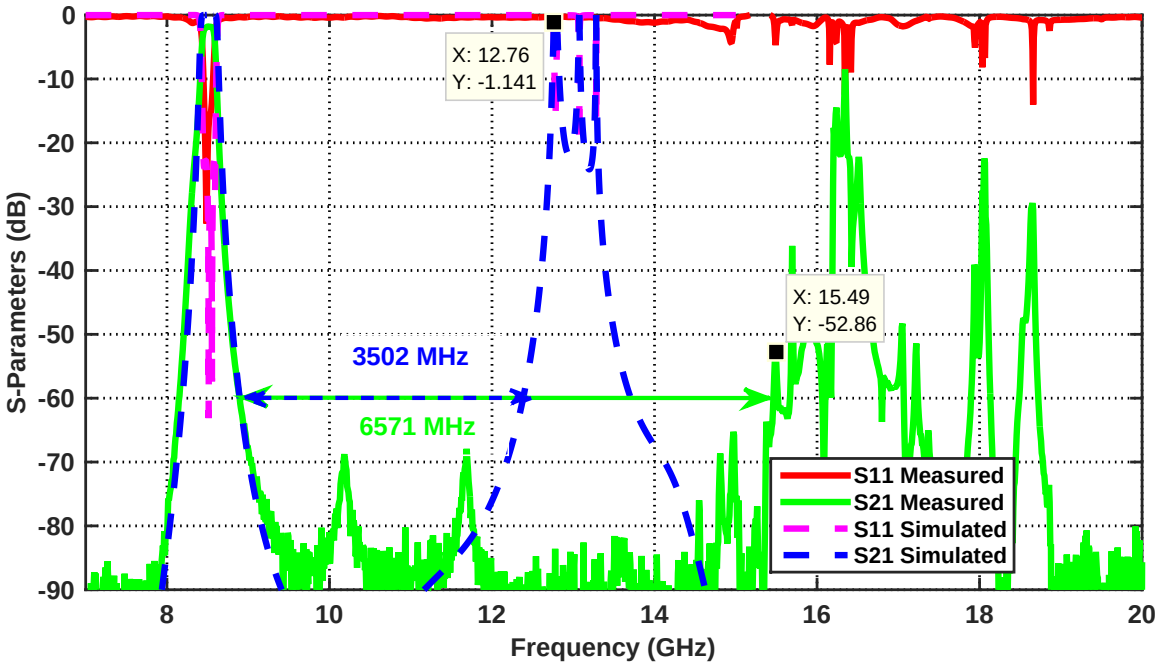

Figure 4.32: Wide band response of the measured and optimised Chebyshev Iris coupled band pass filter (N= 5, RL =25, $f_0 = 8.5\,\text{GHz}$, $\Delta = 1.764\,\%$)

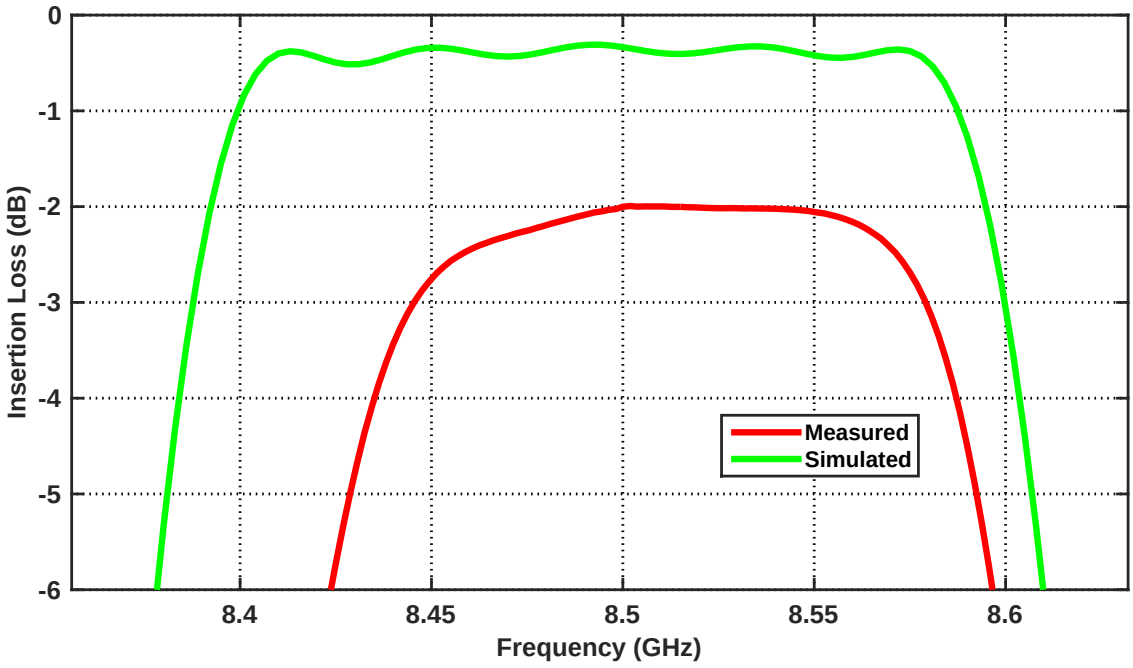

Figure 4.33: Insertion loss response of the measured and simulated Chebyshev iris coupled band pass filter (N= 6, RL =20, $f_0 = 8.5\,\mathrm{GHz}$, $\Delta = 1.764\,\%$)

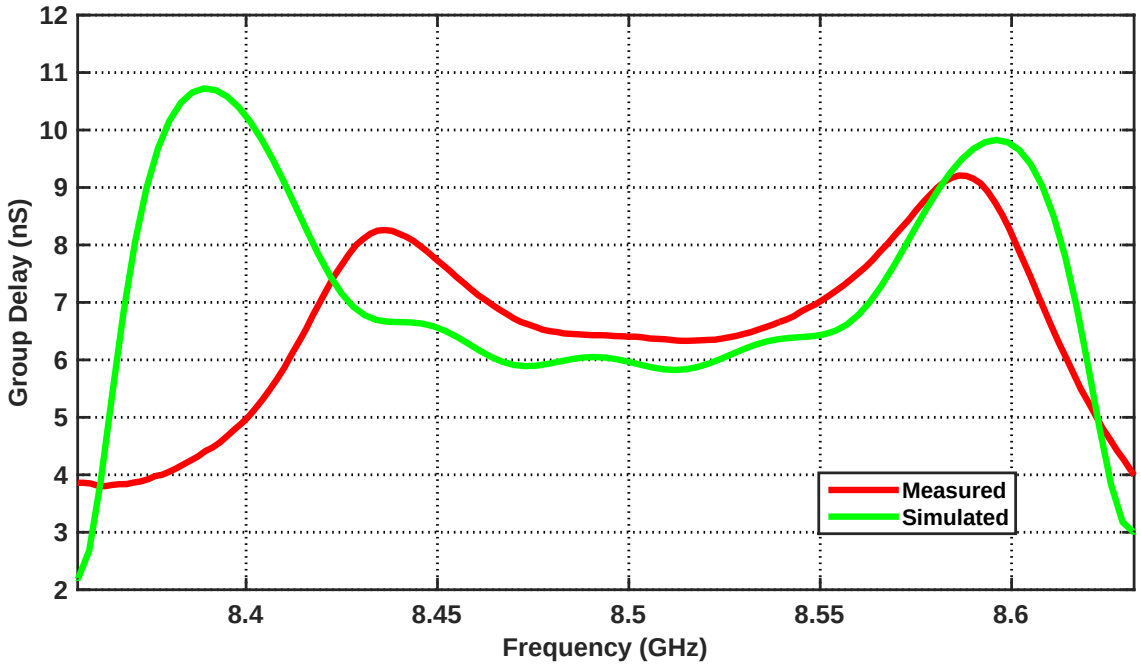

Figure 4.34: Group delay response of the measured and simulated Chebyshev iris coupled band pass filter (N= 6, RL =20, $f_0 = 8.5\,\mathrm{GHz}$, $\Delta = 1.764\,\%$)

a 50 MHz bandwidth, the return loss of the measured filter is 15.5 dB over this bandwidth. Figure 4.35 shows the manufactured filter being used at the RF front end of the NeXtRAD system.

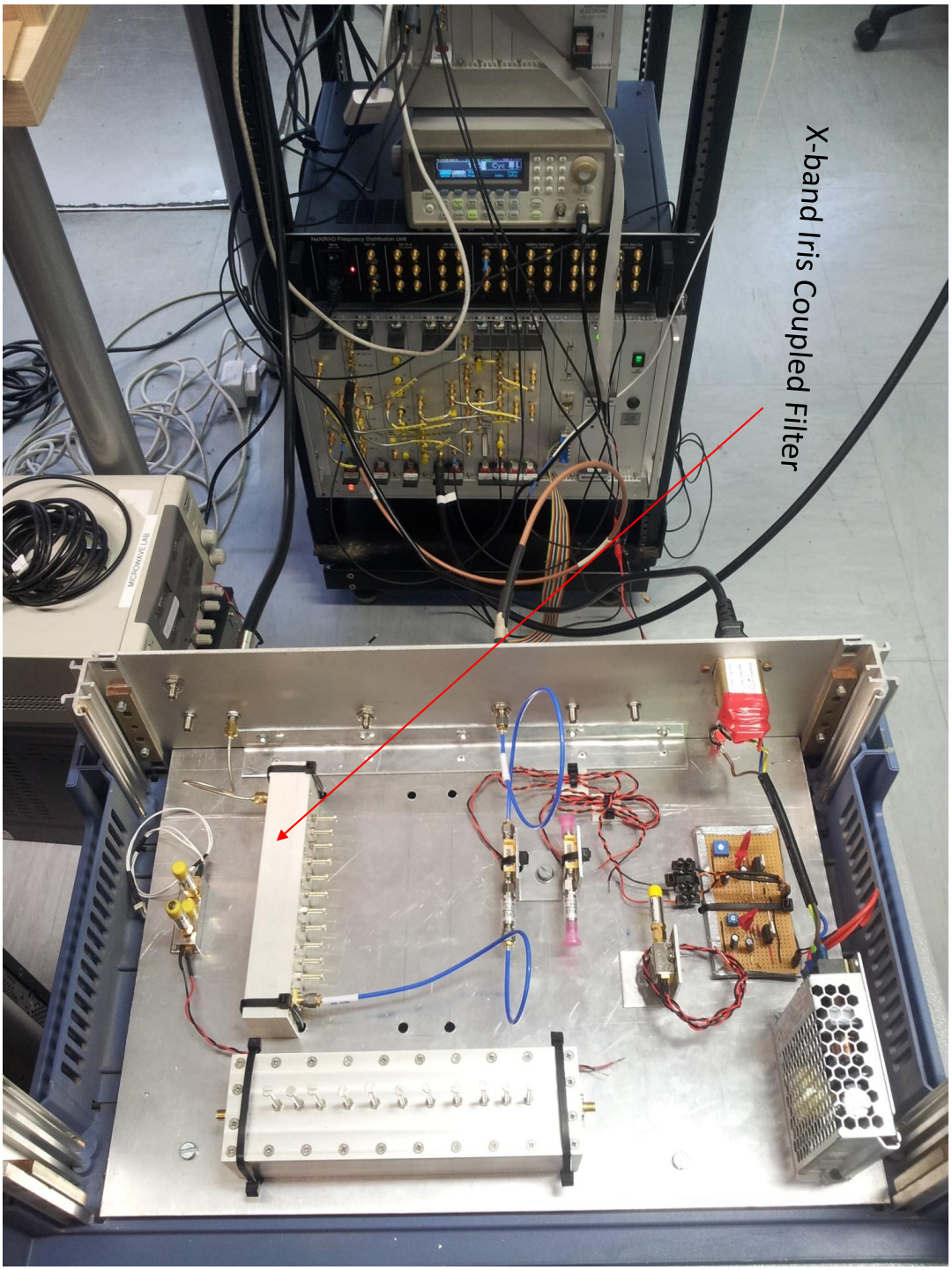

Figure 4.35: X-band Iris coupled Filter used at the RF Front End of the NeXtRAD System

CHAPTER 5

CONCLUSIONS AND FURTHER WORK

5.1 CONCLUSIONS

The purpose of this thesis was to design and implement a coaxial comb-line and an inductive iris coupled waveguide filters. The filters are required at the RF front end of a dual band research radar, called NeXtRAD. A coaxial comb-line filter was designed, manufactured and measured at L-band. The narrow band measurement results showed that the filter was centred at 1300 MHz, with an equal ripple bandwidth of 210 MHz. The filter has a spurious-free window of 2050 MHz at -60 dB, with the first spurious at 2.86 times the operating frequency. The return loss of the filter was 19.52 dB, and the insertion loss at mid-band was 0.14 dB. The measured filter agreed extremely well with the L-band specifications.

The X-band iris coupled filter was also designed, manufactured and measured. The narrow band measurement results showed that the filter was centred at 8.5 GHz, with an equal ripple bandwidth of 121 MHz. The spurious-free window of the measured filter at -60 dB was 6.571 GHz, with the first spurious at 1.82 times the operating frequency. The insertion loss of the filter was measured to be 2 dB at mid-band and the return loss of the filter was measured to be 18.58 dB at mid-band. The measured equal ripple bandwidth of the filter is 29 MHz less than the specified value. However, this is not a problem, since a margin was added to the bandwidth earlier in the design to compensate for manufacturing tolerances and temperature drifts. Also, the measured insertion loss is quite high. This might be due to the use of tuning screws. It was observed during the design of the cavity, that inserting a screw into the cavity had the effect of reducing the unloaded quality factor of the cavity. This might be the reason for the high insertion loss. The filter is well matched at the centre frequency, where the return loss is fairly good. The matching becomes worst below and above the centre frequency. NeXtRAD desired a filter with a 50 MHz bandwidth, the return loss of the measured filter is 15.5 dB over this bandwidth. The L-band and X-band filters are currently being used at the RF front end of the

NeXtRAD system.

5.2 RECOMMENDATIONS FOR FURTHER WORK

An option to improve on the insertion loss of the iris coupled waveguide filter is to build the filter without the tuning screws. The flow of the surface currents on the filter was investigated in CST [7]. It was found that maximum surface current happens at the surface of the tuning screw that is inserted into the centre of the cavity.

BIBLIOGRAPHY

[1] "IEEE standard radar definitions," *IEEE Std 686-2008 (Revision of IEEE Std 686-1997)*, pp. c1–41, May 2008. [i, 2]

[2] M. Inggs, H. Griffiths, F. Fioranelli, M. Ritchie, and K. Woodbridge, "Multistatic radar: System requirements and experimental validation," in *2014 International Radar Conference*, Oct 2014, pp. 1–6. [iv, 2]

[3] S. Maas, "Coaxial resonator filters," Master's thesis, Stellenbosch University, 12 2011. [2, 54, 69]

[4] S. Nassar, P. Meyer, and P. W. van der Walt, "An s-band combline filter with reduced size and increased pass-band separation," in *2015 Conference on Microwave Techniques (COMITE)*, April 2015, pp. 1–4. [2, 45]

[5] R. Cameron, R. Mansour, and C. Kudsia, *Microwave Filters for Communication Systems: Fundamentals, Design and Applications*. Wiley, 2007. [2, 7, 12, 15, 30, 33, 36, 37, 38, 40, 42, 43, 49, 67, 86, 90, 92, 93]

[6] V. Lenive and J. Ness, "Direct-coupled filter utilizing ridge-loaded cavities," in *2003 33rd European Microwave Conference*, Oct 2003, pp. 1251–1254. [2]

[7] "CST Microwave Studio." [Online]. Available: www.cst.com [9, 20, 23, 31, 34, 35, 36, 38, 40, 41, 43, 46, 51, 55, 57, 58, 59, 60, 61, 62, 63, 64, 65, 66, 67, 68, 69, 85, 87, 88, 91, 93, 94, 96, 98, 99, 101, 120]

[8] D. Pozar, *Microwave Engineering, 4th Edition*. Wiley, 2011. [11, 12, 13, 14, 15, 18, 19, 20, 22, 24, 59, 82]

[9] I. Hunter, *Theory and Design of Microwave Filter*, first edition ed., ser. IET Electromagnetic Waves Series 48. The Institution of Engineering and Technology, 2001. [11]

[10] T. G. Brand, "Synthesis methods for multi-band coupled resonator filters," Ph.D. dissertation, Stellenbosch University, 12 2014. [11, 14]

[11] "IEEE standard for microwave filter definitions," *IEEE Std 1549-2011*, pp. 1–22, May 2011. [13, 14]

[12] J. HONG, *Microstrip Filters for RF/Microwave Applications*, second edition ed. Wiley, 2011. [15, 17, 18, 19, 22, 24, 25, 26, 30]

[13] G. Matthaei, L. Young, and E. Jones, *Microwave Filters, Impedance-Matching Networks, and Coupling Structures*. Artech House, Norwood, MA, 1980. [15, 22, 24, 28, 48, 49, 50, 53, 56, 82, 84, 101]

[14] H. Miranda, "Microstrip filters." [Online]. Available: http://paginas.fe.up.pt/~hmiranda/etele/microstrip/, 2003, [Accessed: 11- Mar- 2017]. [33]

[15] "Cavity filters." [Online]. Available: http://micro.apitech.com/cavity.aspx, API Technologies Corp, [Accessed: 11- Mar- 2017]. [33]

[16] "Lumped element filters." [Online]. Available: http://www.dovermpg.com/bscfilters/en/gn/technologies/lumped-element, BSC Filters Ltd, [Accessed: 11- Mar- 2017]. [33]

[17] H.-W. Yao, K. A. Zaki, A. E. Atia, and T. Dolan, "Improvement of spurious performance of combline filters," in *1997 IEEE MTT-S International Microwave Symposium Digest*, vol. 2, June 1997, pp. 1099–1102 vol.2. [45, 57, 68]

[18] S. Han, X. Wang, Y. Fan, and Y. Lin, "Design combline bandpass filter with the stepped impedance resonators," in *2005 Asia-Pacific Microwave Conference Proceedings*, vol. 1, Dec 2005, pp. 2 pp.–. [45]

[19] D. Natarajan, *A Practical Design of Lumped, Semi-lumped & Microwave Cavity Filters*, ser. Lecture Notes in Electrical Engineering. Springer Berlin Heidelberg, 2012. [45, 52]

[20] R. Levy, R. V. Snyder, and G. Matthaei, "Design of microwave filters," *IEEE Transactions on Microwave Theory and Techniques*, vol. 50, no. 3, pp. 783–793, Mar 2002. [46, 50, 52, 53, 57]

[21] B. Wadell, *Transmission Line Design Handbook*. Artech House, Inc, 1991. [48, 49]

[22] D. Swanson and W. Hoefer, *Microwave Circuit Modeling Using Electromagnetic Field Simulation*. Artech House, Inc, 2003. [50, 51]

[23] E. M. Hansmann, "An investigation of coupling mechanisms in narrowband microwave filters," Master's thesis, Stellenbosch University, 12 2008. [51, 54]

[24] "RF and Microwave Filters," [Online]. Available: http://micro.apitech.com/, Api Technologies Corp, [Accessed: 2- Apr- 2017]. [51]

[25] I. C. Hunter, L. Billonet, B. Jarry, and P. Guillon, "Microwave filters-applications and technology," *IEEE Transactions on Microwave Theory and Techniques*, vol. 50, no. 3, pp. 794–805, Mar 2002. [52]

[26] J. Daniel G. Swanson, "Narrowband combline filter design with ansys hfss," [Online]. Available: www.swfilterdesign.com/Narrowband_Combline_Filter_Design.pdf, 5 2015, [Accessed: 20- Jan- 2017]. [52, 53, 54]

[27] "Six-pole band-pass filter with single cross-coupling." [Online]. Available: https://www.cst.com/Applications/Article/Six-Pole-Band-Pass-Filter-With-Single-Cross-Coupling, CST Microwave Studio, [Accessed: 19- Mar- 2017]. [54]

[28] R. Levy, H.-W. Yao, and K. A. Zaki, "Transitional combline/evanescent-mode microwave filters," *IEEE Transactions on Microwave Theory and Techniques*, vol. 45, no. 12, pp. 2094–2099, Dec 1997. [56, 57]

[29] M. Dishal, "Alignment and adjustment of synchronously tuned multiple-resonant-circuit filters," *Proceedings of the IRE*, vol. 39, no. 11, pp. 1448–1455, Nov 1951. [56]

[30] D. R. Design, "Combline filter design using hfss to implement the qex and k method," [Online]. Available: https://www.yumpu.com/en/document/view/1804726/combline-filter-design-using-hfss-to-implement-the-q-and-k-method, [Accessed: 18- Mar- 2017]. [57]

[31] M. Sagawa, M. Makimoto, and S. Yamashita, "A design method of bandpass filters using dielectric-filled coaxial resonators (short papers)," *IEEE Transactions on Microwave Theory and Techniques*, vol. 33, no. 2, pp. 152–157, Feb 1985. [68]

[32] R. M. Kurzrok, "Design waveguide bandpass filters," [Online]. Available: www.rf114.com/lib/download.php?code=tbl_board&seq_name=bseq&seq.., [Accessed: 20- Jan- 2017]. [81]

[33] P. Jarry and J. Beneat, *Advanced Design Techniques and Realizations of Microwave and RF Filters*. Wiley, 2008. [82, 84]

[34] D. Gouveia, "X-band waveguide filter for the nextrad project," University of Cape Town, Tech. Rep., 8 2014. [84]

[35] C. Balanis, *Advanced Engineering Electromagnetics*, second edition ed. Wiley, 2011. [86, 87]

[36] A. Das and S. Das, *Microwave Engineering*. Tata McGraw-Hill, 2000. [86, 87]

[37] "Waveguide receive reject filter." [Online]. Available: http://www.apollomw.com/products/product=WaveguideReceiveRejectFilter, Apollo microwave, [Accessed: 23- Mar- 2017]. [88]

[38] "Waveguide bandpass filters." [Online]. Available: http://www.apollomw.com/products/WaveguideBandpassFilters, Apollo microwave, [Accessed: 23- Mar- 2017]. [88]

[39] Catlash, "Waveguide post filter: a band-pass filter consisting of a length of wg15 (a standard waveguide size for x band use) ." [Online]. Available: https://commons.wikimedia.org/wiki/File:Waveguide-post-filter.JPG, 22 February 2012, [Accessed: 23- Mar- 2017]. [88]

[40] P. Wade, "Rectangular waveguide to coax transition design," [Online]. Available: http://www.w1ghz.org/QEX/Rectangular_Waveguide_to_Coax_Transition_Design.pdf, 8 2006, [Accessed: 1- Apr- 2017]. [89]

[41] A. M. Snchez, F. M. Rizo, and K. Cepero, "Waveguide technology," [Online]. Available: http://www.radio.feec.vutbr.cz/kosy/soubory/zahranicni-lektori/09_mediavilla/mediavilla_03.pdf, 3 2011, [Accessed: 1- Apr- 2017]. [89]

[42] "Transitions and tapers." [Online]. Available: http://www.A1Microwave.com, A1 Microwave, [Accessed: 1- Apr- 2017]. [90]

APPENDIX A

ADDITIONAL INFORMATION

Table A.1: Specifications of the interdigital band pass filter (5845-BB-009) from Reutch Radar Systems

Pass band	1367 MHz to 1235 MHz
Center Frequency	1300 MHz
Insertion Loss	0.2046 dB (max)
Return Loss	23 dB (min)
Passband Ripple	0.0605 dB (max)
Equal Ripple Bandwidth	132 MHz
Number of poles	5
Stop band	
Frequency/MHz	Attenuation/dB (min)
Extended (E-GSM) 900	
880 to 890 Uplink	78
925 to 935 Downlink	74
GSM 1800	
1710 to 1785 Uplink	71.52
1805 to 1880 Downlink	79.47

Specifications

f0=1.3
w0=2*_PI*f0*1e+9 w0: 8.168e9
FBW=0.1615
Rs=50
Gs=1/Rs Gs: 0.02
Rai=77
Gai=1/Rai Gai: 0.01299

Circuit Parameters

Theta=80
Theta_rad= (Theta*_PI)/180 Theta_rad: 1.396
Cot_Theta_rad= 1/tan(Theta_rad) Cot_Theta_rad: 0.1763
Csc_Theta_rad= 1/sin(Theta_rad) Csc_Theta_rad: 1.015
Cap_i= (Gai*Cot_Theta_rad)/w0 Cap_i: 2.804e-13

bi=0.5*Gai*(Cot_Theta_rad)+0.5*Gai*(Theta_rad*(Csc_Theta_rad)^2) bi: 0.01049

g0=1
g1=0.9958
g2=1.413
g3=1.895
g4=1.551
g5=1.727
g6=0.8148
g7=1.222

Coupling inverters

J01 = sqrt((Gs*bi*FBW)/(g0*g1)) J01 : 0.005835
J12 = FBW*sqrt((bi*bi)/(g1*g2)) J12: 0.001429
J23 = FBW*sqrt((bi*bi)/(g2*g3)) J23: 0.001036
J34 = FBW*sqrt((bi*bi)/(g3*g4)) J34: 0.0009889
J45= FBW*sqrt((bi*bi)/(g4*g5)) J45: 0.001036
J56= FBW*sqrt((bi*bi)/(g5*g6)) J56: 0.001429
J67 = sqrt((Gs*bi*FBW)/(g6*g7)) J67: 0.005835

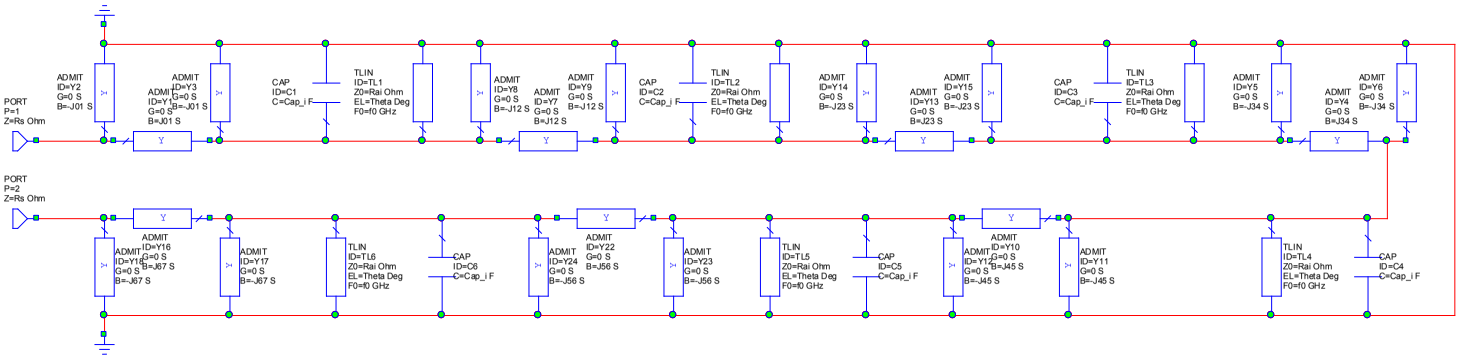

Figure A.1: J-inverter circuit model with transmission lines for a 6^{th} order Chebyshev band pass filter

Bill of Material for Narrow Band L-Band (1-2) GHz Combline Filter

Filter Screws						
Device	**Material**	**Coating**	**Size**	**Units**		
Tunings Screws	Brass	Nickel and Silver	M3 (Simulated Size 3 mm)	13		
Jam-nuts and Thread-lock	Suitable	Suitable	Fit M3 screws	13		
Platic Caps	Suitable	-	Fit M3 screwsPlus Jam-nut assembly	13		
Cover Screws	Brass	Nickel and Silver	M3 (Simulated Size 3 mm)	24		
Feed Screws	Brass	Nickel and Silver	M2 (Simulated Size 2,6 mm)	8		
Filter Feeds						
13_N-50-0-30/133_NE N-type connector	-	-	Dielectric: 4,1 mm and center probe: 1,26mm	2		
Filter Body and Cover						
Filter_Body and Cover	Aluminium6082_T6	Nickel and Silver	Specified in Drawings	2		

Notes

Please buy all the filter screws. These are all the devices in row 5-9. **NB**: The Tuning Screws in row 5 must have very fine pitch.
The filter feed has been bought already. An image of the feed can be found in the folder called additional notes.
All plating/coating must 5um
All Tapping must be platted/coatted too
Please buy Silver Epoxy to set the screws (**Not Applicable**)
The internal length of the rectangular cavity, The dimesions of the Cylinders,The Spacing between the Cylinders, and the position of the feed probe from the base
The tolerence of 0,1mm was decided for all these parameters.

Figure A.2: The List of instruction for the L-band filter

Bill of Material for Narrow Band X-Band (8-12) GHz Waveguide Filter

Filter Screws						
Device	**Material**	**Coating**	**Size**	**Units**		
Tunings Screws	Brass	Nickel and Silver	M3 (Simulated Size 2,76 mm)	13		
Jam-nuts and Thread-lock	Suitable	Suitable	Fit M3 screws	13		
Platic Caps	Suitable	-	Fit M3 screwsPlus Jam-nut assembly	13		
Cover Screws	Brass	Nickel and Silver	M3 (Simulated Size 2,76 mm)	20		
Feed Screws	Brass	Nickel and Silver	M2 (Simulated Size 2,6 mm)	8		
Filter Feeds						
13_N-50-0-30/133_NE N-type connector	-	-	Dielectric: 4,1 mm and center probe: 1,26mm	2		
Filter Body and Cover						
Filter_Body and Cover	Aluminium6082_T6	Nickel and Silver	Specified in Drawings	2		

Notes

Please buy all the filter screws. These are all the devices in row 5-9. **NB**: The Tuning Screws in row 5 must have very fine pitch.
The filter feed has been bought already. An image of the feed can be found in the folder called additional notes.
All plating/coating must 5um
All Tapping must be platted/coatted too
Please buy Silver Epoxy to set the screws
The critical dimesions are; The length of the waveguide, The length of the coupling aperture, and the position of the feed probe to the back wall of the waveguide.
The tolerence of 0,1mm was decided for all these parameters.

Figure A.3: The List of instruction for the X-band filter

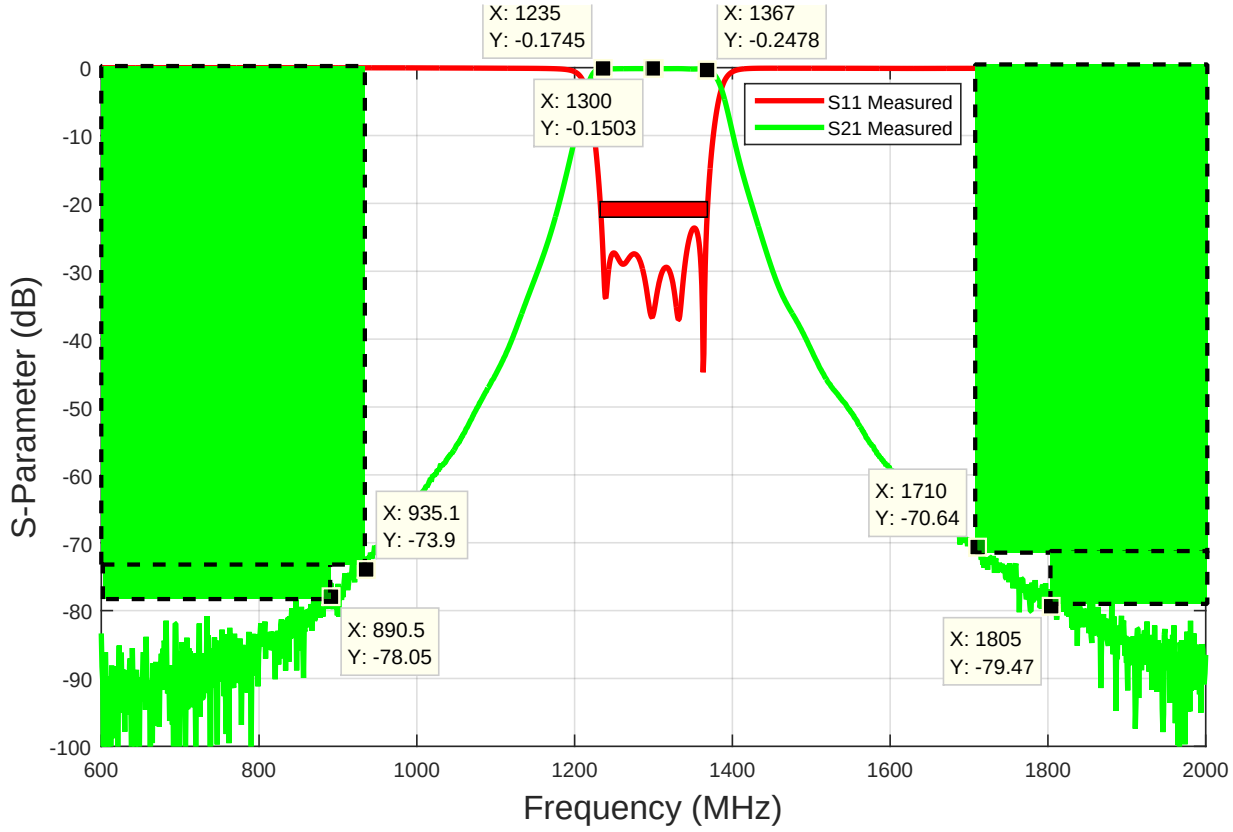

Figure A.4: Narrow band response of interdigital filter from Reutech radars

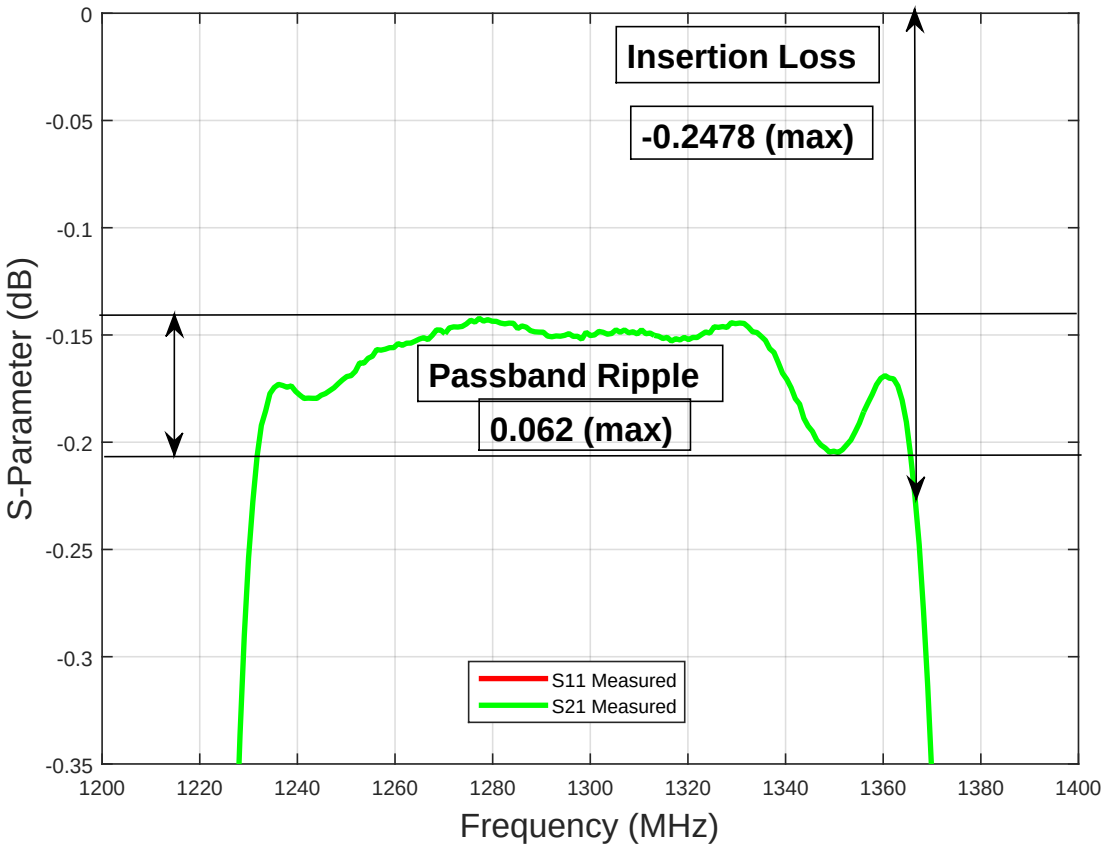

Figure A.5: Insertion loss response of interdigital filter from Reutech radars

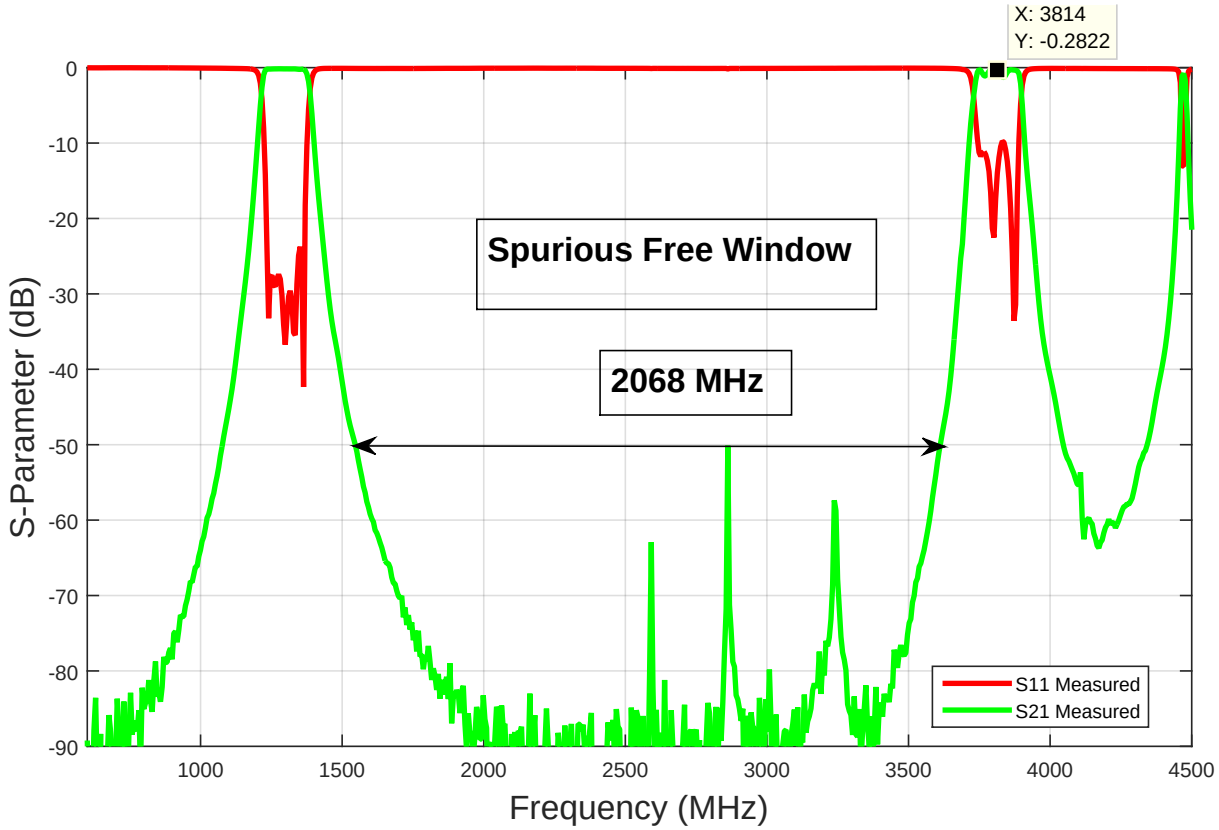

Figure A.6: Wide band response of interdigital filter from Reutech radars

RS Stock No. 5463181

Data sheet

SMA Straight Square Flange Jack Receptacle

RS stock No: 5463181

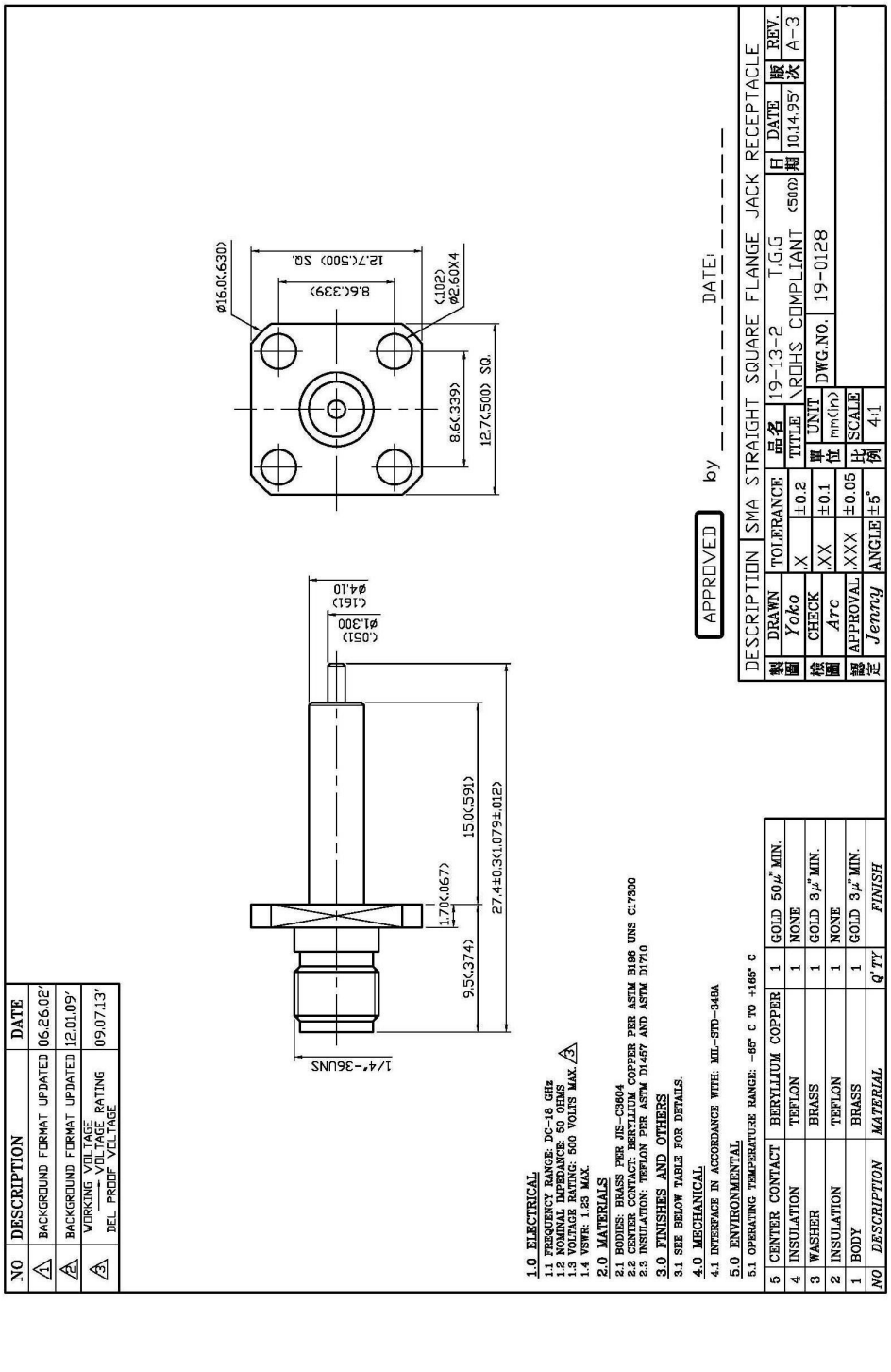

Figure A.7: SMA Straight Square Flange Jack Receptacle: from RS components

Series N 50 Ω – receptacles with solder end

Receptacles, plugs (male)

- Panel mounted
- Extended dielectric

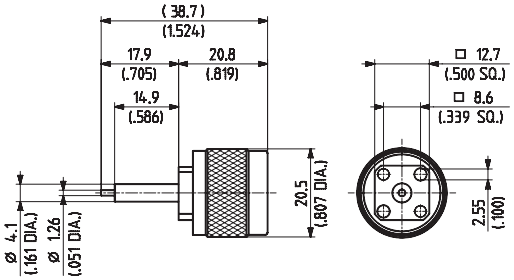

HUBER+SUHNER type	Item no.	Packaging	Weight	Notes
13_N-50-0-30/133_NE	22642831	single	30.0 g/1.05 oz.	SMA flange size

Receptacles, jacks (female)

- Panel mounted
- Extended dielectric

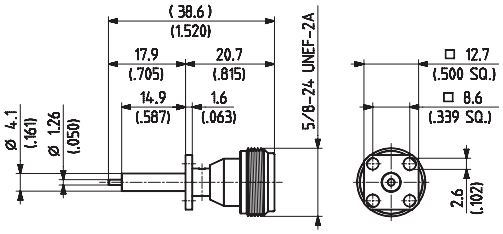

HUBER+SUHNER type	Item no.	Packaging	Weight	Notes
23_N-50-0-30/133_NE	22642835	single	14.0 g/0.49 oz.	SMA flange size

N 50 Ω

- Panel mounted
- Solder pot terminal
- Flush dielectric

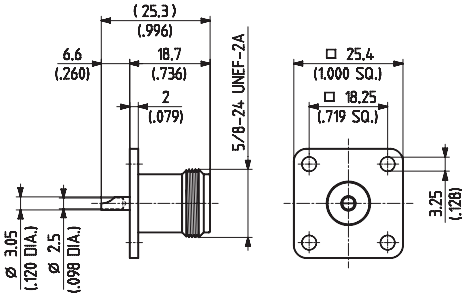

HUBER+SUHNER type	Item no.	Packaging	Weight
23_N-50-0-23/133_NE	22544751	single	24.0 g/0.84 oz.

Cable groups see page 32 Assembly tools see page 441 Mounting holes / PCB layouts see page 465

Figure A.8: Receptacles, jacks (female): from Huber+Suhner

EBE Faculty: Assessment of Ethics in Research Projects (Rev2)

Any person planning to undertake research in the Faculty of Engineering and the Built Environment at the University of Cape Town is required to complete this form before collecting or analysing data. When completed it should be submitted to the supervisor (where applicable) and from there to the Head of Department. If any of the questions below have been answered YES, and the applicant is NOT a fourth year student, the Head should forward this form for approval by the Faculty EIR committee: submit to Ms Zulpha Geyer (**Zulpha.Geyer@uct.ac.za**; Chem Eng Building, Ph 021 650 4791).
NB: A copy of this signed form must be included with the thesis/dissertation/report when it is submitted for examination

This form must only be completed once the most recent revision EBE EiR Handbook has been read.

Name of Principal Researcher/Student: Dominique Gouveia Department: Electrical Engineering

Preferred email address of the applicant: FRGDOM001@MYUCT.AC.ZA

If a Student: Degree: MSc Supervisor: Riana Geschke

If a Research Contract indicate source of funding/sponsorship: N/A

Research Project Title: Design and Implementation of L and X-Band Filters for the NeXtRAD Front-End

Overview of ethics issues in your research project:

Question 1: Is there a possibility that your research could cause harm to a third party (i.e. a person not involved in your project)?		NO
Question 2: Is your research making use of human subjects as sources of data? If your answer is YES, please complete Addendum 2.		NO
Question 3: Does your research involve the participation of or provision of services to communities? If your answer is YES, please complete Addendum 3.		NO
Question 4: If your research is sponsored, is there any potential for conflicts of interest? If your answer is YES, please complete Addendum 4.		NO

If you have answered YES to any of the above questions, please append a copy of your research proposal, as well as any interview schedules or questionnaires (Addendum 1) and please complete further addenda as appropriate. Ensure that you refer to the EiR Handbook to assist you in completing the documentation requirements for this form.

I hereby undertake to carry out my research in such a way that

- there is no apparent legal objection to the nature or the method of research; and
- the research will not compromise staff or students or the other responsibilities of the University;
- the stated objective will be achieved, and the findings will have a high degree of validity;
- limitations and alternative interpretations will be considered;
- the findings could be subject to peer review and publicly available; and
- I will comply with the conventions of copyright and avoid any practice that would constitute plagiarism.

Signed by:

	Full name and signature	Date
Principal Researcher/Student:	Dominique Gouveia Signed	31/03/2017

This application is approved by:

Supervisor (if applicable):	Riana Geschke Signed	2 April 2017
HOD (or delegated nominee): *Final authority for all assessments with NO to all questions and for all undergraduate research.*	Signed EBOSE	11/4/17
Chair : Faculty EIR Committee For applicants other than undergraduate students who have answered YES to any of the above questions.		